SPECTROSCOPIC INVESTIGATION OF SOME RARE EARTH IONS IN FLOURITE TYPE CRYSTALS

A Thesis Submitted
in Partial Fulfilment of the Requirements
for the Degree of
DOCTOR OF PHILOSOPHY

By
D. NARAYANA RAO

to the
DEPARTMENT OF PHYSICS
INDIAN INSTITUTE OF TECHNOLOGY, KANPUR
JANUARY, 1979

PHY-1979-D-RAO-SPE

to

Savitri and Sailaja

CERTIFICATE

This is to certify that the work presented in this thesis entitled SPECTROSCOPIC INVESTIGATION OF SOME RARE EARTH IONS IN FLUROITE TYPE CRYSTALS is the original work of Mr. D. Narayana Rao, carried out under our supervision and the same has not been submitted elsewhere for a degree.

D. Ramachandra Rao
D. Ramachandra Rao

P. Venkateswarlu
P. Venkateswarlu

ACKNOWLEDGEMENTS

I am very grateful to Professor Putcha Venkateswarlu and Professor D. Ramachandra Rao for their kind guidance and encouragement throughout the course of this work.

I am also thankful to Dr. S. Muralidhara Rao, H.P.D., B.A.R.C for his help in using the vacuum furnace. Thanks are also due to Dr. S.D. Soman, Head, H.P.D. and Dr. Ganguli, Director, Chemistry Division, B.A.R.C for their interest in my work.

I have been benefitted a lot from my association with Dr. H. Jagannath and Dr. U.V. Kumar. I am thankful to both of them. It is a pleasure to thank Dr. Bansilal and Dr. A. Sivaram for their cooperation and companionship.

I am also thankful to all the past and present members of Microwave Optical and Laser Spectroscopy Laboratories (MOLS) for their cooperation and help. Particular mention here is to be made of the following MOLS staff members who have been very cooperative: M/S Kuldip Singh Ubhey, D.S. Rawat, Bahadur Singh, N.V.G. Swamy, Pier Singh, Dhingra, S.L. Yadav, R.K. Garg, R.S. Nigam, M.S. Panesar, Jagir Singh, and Miss C. Komala.

I appreciate Mr. Bajpai for the neat tracings and Mr. L.S. Rathaur for cyclostyling the stencils.

Words are inadequate to thank Mrs. B. Rukmini Devi for her love and affection ~~on~~ towards me. Her constant encouragement is gratefully acknowledged. I thank her for the neat and patient typing. It is just not possible to express my feelings towards my parents and other members of our family who are mainly responsible for achieving this goal of mine.

Financial assistance from CSIR during my initial stages of the Ph.D. programme is gratefully acknowledged.

NARAYANA RAO

CONTENTS

SYNOPSIS

CHAPTER 1	:	Introduction	1
CHAPTER 2	:	Experimental Details	14
CHAPTER 3	:	Absorption and Fluorescence of $Sm^{3+}:CaF_2$	37
CHAPTER 4	:	Absorption and Fluorescence of $Ho^{3+}:CaF_2$	89
CHAPTER 5	:	Fluorescence and Excitation Spectra of $Ho^{3+}:BaF_2$	153
CHAPTER 6	:	Fluorescence Spectrum of $Tb^{3+}:CaF_2$	168

SYNOPSIS

SPECTROSCOPIC INVESTIGATION OF SOME RARE EARTH IONS IN FLUORITE TYPE CRYSTALS

D. Narayana Rao
Department of Physics
Indian Institute of Technology Kanpur
India

This thesis deals with the absorption and fluorescence spectra of Ho^{3+} in CaF_2 and BaF_2 and Sm^{3+} in CaF_2 and the fluorescence spectrum of Tb^{3+} in CaF_2.

First chapter of this thesis introduces rare earth spectroscopy, and in particular the optical spectra of the rare earth ions in fluorite type crystals. Different problems faced because of presence of several centres of RE^{3+} ions and the various techniques developed to understand the optical spectrum are cited. Also discussed are the advantages of using concentration series, and the study of decay times and selective laser excitation in the classification of lines due to different centres.

The second chapter deals with the description of the absorption set-up, the spectrophotometer for recording the fluorescence and excitation spectra and the vacuum furnace for crystal growing. Absorption spectra are photographed on a 3.4 m Jarrell-Ash spectrograph in the first order with 5A/mm dispersion. CW Ar^+ laser (Spectra Physics model 165-03), N_2 laser and N_2 laser pumped dye laser (Molectron models UV 1000 and DL 300 respectively) are used as the excitation

sources for recording the fluorescence spectra. The spectrophotometer consists of a 0.75 m Jarrell-Ash grating spectrograph fitted with a photomultiplier tube. The steady state spectra are recorded using a picoammeter. Boxcar integrator and synchronous signal averager are used for the transient studies. $Ho^{3+}:CaF_2$, $Sm^{3+}:CaF_2$ and $Tb^{3+}:CaF_2$ concentration series are grown in a vacuum furnace under fluorine atmosphere created by adding PbF_2 to the melt.

The third chapter presents the work on the absorption and fluorescence of $Sm^{3+}:CaF_2$. The optical absorption spectrum photographed at LNT in the region from 4000 to 6000A consists of seven groups of lines due to Sm^{3+} and a broad band around 4300A due to Sm^{2+}. The seven groups are identified as due to the transitions from $^6H_{5/2}$ ground state to $^6P_{5/2}$, $^4P_{5/2}$, $^4G_{9/2}$, $^4F_{5/2}$, $^4I_{13/2}$, $^4I_{11/2}$, $^4I_{9/2}$ and $^4G_{7/2}$ states. Steady state fluorescence spectra of $Sm^{3+}:CaF_2$ with varying concentrations of Sm are recorded at LNT in the visible region using N_2 laser excitation. Four groups of fluorescence lines due to $^4G_{5/2} \rightarrow {}^6H_{5/2, 7/2, 9/2, 11/2}$ transitions are observed in the region from 5580 to 7150A. A continuum observed in the region from 7000 to 9000A is identified as due to Sm^{2+}. From the variation in the relative intensities of some of the lines, it is concluded that there are two centres A and B for Sm^{3+}.

From the fluorescence spectra recorded by selectively exciting each absorption line and from the excitation spectra

monitoring all the observed fluorescence lines, all the lines in the optical spectrum are classified under these centres A and B. Further confirmation of the classification is obtained from the study of decay times. Decay times of $^4G_{5/2}$ of centres A and B are found to be 4.3 ms and 5.5 ms respectively. Fluorescence from centre B is observed to be very weak, and contains very few lines. The spectrum of this centre is not analysed. The Stark splittings are derived for all the levels involved in the fluorescence and excitation spectra. $^4G_{5/2} \rightarrow {}^6H_{11/2,13/2}$ fluorescence groups which are observed to be very weak with dye laser excitation, are recorded using the 4765A line of the Ar^+ laser. The spectrum recorded using this excitation is found to be exactly the same as that of centre A. With Ar^+ laser excitation, fluorescence from $^4F_{3/2}$, which is $\sim$ 900 cm^{-1} above $^4G_{5/2}$, is also observed, at higher temperatures.

The fourth chapter presents the work on the absorption and fluorescence of $Ho^{3+}:CaF_2$. The absorption spectrum photographed in the region from 3500 to 6500A consists of seven groups which are assigned as due to the transition from $^5I_8$ ground state to $^5G_5'$, $^5G_5$, $^5G_6 + {}^5F_1$, $^3K_8 + {}^5F_2$, $^5F_3$, $^5F_4 + {}^5S_2$, $^5F_5$ states. Fluorescence spectrum is recorded using the 4765A line of Ar^+ laser in the region from 4800 to 7600A for different concentrations of Ho^{3+} in CaF_2. Four groups of lines, assigned as originating from $^5F_3$, $^5F_4 + {}^5S_2$, $^5F_5$ and $^5I_4$, are observed. Two groups around 6500A and 7500A are found to be due to overlapping transitions from $^5F_3$ and $^5F_5$

and $^5F_4 + {}^5S_2$ and $^5I_4$ respectively. All the lines in the fluorescence spectrum are classified under two centres A and B by selective dye laser excitation. This classification is also confirmed by recording the excitation spectrum for each line and from the study of decay times. The times of $^5F_3$, $^5F_4 + {}^5S_2$ and $^5F_5$ levels are measured to be 10, 1100 and 118 μs respectively in centre A and 18, 330 and 145 μs respectively in centre B. From the measurement of decay times and by exciting into different levels, most of the lines belonging to $^5F_3 \rightarrow {}^5I_7$ and $^5F_5 \rightarrow {}^5I_8$ transitions in the 6500A group and $^5F_4 + {}^5S_2 \rightarrow {}^5I_7$ transition in the 7500A group are identified. No lines of the $^5I_4 \rightarrow {}^5I_8$ transition also expected to fall in the same region (around 7500A) are observed.

From the fluorescence and excitation spectra, the Stark components of $^5I_8$, $^5I_7$, $^5F_5$, $^5F_4 + {}^5S_2$, $^5F_3$, $^3K_8 + {}^5F_2$ and $^5G_6 + {}^5F_1$ are derived for both the centres A and B. Variation in the intensity of the fluorescence of the centres A and B for different concentrations of Ho^{3+} is observed by selectively exciting into the absorption lines of each centre.

Work on $Ho^{3+}:BaF_2$ is presented in the fifth chapter. This crystal is bought from the Semi Elements Co., USA. The observed fluorescence and excitation spectra show that there is only one centre of Ho^{3+} which leads to strong fluorescence and absorption. Other centres are also present but their

spectra are found to be too weak to study. The present study in this system is confined to the analysis of the strong centre only. Four groups of fluorescence lines are observed in the region from 4800 to 7600A, as in the case of $Ho^{3+}:CaF_2$. Only two strong groups around 5300A and 7500A due to $^5F_4 + {}^5S_2 \rightarrow {}^5I_8$ and $^5I_7$ transitions respectively could be analysed. The other two groups around 4800A and 6500A are observed to be very weak. The decay time measurements give a value of 2450 μs for the 5300A group. Identical excitation spectra of $^5G_6 + {}^5F_1$ and $^3K_8 + {}^5F_2$ are obtained by monitoring more than three lines in the 5300A group. From the observed excitation and fluorescence data, Stark components of $^5I_8$ (below 150 cm^{-1}), $^3K_8 + {}^5F_2$ and $^5G_6 + {}^5F_1$ are derived.

Results of the studies on $Tb^{3+}:CaF_2$ are presented in Chapter 6. A variation in the relative intensity of some of the fluorescence lines is observed as the concentration is varied. A study of the fluorescence spectrum using Ar^+ laser as the excitation (4880A) source indicates that there are large number of lines in the spectrum which can not be accounted for with the help of the energy level diagram for $Tb^{3+}:CaF_2$ proposed by earlier workers. It is concluded that there are more than one centre for Tb^{3+} in CaF_2. Six groups of fluorescence lines are observed in the region from 5000 to 7000A which are assigned as from $^5D_4$ to $^7F_{5, 4, 3, 2, 1, 0}$.

Only three groups from $^5D_4$ to $^7F_{5,\ 4,\ 3}$ are reported in the literature.

In conclusion, two prominent centres are observed in the case of $Ho^{3+}:CaF_2$ and $Sm^{3+}:CaF_2$. The spectra of $Ho^{3+}:BaF_2$ indicate the presence of only one centre with intense fluorescence. From the observed fluorescence and excitation spectra at LNT, partial energy level diagrams are derived for $Ho^{3+}:CaF_2$, $Sm^{3+}:CaF_2$ and $Ho^{3+}:BaF_2$. The fluorescence spectrum of $Tb^{3+}:CaF_2$ also shows evidence for the presence of more than one kind of terbium centres in the crystal, whereas, only one centre was reported earlier. Most of the fluorescence lines in the overlapping transitions of $Ho^{3+}:CaF_2$ are identified by various studies. Two new groups due to the transitions $^4G_{5/2} \rightarrow {}^6H_{11/2,\ 13/2}$ in the case of $Sm^{3+}:CaF_2$ which are not reported are observed at LNT. Further, $^4F_{3/2}$ level which is $\sim$ 900 cm^{-1} above the $^4G_{5/2}$ level is established from the high temperature studies.

CHAPTER 1

INTRODUCTION

Rare earths (La to Yb) are a class of elements which possess a Xe core of electrons ($1s^2$, $2s^2$, $2p^6$, $3s^2$, $3p^6$, $3d^{10}$, $4s^2$, $4p^6$, $4d^{10}$, $5s^2$, $5p^6$) with N 4f and two or three outer electrons, where N varies from 0 (for La) to 14 (for Yb). In the trivalent state they have only 4f electrons with the Xe core.

The triply ionised rare earth ions have interesting properties in that their $4f^N$ electrons are, to a great extent, shielded by the $5s^2$ and $5p^6$ orbits, and the interaction of these $4f^N$ electrons with the crystal field environment is quite weak. They retain these 'free ion' properties more or less intact even inside solid lattices. The wavefunctions remain to be almost pure angular momentum eigen functions and the centre of gravity of the crystal field split components stay quite close to the 'free ion' values and vary very little from lattice to lattice.

The Hamiltonian of such an f^N electron ion in a crystal field is given in standard form by

$$H = Ho + \sum_{i=j}^{N} \frac{e^2}{2r_{ij}} + \sum_{i} \xi_i(\gamma)\, \bar{l}_i \cdot \bar{s}_i + V$$

where $$Ho = -\sum_{i=1}^{N} \left(\frac{h^2}{2m} \nabla_i^2 + \frac{Ze^2}{r_i}\right)$$

Excepting V, the Hamiltonian in the above equation is exactly the same as the Hamiltonian for the free ion. V is the perturbation due to the crystal field and is given in spherical harmonics as

$$V = \sum_{i}^{N} \sum_{l} \sum_{m} Y_l^m (\Theta_i, \Phi_i) R_{ni} r_i$$

For the rare earth ion in a crystal field $V << \xi$ l.s. The f^N configuration consists of $^{14}C_N$ levels, the degeneracy of which is partly lifted by the interelectronic repulsion and the spin-orbit interaction (second and third terms in H). The electronic repulsion term splits the various terms having different L and S and the levels with different J values are separated out by the spin arbit interaction. The effect of these two terms is usually calculated by a perturbation treatment in which it is assumed that the energy separation between the various configurations is large and hence they do not interact. The off diagonal matrix elements of the spin arbit interaction cause mixtures of levels having the same J but differing in L and S by $\pm$ 1 and $\mp$ 1 respectively. As a result, the levels finally have only one good quantum number J and each level is (2J + 1) fold degenerate.

Because of the perturbation V, the (2J + 1) fold degeneracy is lifted partially or completely depending on the symmetry of the crystal field the rare earth ion experiences.

Thus it becomes important to know the site symmetry of the cation (here RE^{3+}), because V must transform as the totally symmetric representation of the symmetry group of the site. In a crystal field, unless the ion is situated at a centre of inversion, parity is not a good quantum number, and the field brings about a mixture of wave functions belonging to configurations of different parities. This makes the electric dipole transitions between levels formally allowed, which otherwise are forbidden. These are called forced electric dipole transitions and have oscillator strengths of the order of 10^{-6}. The spectra are studied in various solid hosts mainly as, in the free state these transitions are forbidden. The following discussion pertains to the optical spectra of the rare earth ions doped in flurite hosts like MeF_2, where Me = Ca, Ba, Sr and Cd.

The optical spectra of the rare earth ions in fluorite type crystals consist of sets of line groups lying in the ultraviolet, visible as well as infrared regions. Even at liquid helium temperatures, the number of lines in several of these groups is usually found to be considerably larger than the theoretical number calculated with the assumption that all the RE^{3+} ion sites experience a field of same symmetry. This is due to the charge compensation which is not the same for all the rare earth ion sites in the crystal.

Each of these centres has its own set of Stark components and corresponding set of lines in the spectra. This multiplicity of the sites and number of transitions from each site results in a complex spectrum, and thus characterization of the various sites by optical spectroscopy had been a slightly difficult task [1,2]. However, the discovery of laser actions in these crystals and the advent of lasers as the excitation sources have created a new interest in many investigators to obtain energy level structures for these systems through the study of absorption and fluorescence spectra and different relaxation mechanisms.

The fluorine atoms of the MeF_2 crystal form a simple cubic lattice. Alternate body centre positions along the (100) directions of this lattice are occupied by the metal atoms. Rare earth ions can enter the lattice at Ca^{2+} sites. At such sites, divalent rare earth ion experiences a cubic crystalline field of eight fold fluorine coordination. However, rare earths usually enter MeF_2 lattice as trivalent ions (except in the case of Eu and Sm where they enter mostly as divalent ions), and charge compensation is achieved in several ways depending upon many factors associated with the total crystal growth process. Consequently, trivalent rare earth ions can experience crystal fields of different strengths and symmetries [3], cubic, tetragonal, trigonal and orthorhombic being the more commonly occuring symmetries.

The most commonly found RE^{3+} site+ is one of tetragonal (C_{4v}) symmetry. In this case, excess positive charge of the rare earth ion is compensated by the occupation of one of the six nearest interstitial sites along the (100) direction at a distance of a/2 (where a = lattice constant) by an F_i^- ion. All the RE^{3+}:MeF_2 type crystals grown in fluorine atmosphere show the existance of centres+ of tetragonal symmetry.

Cubic symmetry for the RE^{3+} ion results when the charge compensation is not achieved locally. The excess of F_i^- in the interstitial site are loosely bound to the RE^{3+} ion and diffuses though the crystal at high temperature. Tetragonal centres, thus, can be converted to cubic by heating the crystal and then quenching it immediately. The interstitial F_i^- ions which diffuse through the crystal are trapped elsewhere in the crystal. Slow cooling favours a position which is close to the RE^{3+} ion and results in a tetragonal symmetry.

A trigonal site symmetry results when one of the eight nearest neighbour F_i^- (111) ions at a distance of $\sqrt{3}a/4$ is replaced by O_2^-. Formation of this type of site is a function of the oxidation-reduction conditions during the crystal growth. Several statistical theories [4] have been proposed to explain the formation and occurance of these and various other sites.

+ The RE^{3+} ion positions in the lattice are referred to as sites or centres.

It is found that the presence of + ve compensator ions like Na^+ or K^+ (in the form of NaF or KF added to the melt) in the melt results in an increase of cubic and orthorhombic centres. The + ve compensator ion replaces Ca^{2+} ion in the third or sixth coordinate sphere of the RE^{3+} ion resulting in orthorhombic or tetragonal symmetries for the RE^{3+} ion respectively. Ions in the sixth coordinate sphere, because of their large distance, have only a small effect on the crystal field at the rare earth site and the site symmetry remains essentially cubic.

Detailed information about the structure of the RE^{3+} centres may be obtained by the electron paramagnetic resonance method which makes it possible to establish quite reliably, the symmetry of the electric field the RE^{3+} ion experiences and the relative abundance of the various centres [5]. A study of the electron paramagnetic resonance and the optical spectrum gives complete information on the energy level structure of rare earth ions in a particular site.

In this thesis an attempt has been made to obtain the energy level structures for the systems $Ho^{3+}:CaF_2$, $Sm^{3+}:CaF_2$, $Ho^{3+}:BaF_2$ and $Tb^{3+}:CaF_2$ from the studies of optical absorption spectra and steady state and transient fluorescence spectra.

Several methods [1,6] in the past have been used to study the optical spectrum of rare earth ions in the crystals. They are (i) optical Zeeman effect, (ii) the polarized absorption and luminescence and (iii) piezospectroscopic effect. A study by these methods makes it possible to establish the symmetry of the site (centre) corresponding to a given line only if it is well isolated from the rest of the spectral lines. But in practice the spectra due to several centres overlap and none of these methods are useful to analyse the complete Stark structure from the optical spectrum, that is to isolate from the general spectrum the lines belonging to different centres.

The following techniques which have been developed to study the optical spectrum of charge compensated sites in $RE^{3+}:MeF_2$, are used in the present studies.

1. Variation of crystal growth conditions.
2. Varying concentration of RE^{3+} in these crystals.
3. Transient fluorescence studies.
4. Selective laser excitation.

1. Variation of crystal growth conditions:

As just discussed, different crystal growth and heat treatment conditions favour the occurrence of different kinds of centres [7,8]. A study of the variation of intensities of the lines and the appearance of new lines among various

such crystals leads to the classification of lines in the optical spectrum under different centres.

2. Varying concentration of RE^{3+} in MeF_2 [9,10]

This method is to look for sets of lines in the optical spectrum (absorption of fluorescence) whose relative intensity remains constant in all the crystals with different RE^{3+} concentrations. All such lines can be assumed as due to one particular centre. The relative abundances of the various centres is a function of the concentration of the impurity. A brief review of the results of the studies made using the concentration series of crystals is given below. It is considered that at lower concentration cubic centres would predominate. At higher concentrations the distribution should change, as fewer lattice sites are available for distant compensation that a cubic site requires [4]. Experimental evidance [11,12] does not seem to confirm this theoretically predicted behaviour of the different sites with concentration. An increase of cubic centres with increase in concentration of RE^{3+} in CaF_2 has been observed by many investigators. At still higher concentration dipolar interaction of $RE^{3+} - F_i^-$ increases leading to the formation of clusters in the lattice Formation of dimers is observed in $Er^{3+}:CaF_2$ and $Er^{3+}:SrF_2$ by Wright and others [13,14]. A theoretical frame work developed for dimers by Neberhuis and Fong agrees with

McClure's observation of the optical absorption line intensity increasing as N^2, where N is the number of cations per unit volume of the crystal [15].

3. Transient fluorescence studies:

It is observed that the fluorescence lines involving the Stark ~~levels~~ components of an SLJ level of a particular centre show the same decay time at all but the lowest temperatures. This phenomenon is used in this method to isolate the fluorescence lines of each centre in the observed spectrum. Here all the fluorescence lines (assigned to a particular SLJ level) having the same decay time are classified under the same centre. However, this method cannot be applied when the decay times of the corresponding SLJ levels of different centres are very close to each other.

4. Selective laser excitation:

The three methods discussed so far have some practical limitations. At very low concentrations, the fluorescence from some of the centres may be very weak. At higher concentrations, fluorescence from different centres may overlap and lead to a complicated spectrum. Thus the actual line intensities cannot be measured in such cases. Further, the decay times in the case of overlapping lines result in erroneous values, and may lead to the different site origins.

In this method, a narrow band dye laser is used to selectively excite the absorption lines of specific sites in a crystal. The resulting fluorescence arises from the site excited only. Nonresonant energy transfer between different sites is not observed [13,14]. Excitation of more than one site is observed only when absorption lines of different sites overlap. The selective excitation thus simplifies the fluorescence spectrum compared to a conventional (broad band) excitation. Conversely, single site excitation spectrum can be obtained by monitoring fluorescence line of a specific site.

In the present work, all the four methods discussed above have been used to study the optical spectrum of Ho^{3+}: CaF_2 [16], Sm^{3+}:CaF_2,[17], Tb^{3+}:CaF_2 [18] and Ho^{3+}:BaF_2 [16] and to identify the energy levels of the different centres in these systems. Earlier work [16,17,18] on these systems has been limited mainly to the analysis of the spectra in terms of one centre, using a 'broad band' excitation source. Using a concentration series for each of the above systems (except Ho^{3+}:BaF_2, only one crystal of which has been bought from Semi Elements Inc. USA), which are grown in a fluorine atmosphere, the spectra are reinvestigated at LNT using CW Ar^+ laser, N_2 laser and N_2 laser pumped dye laser. All the fluorescence and absorption lines observed in the spectra

are classified into different centres in the case of Ho^{3+}: CaF_2, Sm^{3+}:CaF_2 and Ho^{3+}:BaF_2 and possible sets of partial energy level schemes are constructed. Presence of different centres is also observed in the case of Tb^{3+}:CaF_2.

REFERENCES

1. R.H. Heist, C.R. Chilver and F.K. Fong, Phys. Rev. B5, 4237 (1972).

2. R.E. Bradbury and E.Y. Wong, Phys. Rev. B4, 690, 694 702 (1971).

3. M.J. Weber and R.W. Bierig, Phys. Rev. 134A, 1492 (1964).

4. F.Z. Gilfanov, L.D. Livanova, A.L. Stolov, Soviet Phys. Solid State 8, 108 (1966).

4. V.V. Osiko, Soviet Physics-Solid State 7, 1047 (1965).

5. R.H. Heist and F.K. Fong, Phys. Rev. B1, 2970 (1970) and the references 7 to 16 contained therein.

6. P.P. Feofilov and A.A. Kaplyanskii, Soviet Physics Uspekhi 5, 79 (1962).

7. U. Ranon and A. Yaniv, Phys. Letters 9, 17 (1964).

8. E. Friedman and W. Low, J. Chem. Phys. 33, 1275 (1960).

9. Yu.K. Boron'ko, L.V. Krotova, V.V. Osiko, V.T. Udovenchik, M.M. Fursikov, Soviet Phys. Solid State 7, 1450 (1965).

10. Yu.K. Voron'ko, A.A. Kaminskii and V.V. Osiko, Soviet Physics JETP 22, 501 (1966).

11. M.R. Brown, K.G. Roots, J.M. Williams, W.A. Shand, C. Groter and H.F. Kay, J. Chem. Phys. 50, 891 (1969).

12. G.K. Miner, T.P. Graham and G.T. Johnston, J. Chem. Phys. 57, 1263 (1972).

13. D.R. Tallant and J.C. Wright, J. Chem. Phys. 63, 2074 (1975).

14. M.D. Kurz and J.C. Wright, J. Luminescence 15, 169 (1977).

15. S.L. Neberhuis and F.K. Fong, J. Chem. Phys. 56, 1174 (1972).

16. Bansilal, Ph.D. Dissertation, I.I.T. Kanpur, India (1977).

17. N. Rabbiner, Phys. Rev. 130, 502 (1963).

18. N. Rabbiner, J. Opt. Soc. Am. 55, 436 (1965).

19. A. Sivaram, D. Ramachandra Rao, P. Venkateswarlu, J. Phys. C11, L401 (1978).

CHAPTER 2

EXPERIMENTAL DETAILS

ABSTRACT

Absorption spectra are photographed on a 3.4 m Jarrell-Ash spectrograph in the first order with 5A/mm dispersion. CW Ar^+ laser, N_2 laser and N_2 laser pumped dye laser are used as the excitation sources for recording the fluorescence spectra. The fluorescence and excitation spectra are recorded using a spectrophotometer set-up assembled around a 0.75 m Jarrell-Ash grating spectrograph. N_2 laser pumped dye laser, tunable continuously in the visible region, is used for recording the excitation spectra. Transient measurements are made using a boxcar integrator and a synchronous signal averager. $Ho^{3+}:CaF_2$, $Sm^{3+}:CaF_2$ and $Tb^{3+}:CaF_2$ concentration series are grown in a vacuum furnace, under fluorine atmosphere created by adding PbF_2 to the melt.

2.1 Experimental Set-up for Recording the Optical Absorption Spectrum

The optical absorption spectra are recorded photographically on a Jarrell-Ash 3.4 m Ebert grating spectrograph. The spectrograph is provided with interchangeable 15000 LPI and 30000 LPI gratings which provide a dispersion of 5A/mm and 2.5 A/mm in the first order. Color glass filters are used to cut-off the higher orders, where needed.

A 750 W tungsten lamp is used as a source of continuum. Light from the lamp is focussed on to the crystal through a water filter to cut off the IR radiation (to reduce the heating of the crystal) and is collected on to the slit of the spectrograph with a cylindrical lens. A slit width of 25 μ is used for photographing the spectra. A standard demountable cold finger liquid N_2 dewar is used to cool the crystals to liquid nitrogen temperature (LNT). The crystals are mounted so as to have (1) maximum path length for the light in the crystal, (2) maximum thermal contact with the cold finger.

Iron arc is used as a standard for wavelength measurements. Exposure times for photographing the spectra are varied from 1/2 minto 20 mins depending upon the intensity of the lines. All the spectra are photographed on Kodak NP27:400 ASA films and are measured on a Carl-Zeiss Abbe comperator which has a least count of 1 μ. Weak and broad

lines are measured from the densitometer traces of the absorption spectra obtained on a Carl-Zeiss Microdensitometer.

2.2 Experimental Set-up for Recording the Steady State Fluorescence and Excitation Spectra

The steady state fluorescence spectra, excited by the CW Ar^+ laser, pulsed N_2 laser and N_2 laser pumped dye laser are recorded by the experimental set-up shown in figure 2.1.

2.2.1 Excitation Sources/the Lasers Used

The CW Ar^+ laser used is a Spectra Physics model 165-03, equipped with an intracavity tuning prism to select the lasing wavelength. Maximum powers of 1300, 500 and 250 mw can be obtained at 4880A, 4765A and 4579A respectively as per the manufacturer's specifications. The output power can be varied by varying the discharge current of the plasma tube from 10 to 35 Amps.

The Molectron model UV 1000 N_2 laser, which is used mainly for the present studies, is capable of producing a peak output power of 1 mw at 3371A with a pulse width of 10 ns. The repetition rate can be varied from 5 Hz to 50 Hz. A repetition rate of 10 Hz is chosen for the present studies. This amounts to an average power of 100 mw. The cross-section of the laser beam is a rectangle of dimensions 6 mm x 25 mm.

Molectron model DL 300 dye laser is pumped by the UV 1000 N_2 laser. Various organic dyes can be excited to lase within their fundamental fluorescence bands of 20 to 60 nm width and a continuous tuning can be achieved from 360 nm to 750 nm. Present work is carried out with coumarin, fluorescein, umbelliferon, R6G, RB and CVP dyes. Table 2.1 gives the tuning range of the laser for each of the above dyes used in the experiments. Because of the nonavailability of some of the dyes, the experiments could not be conducted in the spectral range 4900-5300A. The grating of the DL 300 dye laser is a glass replica blazed at 2.70 μm with 600 lines (grooves) per millimeter of grating width. To operate over a broad range of output wavelengths, orders (n) 4 through 7 of the grating are used, there by maintaining high efficiency at all wavelengths. The grating is driven through a sinebar to provide linear wavelength scanning. A provision is made to rotate the grating shaft with a hand crank. We have added a stepper motor+ (Step-Syn™ of Automatic Electric Co. India) for driving the grating shaft, making it convenient for recording the excitation spectrum. The speed of the stepper motor can be varied in nine steps, viz., 10, 5, 2, 1, 0.5, 0.25, 0.1, 0.05 and 0.025 rpm. Each revolution of the grating shaft corresponds to the scanning of 100A in the first order and 100 A/n in the nth. order. Table 2.1 lists the wavelength increment

---

+ Stepper motor drive has been fabricated under a joint project of Lasers Laboratory, Department of Physics and Advanced Centre for Electronic Systems of Electrical Engineering Department, I.I.T. Kanpur.

Name of the dye	Solvent	Peak wavelength A	Wavelength range (10 per-cent points) A	Power output relative to R6G at the peak	Grating order n	Wavelength range per one revolution of the grating shaft
Diethylamino 4 methyl coumarin	Ethanol	4570	4400-4780	1.4	6	17.2
4-methyl umbelliferon	Ethanol	4500	4300-4900	< 1.0	6	17.2
Disodium fluorescein	Ethanol	5400	5300-6000	> 1.0	5	20.5
R6G	Ethanol	5790	5680-6050	1.0	5	20.5
RB	Ethanol	6090	5940-6430	0.9	4	25.8
R6G + CVP	Ethanol	6390	6280-6510	0.5	4	25.8
RB + CVP	Ethanol	6600	6410-6870	0.5	4	25.8

per one revolution of the grating shaft in the appropriate order and the approximate power output in comparison to R6G dye, for each of the dyes used.

2.2.2 Spectrophotometer [1]

The beam from the N_2 laser pumped dye laser (or N_2 laser or Ar^+ laser), bent upwards by a mirror, is focussed on to the crystal under study by a lens. The fluorescence light is collected in a direction perpendicular to the incident light and is focussed on to the slit of the 0.75 m plane grating spectrograph which has an asymmetric Czerny-Turner mounting for the grating and a worm and gear arrangement to rotate the grating table. The grating used is blazed at 5000A and has 1200 grooves/mm. One revolution of the grating shaft results in a 0.1 degree rotation of the grating. A mechanical counter on the spectrograph indicates the grating setting in hundredths of a degree. A stepper motor similar to the one described in section 2.2.1 is also added to rotate the grating shaft of the spectrometer. This results in different scanning speeds in the range from 520A/min. to 1.3A/min. Different color glass filters are used to suppress the higher order spectra.

A photomultiplier tube (PMT) ITT No. FW 130 is placed in front of the exit slit which replaces the plate holder arrangement. The response of the FW 130 tube is S 20 and

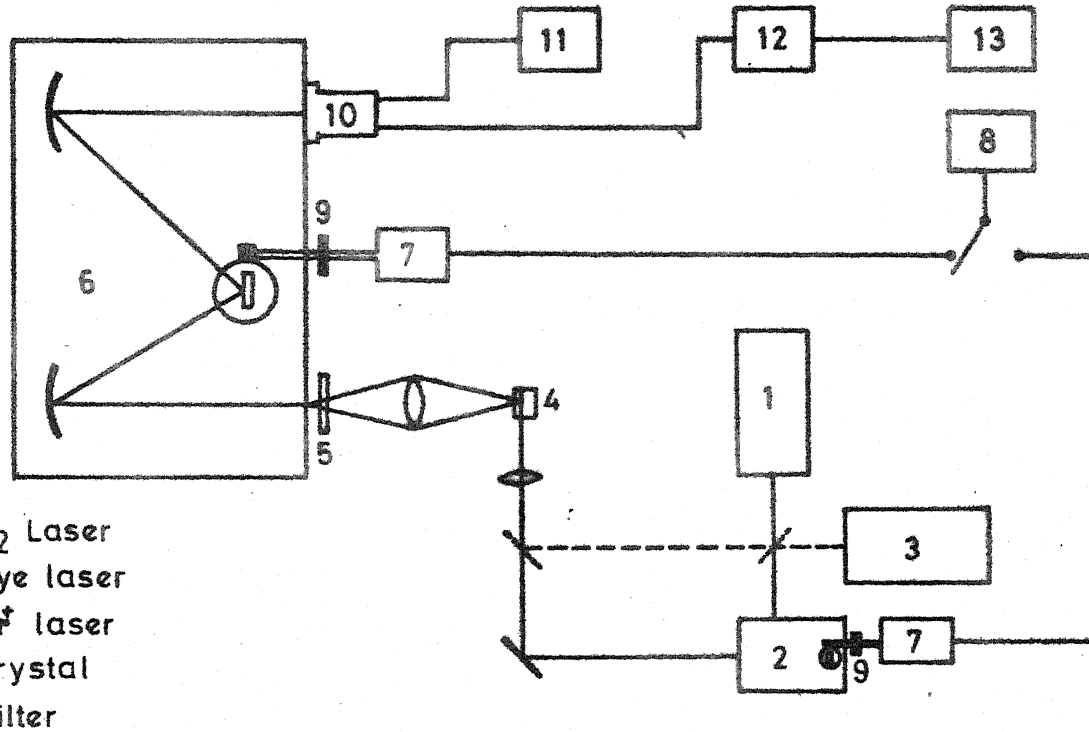

1. N_2 Laser
2. Dye laser
3. $A\overset{+}{r}$ laser
4. Crystal
5. Filter
6. Monochromator
7. Stepper motor
8. Stepper motor drive
9. Cam and microswitch
10. Photomultiplier tube
11. H V power supply
12. Picoammeter
13. Strip chart recorder

FIG. 2.1 BLOCK DIAGRAM OF THE RECORDING SPECTROPHOTOMETER.

its dark current is 1.5 nA when operated at 1500V and room temperature. The input and exit slits of the spectrometer can be varied from 20 μ to 440 μ. The current from the PMT is measured with a picoammeter (Keithley model No. 417), which has an output of 3V for full scale deflection, and the sensitivity is variable from 3×10^{-14} amps to 3×10^{-5} amps. Most of the spectra in the present case are recorded using slit widths (input x output) varying from 40 μ x 40 μ (for strong signals) to 100 μ x 100 μ (for weak signals), and the typical picoammeter current ranges at $(3, 1, 0.3) \times 10^{-7}$ amps. The output of the picoammeter is used to drive a strip-chart recorder (Varian model No. G-14A-2) which has two speeds of 2.5 cms/min. and 10 cms/min. Generally 2 rpm and 1 rpm for the grating shaft rotation (both the spectrophotometer and the dye laser gratings) and 10 cms/min. chart for the recorder are used. These correspond to a dispersion of 1 A/mm and 0.5 A/mm (0.3 A/mm and 0.15 A/mm in the case of the dye laser scanning, excitation spectrum) on the chart paper.

'Wavelength markers' on the chart paper are obtained [2] for every rotation of the grating shaft with a cam and microswitch arrangement shown in figure 2.2. A cam attached to the grating drive shaft (of both the dye laser and the spectrometer) closes a microswitch contact once every rotation and connects a 1.5 V dry cell across the recorder

terminals through a capacitor. The capacitor allows a sharp spike of voltage to pass through, at the instant the contact is closed. During the off period of the microswitch, the capacitor is discharged through the resistor R_1 to make it ready for the next marker. R_2 is an isolation resistor inserted in the picoammeter output lead to prevent the shunting of the 1.5 V pulse by the low output impedence of the picoammeter.

The wavelength markers are calibrated by recording the spectra of He-Ne, Ar and Xe low pressure discharge tubes. An accuracy of $\pm$ 1 A and $\pm$ 0.3A are obtained for the spectrophotometer and the dye laser markers respectively.

2.3 Experimental Set-up for Recording the Transient Fluorescence

The transient fluorescence spectra excited by N_2 laser pumped dye laser are recorded with the experimental set-up shown in figure 2.3.

Here, the output from the PMT is fed to an ac coupled pre-amplifier (Tektronix model 1121) through an emitter follower. The emitter follower with a large input impedence and an output impedence of 50Ω is used to avoid the distortion of the decay curve due to impedence mismatch. The preamplifier gain can be varied from 0.2 to 100 in nine steps

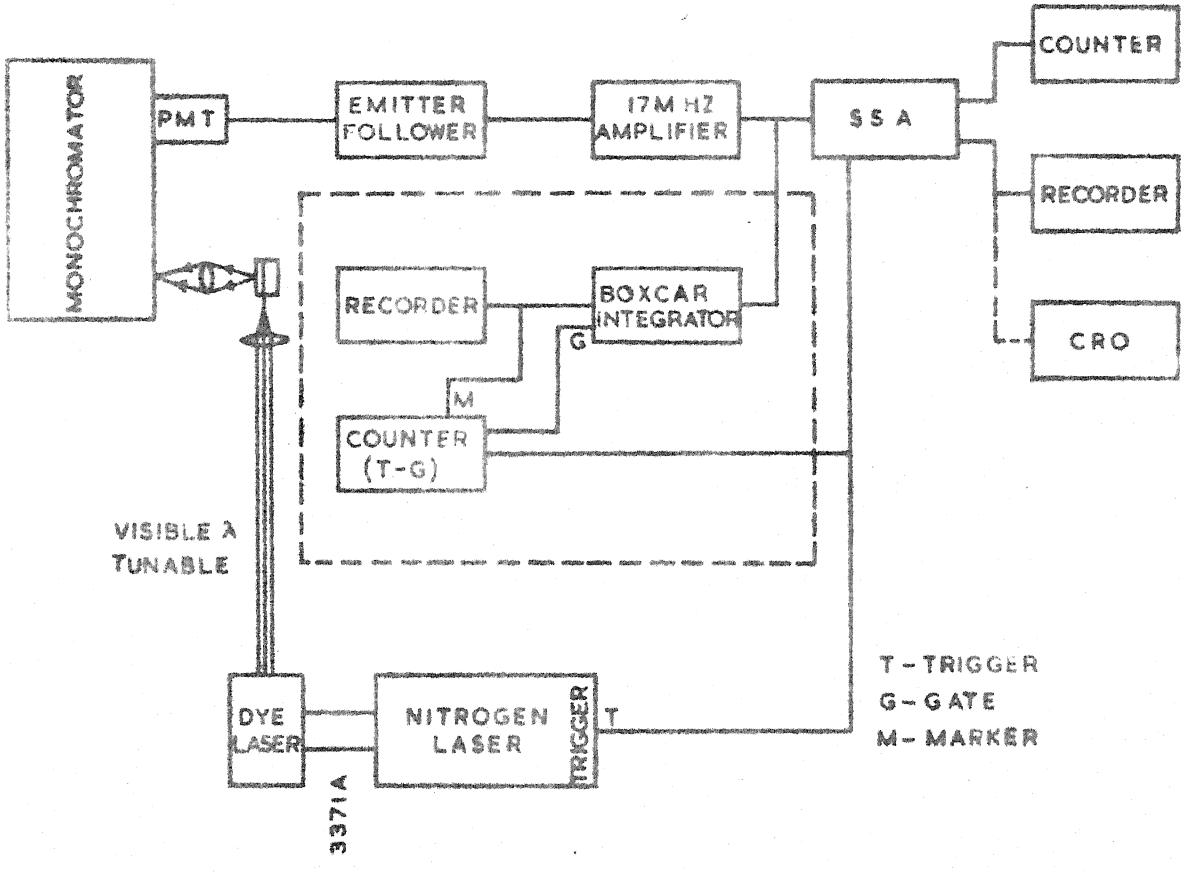

FIG. 2.3 BLOCK DIAGRAM OF THE EXPERIMENTAL SET-UP FOR LIFE-TIME MEASUREMENTS.

through an input attenuator. Output from the pre-amplifier is fed to either a boxcar integrator+ or a synchronous signal averager+ (SSA) for signal processing. The output of these is fed to the strip-chart recorder.

2.3.1 Boxcar Integrator [3]

The boxcar integrator is a gated signal averaging device which allows recovery of waveforms burried in noise. This instrument utilizes a variable delay gate of selectable width which can be fixed at any point on a repetitive waveform. This sampled portion of the input waveform is averaged by an integrator with adjustable time constant. Because the mean value of the noise is zero, the output of the integrator will approach the true form of the signal with an improvement in the S/N ratio given by

$$\text{S/N improvement} = \left[\frac{2 \times \text{time constant}}{\text{gate width}}\right]^{\frac{1}{2}}$$

In the 'scan' mode of operation, the gate is slowly scanned across the signal and the total wave form of the signal is reproduced at the output. The scan period to be used for achieving the optimum S/N improvement is directly proportional to the time constant and time base duration and inversely proportional to the repetition rate and square

---

+ Both the units are fabricated under a joint project of Lasers Laboratory, Department of Physics and Advanced Centre for Electronic Systems of Electrical Engineering Department, I.I.T. Kanpur.

of the gate width. The minimum scan period (MSP) to be used is given by

$$\text{MSP(mins.)} = \frac{\text{Time Constant (sec.)} \times \text{Time Base (sec.)}}{12 \times \text{Repetition Rate } (\text{sec}^{-1}) \times (\text{Gatewidth})^2 (\text{sec.})^2}$$

The averaging time constant can be varied from 0.01 ms to 100 secs in 1-3 sequence, while the time base duration is adjusted between 100 μs to 20 secs in 1-2-5 sequence. The gate width is continuously variable from 0.5 μs to 0.5 sec.

The sensitivity of the boxcar integrator is adjustable from 50 mV to 10 V in a 1-2-5 sequence and provides an output of ± 10 V for driving servo-type recorders.

The 'sync. output' (4 V - 400 ns) from the Molectron N_2 laser is used to trigger the boxcar, the scope and a digital counter (Yamuna (India) model No. 614). The moving gate of the boxcar is used to stop the digital counter thus giving the location of the gate across the fluorescence signal. Markers in this case are obtained in the following manner. The counter is used in the 'count disabled' mode and the readings are taken only when the counter is 'reset'. This reset voltage (~20 V) tapped out of the counter is used to provide a marker on the chart paper [2].

2.3.2 Synchronous Signal Averager [4]

The synchronous signal averager (also known as waveform eductor) utilizes an efficient waveform averaging technique to produce an output which is smooth point by point 'average' of the input waveform. It has 64 channels of capacitor memory, each channel storing the information of a minimum of 1μs. The signal waveform is therefore divided into 64 time segments, and information contained in these segments is charged on to 64 capacitors which are serially gated in, each time the signal repeats. After sufficient number of repetitions, the noise (in each segment) gets averaged to small values, but the signal builds up. The capacitors are charged through a resistor which is chosen to be as high as is compatible with the speed of acquisition to provide noise smoothening.

The characteristic time constants provided with the instrument cover a range from 1 to 100 secs in a 1-2-5 sequence. For initial build up of the waveform, a lower time constant is chosen. Time constant is then slowly increased to the highest value to obtain a smooth curve at the output.

Sweep duration is continuously variable from 45 μs to few secs. A provision is made for introducing any delay between trigger initiation and the start of the sweep. This

delay can be continuously adjusted between a few μs & few secs. With proper adjustements of the sweep duration and the delay, it is possible to read either the complete waveform or any part of it.

In the 'analyse' and 'read' out modes provided in the instrument, the input waveform is stored in the memory capacitors and can be read out simultaneously. Provision is made to observe the waveform on an oscilloscope as it grows towards a final value. The analysed waveform is then retained in the memory capacitors and can be read out at any time desired into a strip-chart recorder at a slow rate. The waveform can also be stored for longer times in the 'hold' mode. The leakage of the memory capacitors is approximately 1 percent in about 15 mins.

As in the case of boxcar, the sync. output from the N_2 laser is used to trigger the SSA and the scope. Here the scan time (or time base) is measured using the digital counter. The rise of the time base, which is a square pulse, is used to trigger the counter and its fall is used to stop the counter.

The SSA is very much more time efficient than the boxcar integrator (64 times faster in the present case), but the minimum time base available is approximately 50 μs with SSA. Thus all the signals with the decay times above 100 μs

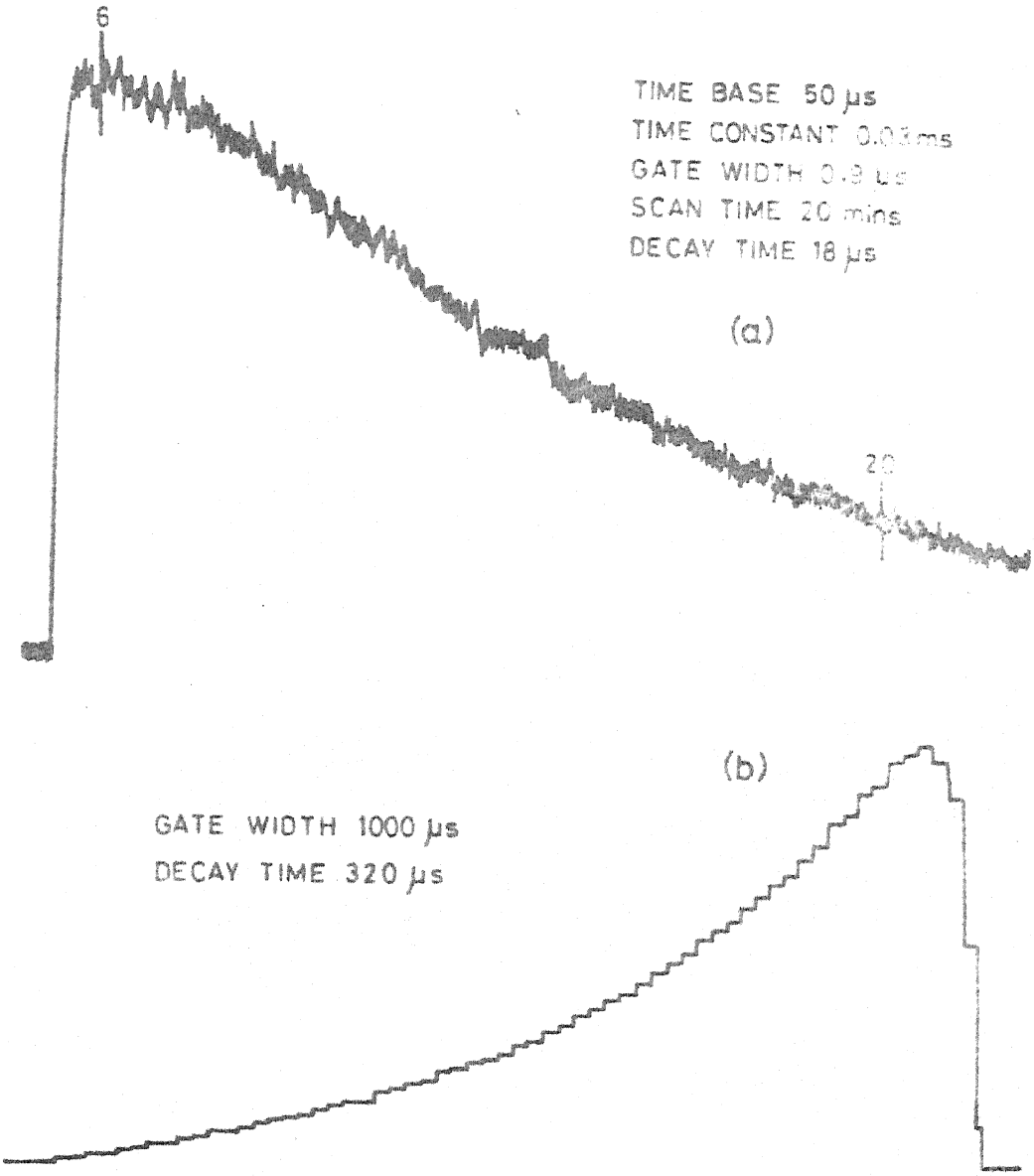

FIG. 2.4 TYPICAL DECAY CURVES
(a). USING BOXCAR INTEGRATOR
(b). USING SSA

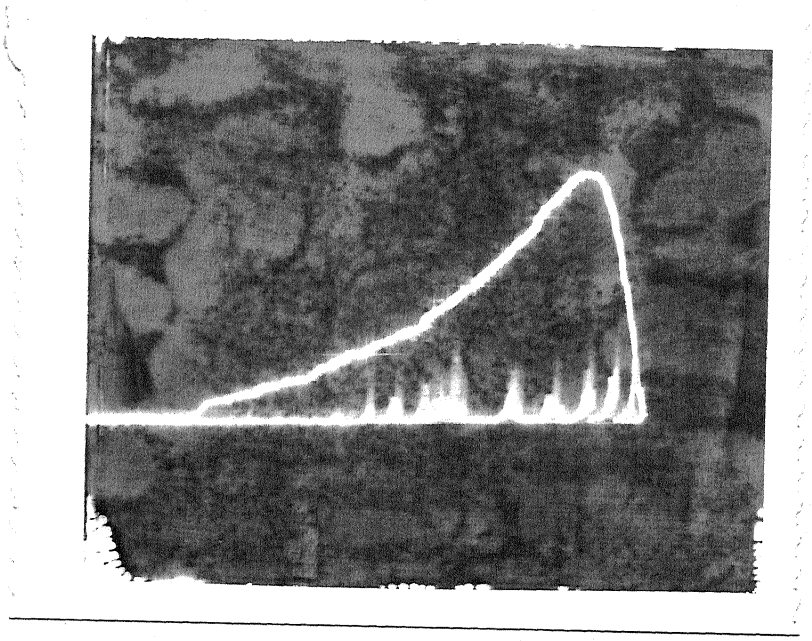

FIG. 2.5 S/N IMPROVEMENT USING SSA

are processed with the SSA. For faster signals, boxcar integrator is used.

Estimated values of errors in the measurement of decay times due to boxcar and SSA are about 5 percent and 1 percent respectively. The error is mainly due to the drift in the d.c. level of the boxcar and the SSA outputs. Typical decay curves recorded using boxcar integrator and SSA are shown in figures 2.4a and 2.4b. Figure 2.5 shows the signal to noise ratio improvement by using SSA.

2.4 The Crystals

Single crystals of Ho:CaF_2 and Sm:CaF_2 free from O_2 contamination are grown by the author in association with Dr. S. Muralidhara Rao using a Bridgeman vacuum furnace [5] developed at Bhabha Atomic Research Centre, Bombay, by the latter. The author is also associated with the building of a similar furnace for the Laser Laboratory, I.I.T. Kanpur, under the guidance of Dr. S. Muralidhara Rao and Tb:CaF_2 crystals are grown in this furnace. Design details of this furnace are briefly discussed below.

The vacuum furnace (fig. 2.6a) which can go upto a temperature of 1700 C, uses a squirrel cage heater shown in figure 2.6b. The heater is made out of a graphite rod of 9'' length and 4'' dia and has a resistance of 0.25Ω

Figure 2.6a : Legend

1. Heater
2. Graphite plate
3. Water cooled stainless steel electrode
4. Baseplate(stainless steel)
5. Vacuum tight seal
6. Molybdenum shields
7. Stainless steel shields
8. Graphite crucible
9. Graphite support
10. Water cooled jacket (stainless steel rod)
11. Wilson seal
12. Pt; Pt, Rh. thermocouple
13. Thermocouple gauge head
14. Penning gauge head
15. Stainless steel chamber
16. Tubes for water circulation
17. Windows

approximately. The heater is supported on ½'' thick and 4'' wide graphite plates which are screwed to the water cooled electrical feed throughs. These electrical feed throughs project out of the base plate (made of 1'' thick stainless steel sheet) of the furnace through vacuum tight seals. A transformer (0-40 V, 250 A) connected to the a.c. mains through a variac (0-250 V) supplies necessary current for the heater.

To reduce the radiation losses, the heater is enclosed with a set of radiation baffles. An inner set of these are made of molybdenum and the outer set with stainless steel. All these radiation baffles are mounted on a molybdenum sheet (dia 12'') which is again supported by four ½'' dia stainless steel rods fixed to the base plate.

The crucible for the crystal growth is made of a graphite rod of ½'' dia and 7'' length. A provision is made by making seven holes (5'' deep and 1/4'' dia) in this rod, to grow a set of seven crystals simultaneously. This crucible is mounted on a water cooled stainless steel rod (1'' dia). This stainless steel rod passes through a Wilson seal in the base plate of the furnace (the Wilson seal is tight enough to prevent its sliding under gravity). The crucible is lowered through the heater for growing the crystal. This is effected by pulling the stainless steel rod down by a

wire wound on a motor driven pulley. Present crystals are grown using a lowering speed of 6 mm/hr.

The temperature near the crucible is measured with a Pt; Pt.Rh. thermocouple, the leads of which pass through the base plate. The base plate is also fitted with I.B.P. Co. (India) thermocouple and penning gauge heads for vacuum measurements. A vacuum of 1.5×10^{-4} torr is maintained during the crystal growth. The base plate, and the stainless steel chamber which is fitted to the base plate to enclose the above assembly are cooled by circulating water through coils welded to them.

A batch of crystals, with the dopant (HoF_3 or SmF_3 or TbF_3) concentrations varying from 0.01 to 5 percent by weight of the host material CaF_2, are grown at a time to ensure identical crystal growth conditions. The concentration series grown are: 0.01, 0.03, 0.09, 0.3, 0.65, 1.0 and 5 percent of HoF_3 in CaF_2; 0.01, 0.03, 0.09, 0.3, 1.0 and 5 percent of SmF_3 in CaF_2; and 0.03, 0.09, 0.3, 1.0 and 5 percent of TbF_3 in CaF_2. The exact concentration of the dopant in the crystals is not analysed. A small amount of PbF_2 is added to the charge to remove the traces of oxygen. 3/4'' long pieces cut out from these rods are polished and used for recording the spectra.

REFERENCES

1. D. Ramachandra Rao, U.V. Kumar, Bansilal and P. Venkateswarlu; J. Instr. Soc. of India, 6, 5 (1976).

2. Bansilal; Ph.D. Thesis, I.I.T. Kanpur, India (1977).

3. Bh.A.R.B. Raju, P.R.K. Rao, D. Ramachandra Rao; I.I.T. Kanpur (India) Technical Report (to be published).

4. Bh.A.R.B. Raju, K.R. Sarma, D. Ramachandra Rao; I.I.T. Kanpur (India) Technical Report (to be published).

5. S. Muralidhara Rao, Ind. J. of Phys. 50, 378 (1976).

CHAPTER 3

ABSORPTION AND FLUORESCENCE SPECTRA OF $Sm^{3+}:CaF_2$

ABSTRACT

Measurements are reported, of the absorption, fluorescence, and excitation spectra of $Sm^{3+}:CaF_2$, and also of the fluorescence life times. The absorption spectrum is photographed at LNT using a 5 percent concentration crystal. The fluorescence spectrum is recorded using several laser excitations and for different concentrations of Sm^{3+} in CaF_2. The steady state fluorescence spectrum recorded using N_2 laser excitation is identified as originating from $^4G_{5/2}(A)$ level and is found to be identical to that of Rabbiner's spectrum II [11]. Decay times are measured for most of the intense lines using synchronous signal averager. From the observed fluorescence and excitation spectra, it is concluded that there are two centres A and B for Sm^{3+} in CaF_2. A revised energy level scheme is proposed for Sm^{3+} in centre A. Centre B could not be analysed because of the poor intensity of fluorescence and absorption. Fluorescence from $^4F_{3/2}(B)$ is observed for the first time when the crystal was maintained at room temperature and excited by a CW Ar^+ laser.

3.1 Introduction

Samarium as a dopant has been studied extensively in a large number of hosts yielding information on energy levels, transition probabilities, etc., in the divalent as well as trivalent states. The study of the spectra in CaF_2 has added attraction or complication because of the different site symmetries of Sm^{3+}. The object of the present reinvestigation of $Sm^{3+}:CaF_2$ is, to use a number of experimental techniques, and to study crystals of different concentrations grown under similar conditions. The experimental observations include, in addition to traditional absorption and fluorescence, recording the excitation spectrum using N_2 laser pumped dye laser, determining life times of most of the fluorescence lines from pulsed laser excitations, and study of fluorescence at low and high temperatures.

Samarium is the sixth element in the lanthanide series and has $4f^5$ as the lowest configuration in its trivalent state and $4f^6$ in its divalent state. Since Sm^{2+} occurs very readily in MeF_2 type crystals, more information is available on Sm^{2+}. The optical spectrum of Sm^{2+} in MeF_2 [1,2,3] has been investigated in greater detail partly because of the laser action observed in $Sm^{2+}:CaF_2$.

Spedding and Bear [4] and Lammermannet al [5] have made extensive studies of the optical absorption of Sm^{3+} in

various salts like $SmCl_3.6H_2O$, $Sm(C_2H_5SO_4).9H_2O$, $Sm(NO_3)_3.6H_2O$ and $Sm_2Mg_3(NO_3)_{12}.24H_2O$. Magno and Dieke [6,7] later reported the absorption and fluorescence spectra of Sm^{3+} in anhydrous $SmCl_3$ and $LaCl_3$. Wybourne [8] and Dieke [9] have calculated the complete energy level matrices of the f^5 configuration using the methods of Racah and constructed the energy level schemes for Sm^{3+} ion. Rast et al [10] have analysed the fluorescence and infrared spectrum of Sm^{3+} in the single crystal of LaF_3. The energies of all the free ion states of Sm^{3+} below 40000 cm^{-1} have been approximately established in the literature [11]. Of the ^6H ground multiplet, $^6H_{7/2}$, $^6H_{9/2}$, $^6H_{11/2}$ and $^6H_{13/2}$ states and the upper three fluorescing levels A,B and C are approximately 1200, 2400, 3500, 4800, 17800, 18700 and 19800 cm^{-1} above the $^6H_{5/2}$ ground state respectively. Different investigators have identified the three fluorescing levels A,B and C differently. Wybourne [8], Dieke [9] and Rast [10] have identified these three fluorescence levels as $^4G_{5/2}(A)$, $^4F_{3/2}(B)$ and $^4G_{7/2}(C)$. Other investigators [12,13,14] have designated the lowest fluorescing level A to $^4F_{5/2}$. Because of this ambiguity, the identification given by Dieke [15] is followed in the present analysis of the $Sm^{3+}:CaF_2$ spectra.

Rabbiner [12,13], who reported two types of spectra for $Sm^{3+}:CaF_2$ - spectrum I and spectrum II, has identified

the three fluorescing levels A,B and C as $^4F_{5/2}$, $^4F_{7/2}$ and $^4F_{9/2}$ respectively. Rabbiner's spectrum I was recorded using a light green crystal grown by deliberately adding YF_3 to the melt. Spectrum II was obtained using a colorless crystal grown by using either SmF_3, or SmF_3 plus NaF. He assigned the spectrum I as due to the transition from $^4F_{7/2}$ to $^6H_{7/2}$, $^6H_{9/2}$ and $^6H_{11/2}$ and the spectrum II as due to the transition from $^4F_{5/2}$ to $^6H_{5/2}$, $^6H_{7/2}$ and $^6H_{9/2}$. However the reason for the occurance of fluorescence from different SLJ levels in crystals grown under different conditions was not discussed. Rabbiner has also constructed partial energy level schemes for both types of spectra, assuming that the spectrum in each case arises from a single centre of Sm^{3+}. Both the crystals showed some lines above 6830A which are characteristic of Sm^{2+}. Infact, the light green color of the first crystal is due to the presence of a large fraction of Samarium in its divalent state.

The absorption spectrum of Sm^{3+}:CaF_2 (0.05 percent Sm^{3+}; 0.01 percent Sm^{2+}) was first reported by Kaiser et al [2] and later by Wood and Kaiser [3]. The spectrum reported by them consists of a few sharp lines due to Sm^{3+} overlapping a broad absorption band due to Sm^{2+}. Voronko et al [16] have studied the absorption, fluorescence and excitation spectra of Sm^{3+} in CaF_2 grown under various conditions. They have observed three types of spectra - I, II and III. However,

none of them have given the complete details of the absorption spectrum in the visible region.

This chapter mainly deals with the absorption and fluorescence spectra of $Sm^{3+}:CaF_2$. The optical spectra are recorded using different concentrations of Sm and different excitations. Two centres A and B are identified for Sm^{3+} from the observed spectra. A revised partial energy level scheme is proposed for centre A.

3.2 Experimental Details

The experimental set-ups used for recording the absorption and fluorescence spectra are discussed in Chapter 2. Crystals used for these studies are grown with 0.01, 0.03, 0.09, 0.3, 1.0 and 5.0 percent by weight of SmF_3 in CaF_2 in a vacuum furnace, also described in Chapter 2. A 5 percent concentration crystal is used for the absorption studies. Absorption in crystals with lower concentrations of Sm is found to be very weak. Steady state fluorescence spectra of the concentration series are recorded using N_2 laser and N_2 laser pumped dye laser. CW Ar^+ laser is used for recording the fluorescence from $^4F_{3/2}(B)$.

3.3 The Optical Absorption Spectrum

The optical absorption spectra photographed at LNT in the region from 4000 to 6000A consists of seven groups of sharp lines and a broad band at 4300A (Fig. 3.2a). This band attributed to Sm^{2+} starts appearing approximately from 4200A and extends upto 4500A with a peak at 4246A. Few groups of sharp lines (Fig. 3.2b and c)due to Sm^{3+} are located on the shoulder of this broad band on the higher wavelength side. Half width (full width at half maximum) of most of the absorption lines is found to be $\sim$3A. Few lines are also observed to be sharper with a half width of $\sim$ 1A. Figures 3.1 and 3.2 show the densitometer traces of the different absorption groups and table 3.1 lists the absorption lines.

A comparison of this observed spectrum with the spectrum of Sm^{3+} in LaF_3 [10] and $LaCl_3$ [7] lead to the following assignments (shown also in table 3.1):

Absorption Group	Transition Assignment +
4130 - 4180A	$^6H_{5/2}(Z) \rightarrow {}^6P_{5/2}(I)$
4430 - 4470A	$^6H_{5/2}(Z) \rightarrow {}^4G_{9/2}(H)$
4510 - 4550A	$^6H_{5/2}(Z) \rightarrow {}^4F_{5/2}(G)$
4580 - 4660A	$^6H_{5/2}(Z) \rightarrow {}^4I_{13/2}(F)$
4730 - 4850A	$^6H_{5/2}(Z) \rightarrow {}^4I_{11/2}(E)$

+ The alphabatical notation used in the parenthesis is similar to the one given by Dieke [15].

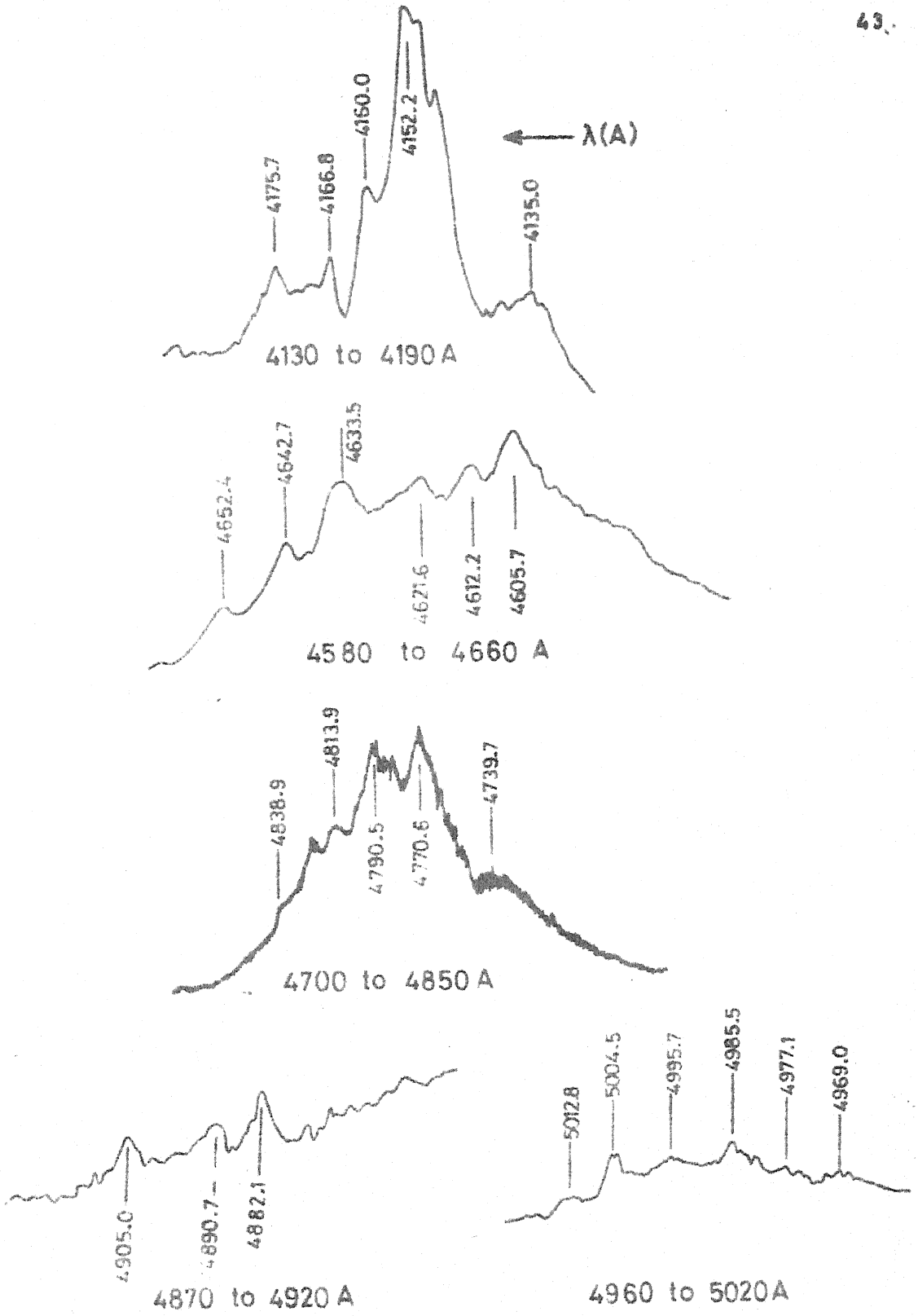

Fig. 3.1 Sm^{3+}: CaF_2 absorption at LNT, 5%. Conc.

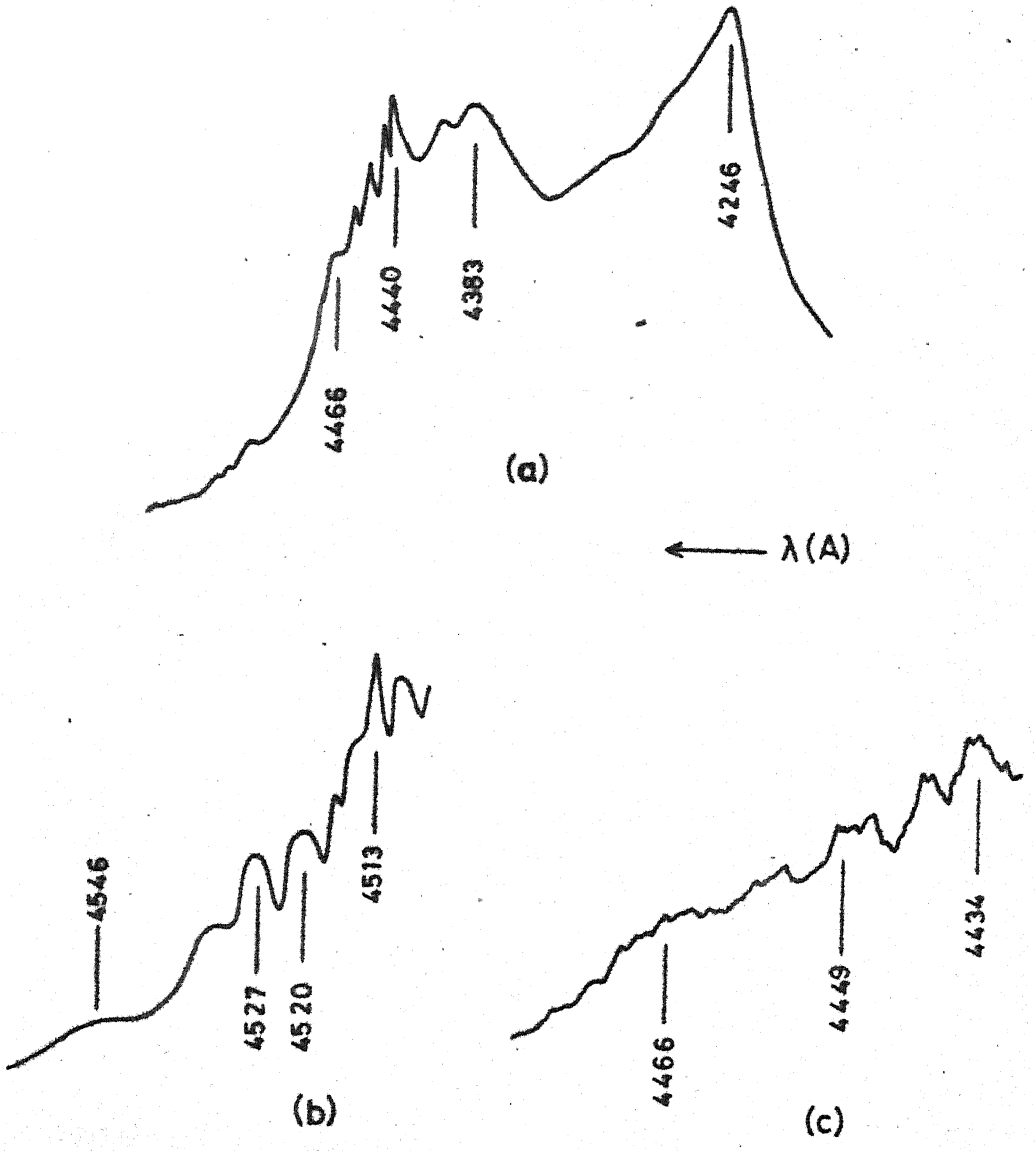

FIG. 3.2 ABSORPTION SPECTRUM 4200 to 4560 A

a. BROAD BAND DUE TO Sm^{2+}

b&c. SHOULDER LINES DUE TO Sm^{3+}

Table 3.1 : Absorption Spectrum of $Sm^{3+}:CaF_2$ at LNT
(5 percent concentration crystal)

Wavelength A	Energy cm^{-1}	Wavelength A	Energy cm^{-1}
$^6H_{5/2}(Z) \rightarrow {}^6P_{5/2}(I)$		$^6H_{5/2}(Z) \rightarrow {}^4I_{13/2}(F)$	
4135.0	24177	4588.8	21786
4149.1	24095	4605.7	21706
4152.2	24077	4612.2	21676
4154.3	24065	4621.6	21632
4160.0	24032	4633.5	21576
4161.5	24023	4642.7	21533
4166.8	23993	4652.4	21488
4175.7	23941		
$^6H_{5/2}(Z) \rightarrow {}^4G_{9/2}(H)$		$^6H_{5/2}(Z) \rightarrow {}^4I_{11/2}(E)$	
4434.3	22545	4731.1	21131
4440.3	22515	4739.7	21093
4443.2	22500	4770.6	20956
4446.7	22482	4784.0	20897
4449.5	22468	4789.0	20875
4456.0	22435	4804.9	20806
4465.8	22386	4813.9	20767
		4825.4	20718
$^6H_{5/2}(Z) \rightarrow {}^4F_{5/2}(G)$		4835.8	20673
4513.3	22151	4841.0	20651
4516.0	22137	4845.6	20632
4520.2	22117		
4527.0	22084	$^6H_{5/2}(Z) \rightarrow {}^4I_{9/2}(D)$	
4532.8	22055	4882.1	20477
4546.0	21991	4890.7	20441
		4905.0	20382

Table 3.1 : (Continued)

Wavelength A	Energy cm^{-1}	Wavelength A	Energy cm^{-1}
$^6H_{5/2}(Z) \rightarrow {}^4G_{7/2}(C)$			
4969.0	20119	4995.7	20012
4977.1	20086	5004.5	19977
4985.5	20053	5012.8	19943

Absorption Group	Transition Assignment
4880 - 4910A	$^6H_{5/2}(Z) \rightarrow {}^4I_{9/2}(D)$
4960 - 5020A	$^6H_{5/2}(4) \rightarrow {}^4G_{7/2}(C)$

3.4 Fluorescence Spectrum of $Sm^{3+}:CaF_2$ using N_2 Laser

Steady state fluorescence spectra of CaF_2 with varying concentrations of Sm are recorded at LMT in the visible region using N_2 laser excitation. Excitation with N_2 laser is **non**resonant leading to a pumping of Sm^{3+} ions into the excited states of all the centres through phonon coupling in much the same way as a 'broad band' excitation. Thus the spectrum contains information about all centres of Sm^{3+}. Figures 3.3 to 3.5 illustrate the observed spectrum in the region from 5580A to 6550A as the concentration is varied from 0.01 percent to 5 percent. All the fluorescence lines are identified to be arising as due to the transitions from $^4G_{5/2}$ [+] level to the various lower levels. The groupwise assignment is given below:

Fluorescence Group	Transition Assignment
5580 - 5630A	$^4G_{5/2} \rightarrow {}^6H_{5/2}$
5900 - 6100A	$^4G_{5/2} \rightarrow {}^6H_{7/2}$

[+] This fluorescing level has been assigned as $^4F_{5/2}$ by Rabbiner [12] and Babkina [14].

Fluorescence Group	Transition Assignment
6350 - 6550A	$^4G_{5/2} \rightarrow {}^6H_{9/2}$
Around 6950A (not shown in figures 3.3 to 3.5)	$^4G_{5/2} \rightarrow {}^6H_{11/2}$

The energy of N_2 laser (29656 cm^{-1}) is adequate to excite all the three fluorescing levels $^4G_{5/2}$ (17990 cm^{-1})$^+$, $^4F_{3/2}$ (18860 cm^{-1})$^+$ and $^4G_{7/2}$ (20030 cm^{-1})$^+$, but fluorescence from only level $^4G_{5/2}$ is observed at LNT. A continuum starts appearing from $\sim$ 7000A and extends beyond 9000A (which is the approximate limit of the PMT sensitivity). This continuum is assigned as due to the Sm^{2+} present in the crystal.

The spectrum is analysed as due to two sets of lines. The relative intensity of these two sets show some change with concentration. This indicates that these two sets arise probably from two different centres of Sm^{3+} in the crystal. The spectrum whose relative intensity decreases with increase in concentration is referred to as A set (lines at 5584.6, 5599.1, 5606.8, etc., belong to this set). The second set of lines referred to as B set show an increase in intensity from 0.01 percent to 1.0 percent concentration. But in 5.0 percent concentration crystal fluorescence intensity of both the sets become weak.

+ Barycentres of each level as observed in the present experiments.

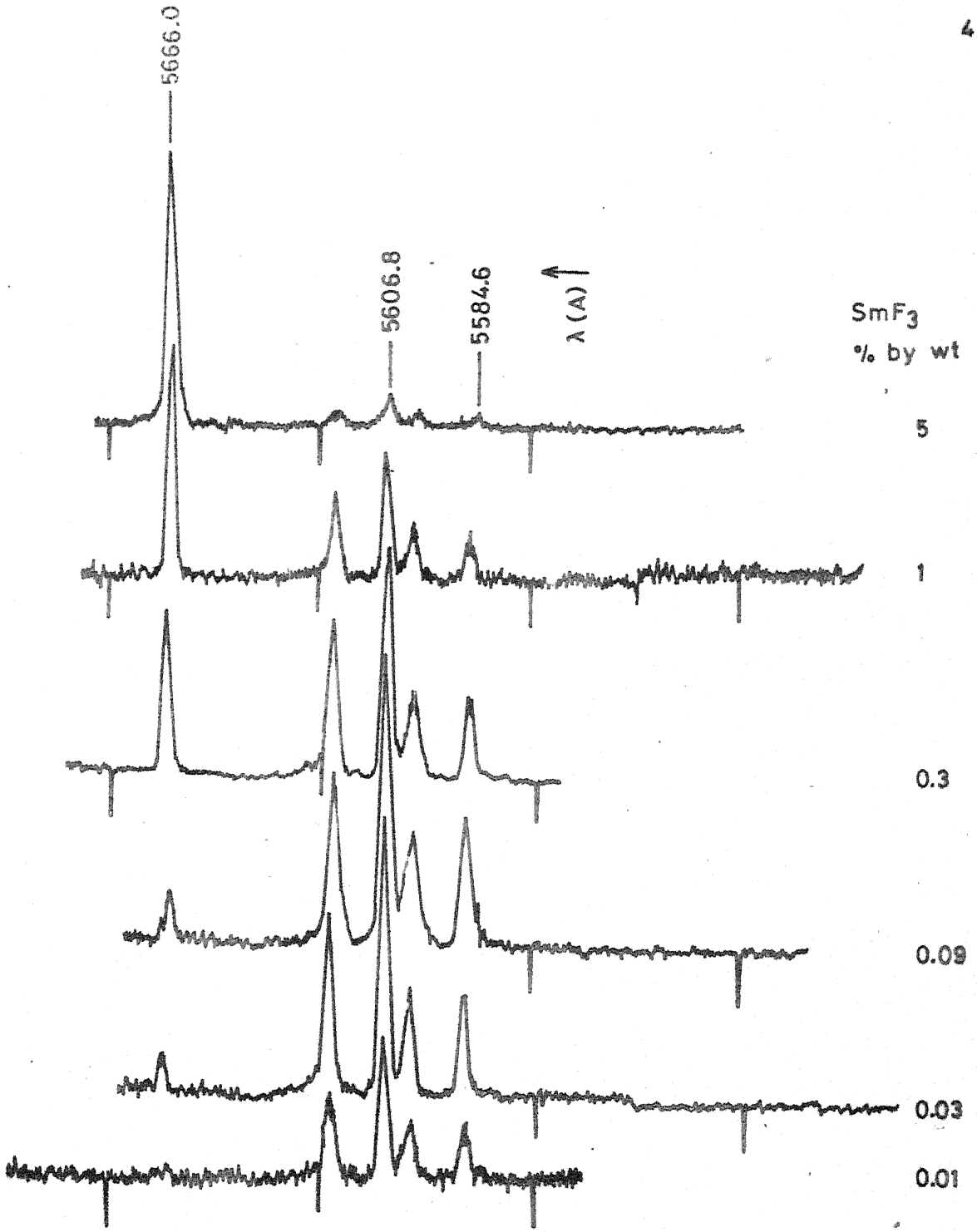

FIG. 3.3 FLUORESCENCE SPECTRUM OF Sm^{3+}: CaF_2 AT LNT; CONCENTRATION SERIES; $^4G_{5/2}(A) \longrightarrow {}^6H_{5/2}(Z)$; EX: 3371 A.

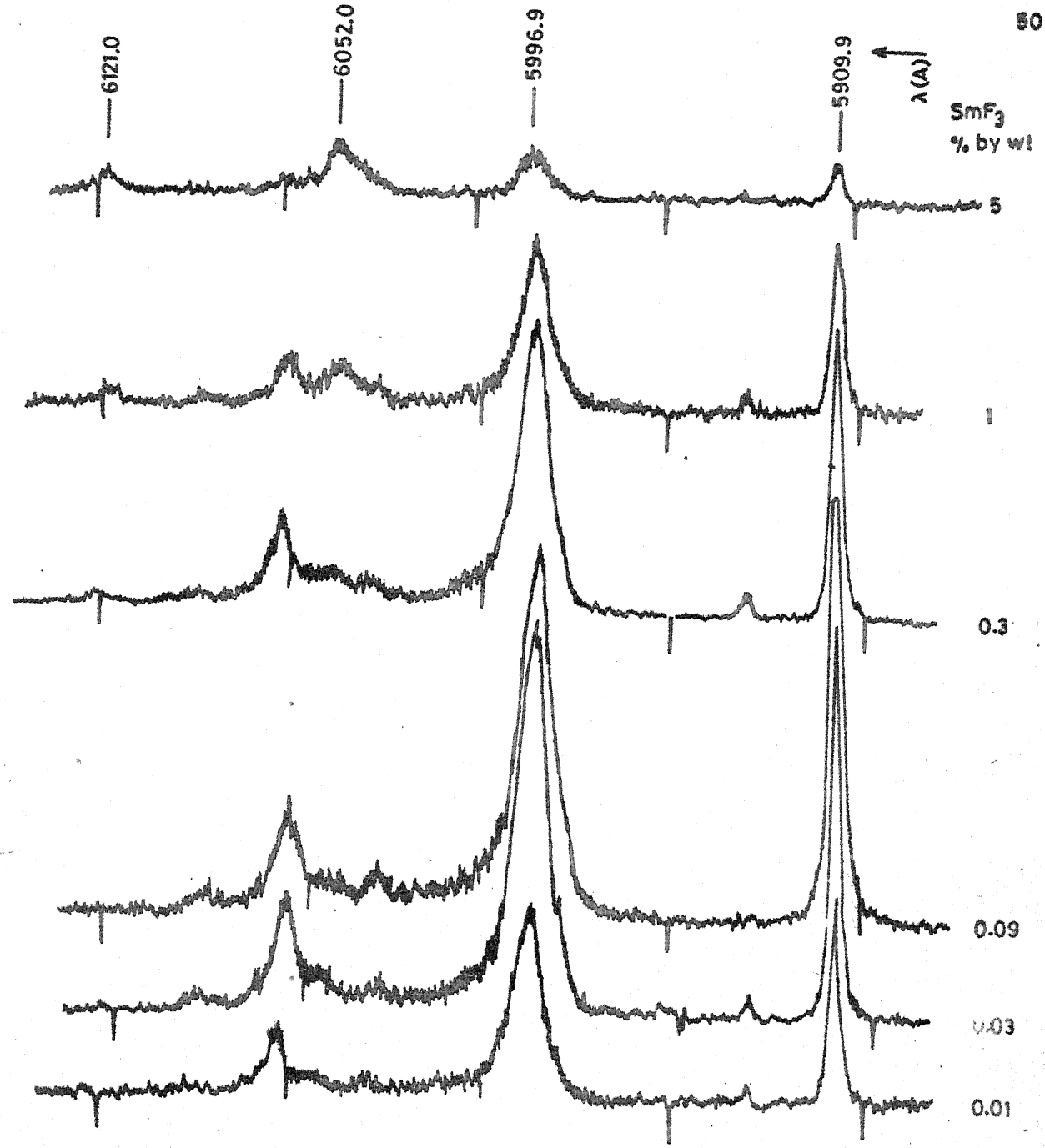

FIG. 3.4 FLUORESCENCE SPECTRUM OF Sm^{3+}: CaF_2 AT LNT; CONCENTRATION SERIES; $^4G_{5/2}(A) \longrightarrow {}^6H_{7/2}(Y)$; EX: 3371 A

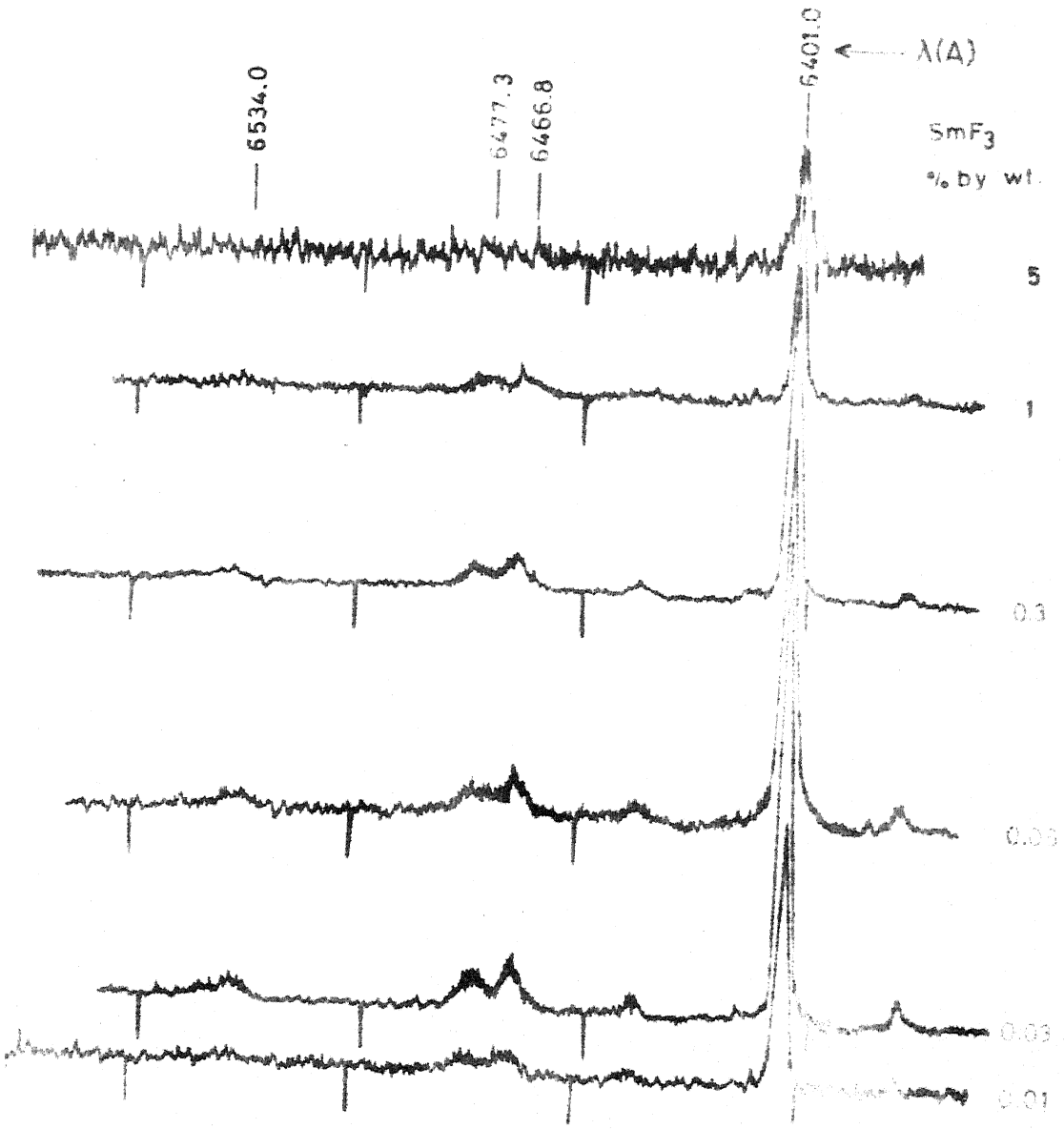

FIG. 3.5 FLUORESCENCE SPECTRUM OF Sm^{3+} : CaF_2 AT LOW CONCENTRATION SERIES; $^4G_{5/2}(A) \longrightarrow {}^6H_{9/2}(B)$, EX: 3371 A

3.5 Fluorescence and Excitation Spectra of $Sm^{3+}:CaF_2$ using N_2 Laser Pumped Dye Laser

Further information about the A and B sets of lines is obtained by recording the excitation spectra and selectively excited fluorescence with N_2 laser pumped dye laser. The 1.0 percent concentration crystal is chosen for this detailed study as the intensity of both the sets of lines are comparable in it.

Excitation spectra (where fluorescence intensity is recorded as a function of exciting wavelength) are recorded by setting the spectrophotometer for each fluorescence line and scanning the dye laser from 4500A to 5700A. The excitation spectrum of $Sm^{3+}:CaF_2$ was first reported by Voronko et al [16]. Their interest, however, was mainly concentrated on the ultra-violet region to study the content of O_2 in the crystals grown under different conditions. In the present work excitation spectrum is obtained in the visible region.

The excitation spectra are recorded at LNT by monitoring each fluorescence line recorded with N_2 laser excitation. Conversely the fluorescence spectra are obtained by selectively exciting each absorption line recorded in the absorption spectrum (Section 3.3). The selective excitation of most of the absorption lines has lead to fluorescence spectra containing exclusively either the A or B sets of

lines. In the case of overlapping absorption (or fluorescence) lines, the resulting fluorescence (or excitation) spectrum contained lines from both the sets. Excitation spectrum recorded in the region from 4500 to 5700A is seen to contain two sets of lines A and B obtained by monitoring A and B sets of fluorescence lines respectively. These two sets A and B are identified as due to the A and B centres of Sm^{3+} in CaF_2. Figures 3.6 to 3.9 show a comparison of the excitation spectra of centres A and B obtained by monitoring A and B centre fluorescence lines. Details of the excitation spectrum along with the transition assignments for each group are given in table 3.2.

The selective excitation of most of the absorption lines recorded in the excitation spectra has lead to fluorescence spectra containing exclusively either A or B centre lines. Further most of the fluorescence lines that are classified as originating from a given centre (A or B) are seen to possess identical excitation spectra. The list of the observed fluorescence lines and their centre classifications are given in table 3.3. Figures 3.10 to 3.13 show the fluorescence spectra obtained using the selective excitation.

The continuum beyond 7000A is found to appear with all the excitations of centre A as well as centre B. Part of this continuum is shown in figure 3.13. An excitation

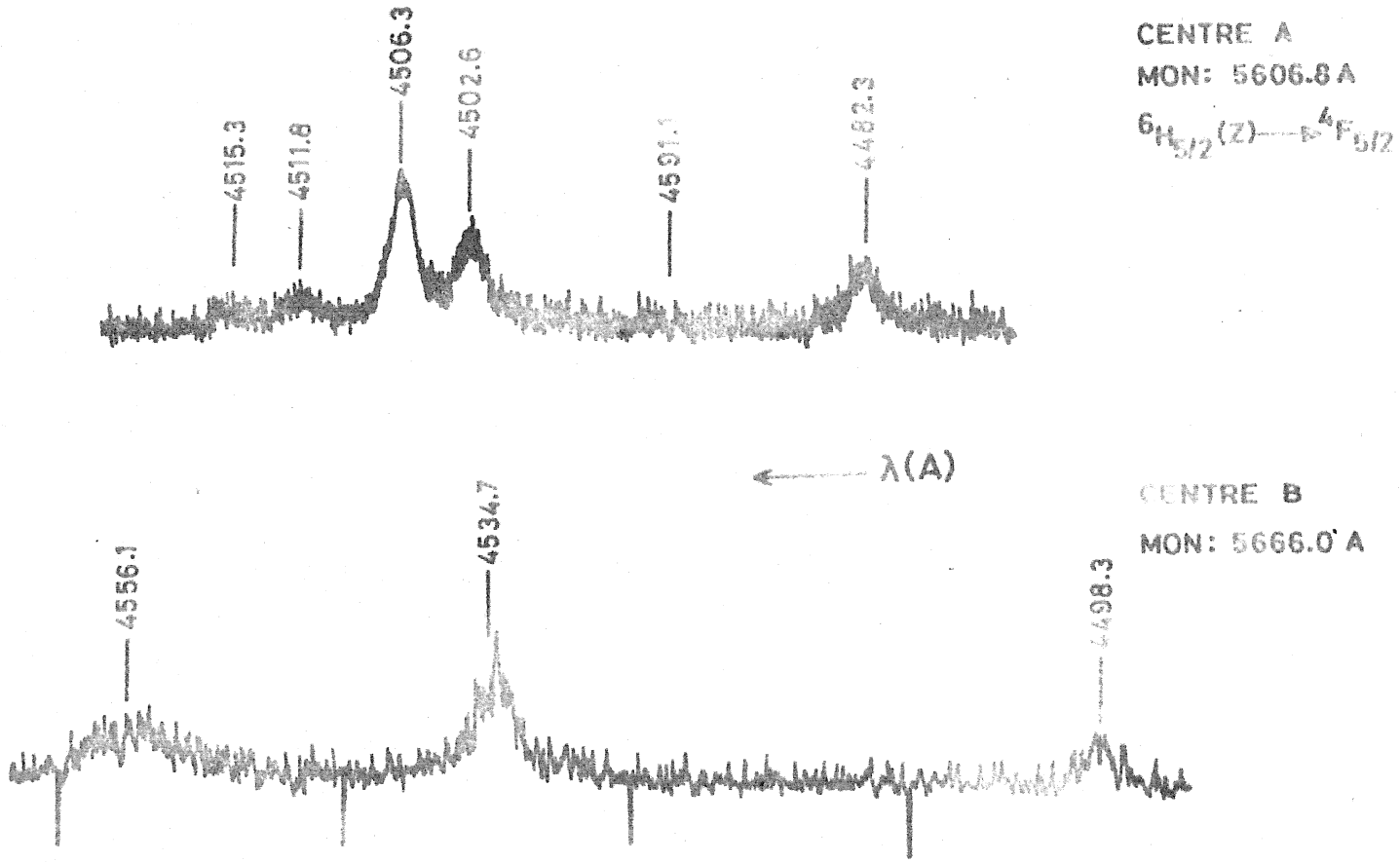

FIG. 3.6 EXCITATION SPECTRUM OF Sm^{3+}: CaF_2 AT LNT; 4500A GROUP.

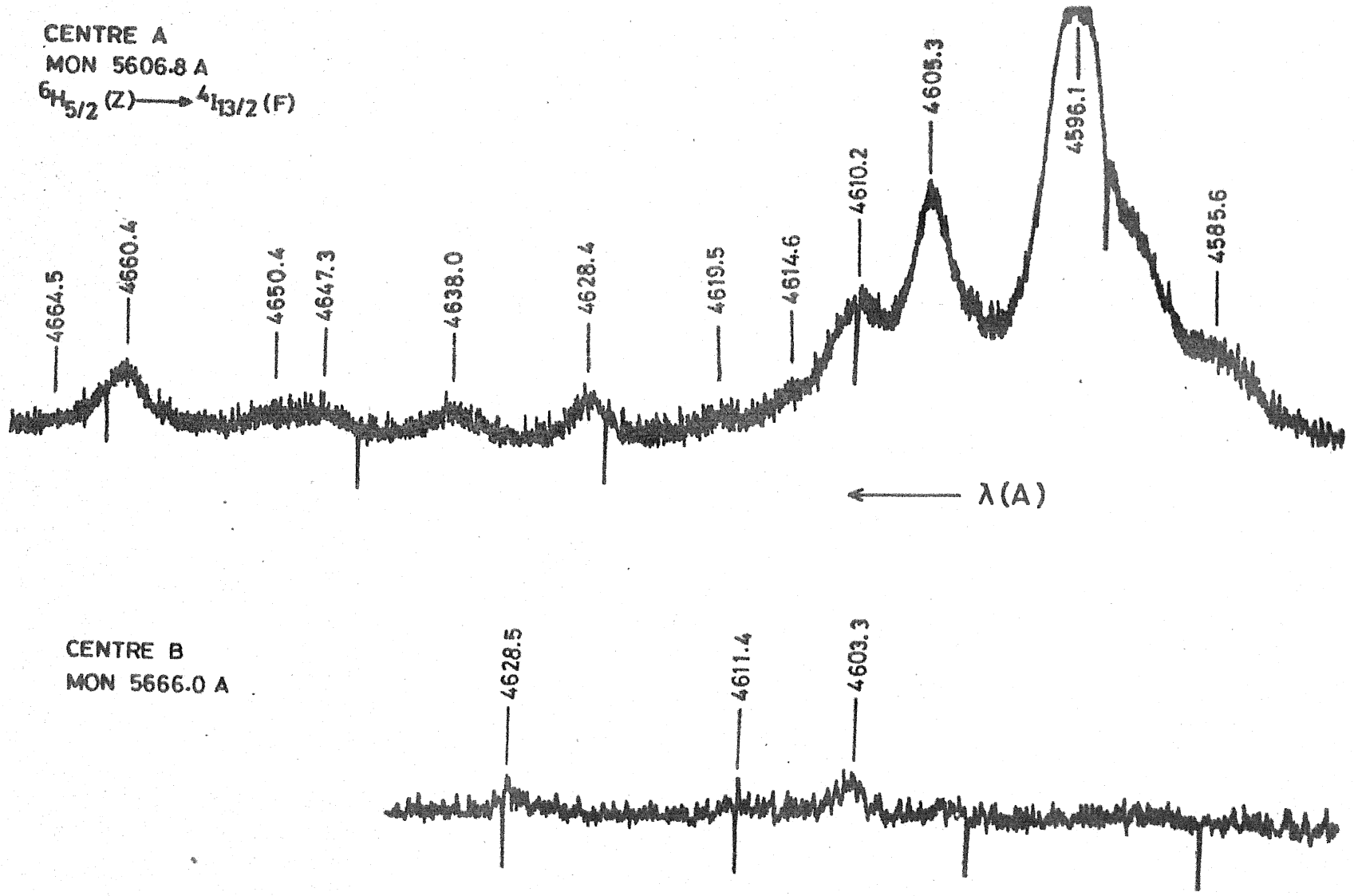

FIG. 3.7 EXCITATION SPECTRUM OF Sm^{3+}: CaF_2 AT LNT; 4600A GROUP.

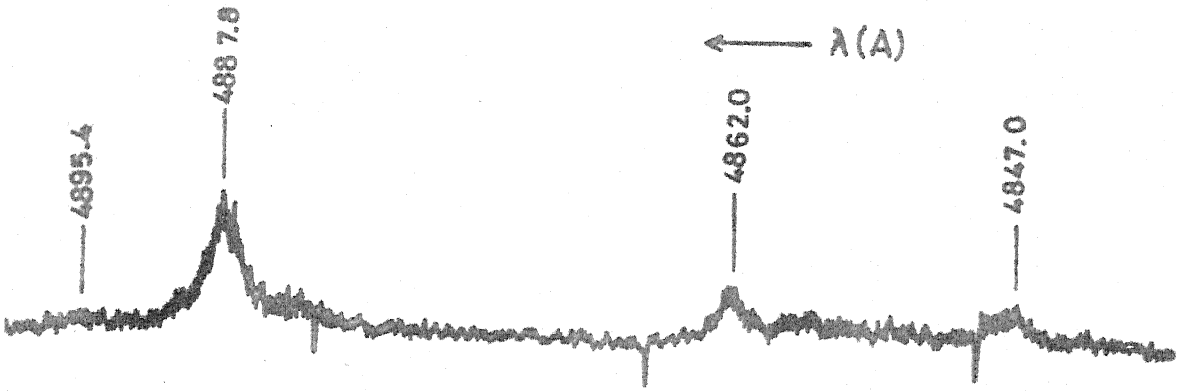

FIG. 3.8a $^6H_{5/2}(Z) \longrightarrow {}^4I_{9/2}(D)$ EXCITATION SPECTRUM OF Sm^{3+}: CaF_2 ; CENTRE A AT LNT.

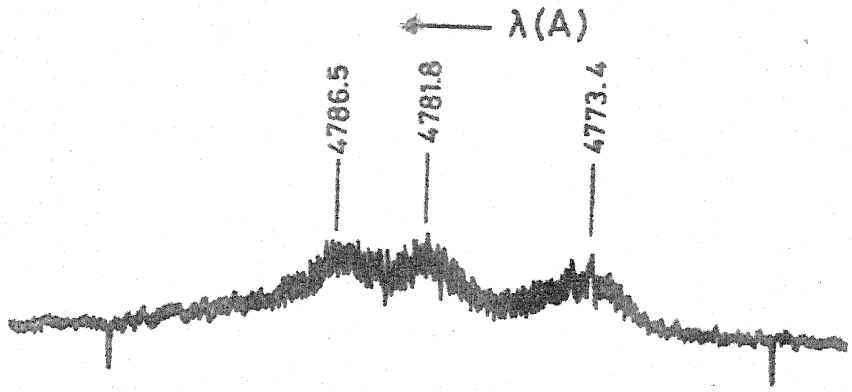

FIG. 3.8b $^6H_{5/2}(Z) \longrightarrow {}^4I_{11/2}(E)$ EXCITATION SPECTRUM OF Sm^{3+}: CaF_2 ; CENTRE A AT LNT.

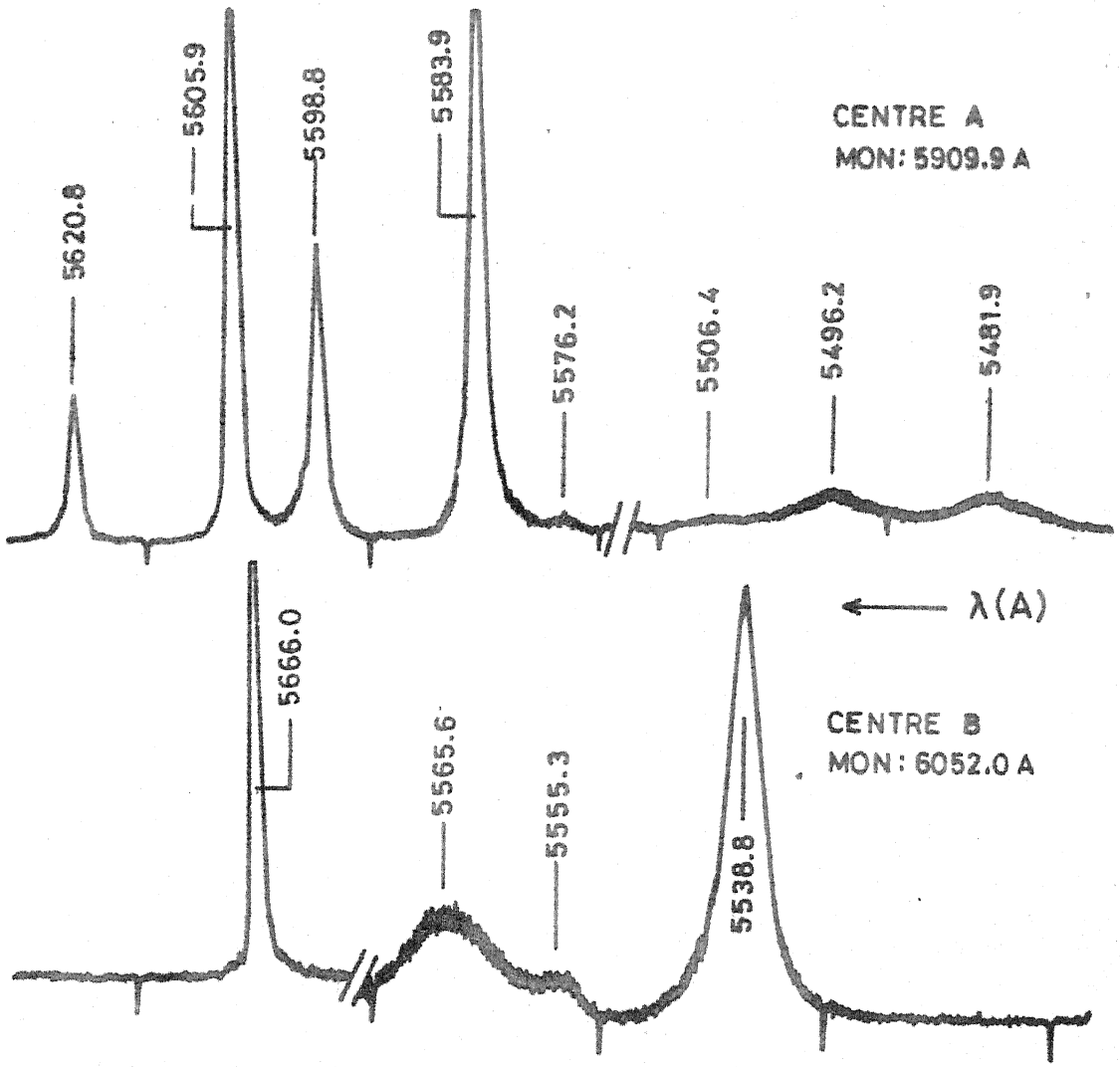

FIG. 3.9 $^6H_{5/2} \longrightarrow {}^4G_{5/2}$ EXCITATION SPECTRUM OF Sm^{3+}: CaF_2 AT LNT.

Table 3.2 : Excitation Spectrum of $Sm^{3+}:CaF_2$ at LNT

Centre A			Centre B		
Wavelength A	Energy cm^{-1}	Intensity (arb.units)[β]	Wavelength A	Energy cm^{-1}	Intensity (arb.units)
$^6H_{5/2}(Z) \rightarrow {}^4F_{5/2}(G)$					
4482.3	22304	6	4498.3	22224	7
4491.1	22260	1	4534.7	22046	17
4502.6	22203	8	4556.1	21943	10
4506.3	22185	15	4603.0	21718	9
4511.8	22158	4	4611.4	21679	4
4515.3	22141	2	4628.5	21599	4
$^6H_{5/2}(Z) \rightarrow {}^4I_{13/2}(F)$					
4585.6	21801	25			
4591.8	21772	56			
4596.1	21752	150			
4605.3	21708	56			
4610.2	21685	32			
4614.6	21664	14			
4619.5	21641	8			
4628.4	21600	10			
4638.0	21555	8			
4647.3	21507	7			
4650.4	21498	7			
4653.1	21485	3			
4660.4	21451	15			
4664.5	21432	2			
$^6H_{5/2}(Z) \rightarrow {}^4I_{11/2}(E)$					
4773.4	20944	8			
4781.8	20907	10			
4786.5	20886	10			

[β] The numbers indicate relative intensities of the lines in each group in an arbitrary scale.

Table 3.2 : (Continued)

Centre A			Centre B		
Wavelength A	Energy cm^{-1}	Intensity (arb.units)	Wavelength A	Energy cm^{-1}	Intensity (arb.units)
$^6H_{5/2}(Z) \rightarrow {}^4I_{9/2}(D)$					
4847.0	20626	7			
4862.0	20562	10			
4887.8	20453	20			
4895.4	20422	3			
$^6H_{5/2}(Z) \rightarrow {}^4G_{5/2}(A)$					
5481.9	18237	8			
5496.2	18189	8			
5506.4	18156	2	5538.8	18049	95
5576.2	17928	3	5555.3	17996	10
5583.9	17904	~150	5565.6	17963	23
5598.8	17856	56	5666.0	17643	~100
5605.9	17833	120			
5620.8	17786	30			

Table 3.3 : Fluorescence Spectrum of $Sm^{3+}:CaF_2$ at LNT

Centre A Ex:4596.1A			Centre B Ex:4534.7A		
Wavelength A	Energy cm^{-1}	Intensity (arb.units)	Wavelength A	Energy cm^{-1}	Intensity (arb.units)
		$^4G_{5/2}(A) \rightarrow {}^6H_{5/2}(Z)$			
5584.6	17901	20	5666.0	17648	Very strong
5599.1	17855	20			
5606.8	17831	67			
5621.2	17785	35			
		$^4G_{5/2}(A) \rightarrow {}^6H_{7/2}(Y)$			
5909.9	16916	70	6043.3	16543	20
5936.2	16841	3	6052.0	16519	50
5996.9	16671	78	6100.0	16389	3
6041.4	16548	3	6106.4	16372	3
6057.4	16504	3	6120.9	16335	17
6069.2	16472	17			
6092.2	16420	2			
		$^4G_{5/2}(A) \rightarrow {}^6H_{9/2}(X)$			
6370.9	15692	16			
6401.0	15618	>200			
6436.7	15530	13			
6448.1	15504	4			
6466.8	15458	32			
6477.3	15434	26			
6506.0	15366	2			
6534.0	15300	10			
6545.0	15275	4			
		$^4G_{5/2}(A) \rightarrow {}^6H_{11/2}(W)$			
6941.5	14402	7			
6975.8	14331	19			

spectrum obtained by monitoring the peak of this broad band at 7050A shows broad bands of absorption in the region from 4500A to 5700A approximately. This fluorescence and the broad absorption band around 4300A coincide well with the already reported data on Sm^{2+} in CaF_2 [2,3].

The decay times are studied using synchronous signal averager for all the fluorescence lines of centres A and B. Decay times are also measured using several of the A centre and B centre excitations. All the fluorescence lines that are classified as originating from a given centre are seen to possess identical decay times. Following decay times are observed.

	Fluorescing Level	Decay Time
Sm^{3+}	$^4G_{5/2}$ (A centre)	4.3 ms
Sm^{3+}	$^4G_{5/2}$ (B centre)	5.5 ms
Sm^{2+}	$^5D_0$	$\sim$1 μs

Intermediate times are also observed for the overlapping lines. For example lines at 6055.7, 6041.4A, etc., showed decay times around 4.7 ms.

3.6 Results and Discussion

The number of lines in several groups of the fluorescence and excitation spectra is more than what could be

expected if the site symmetry of A centre is assumed as cubic (see table 3.4). Also the fluorescence from A centre was observed to be polarised [17], thus indicating the symmetry to be non-cubic. Further there is reason to believe that the symmetry of B centre could be cubic [18] because of its increase in intensity with increase in concentration. The symmetry of the A centre is therefore taken to be non-cubic and consequently all the levels are considered to be split into J + ½ Kramer's doublets. For tetragonal and other symmetries which occur usually for the rare earth ions in MeF_2 type crystals, transitions between all Stark components of Kramer's ions are allowed. Therefore the crystal field splitting for the levels with J = 5/2, 5/2, 7/2, 9/2, 11/2 and 13/2 are respectively 2,3,4,5,6 and 7. The resulting maximum number of transitions from J = 5/2 to J = 3/2, 5/2, 7/2, 9/2, 11/2 and 13/2 are 6, 9, 12, 15, 18 and 21 respectively. Details of the maximum number of transitions expected in cubic and the other centres in MeF_2 are given in table 3.4. The intensity and number of lines from A centre are found to be adequate to enable deriving the Stark splitting of the levels involved ($^6H_{5/2}$, $^6H_{7/2}$, $^6H_{9/2}$, $^4G_{5/2}$, $^4I_{9/2}$, $^4I_{11/2}$, $^4I_{13/2}$ and $^4F_{5/2}$) in the observed fluorescence and excitation spectra. Fluorescence and excitation spectra of centre B are observed to be weak and contain few lines. Therefore the spectrum of centre B is not analysed. The following discussion pertains mainly to the centre A.

Table 3.4 : Splittings and Transitions Involving J = 5/2

J	Stark Splitting		No. of Transitions from J = 5/2 Level to Different J Levels			
			Expected for		Observed in centre A	
	Cubic sym.	Other syms.	Cubic sym.	Other syms.	Fluorescence+ Spectrum	Excitation++ Spectrum
3/2	1	2				
5/2	2	3	4	9	4	8 and 6
7/2	3	4	6	12	7	
9/2	4	5	8	15	8	4
11/2	5	6	10	18		3
13/2	6	7	12	21		14

\+ Corresponding to $^4G_{5/2}(A) \rightarrow {}^6H_{5/2}(Z)$, $^6H_{7/2}(Y)$ and $^6H_{9/2}(X)$ transitions.

++ Corresponding to $^6H_{5/2}(Z) \rightarrow {}^4G_{5/2}(A)$, $^4F_{5/2}(G)$, $^4I_{9/2}(D)$, $^4I_{11/2}(E)$ and $^4I_{13/2}(F)$ transitions.

To derive the Stark splittings of each SLJ level, differencetables are constructed for each group in the excitation and fluorescence spectra. From these difference tables a set of Stark components, which can explain all the groups in the excitation spectra and the $^4G_{5/2}(A) \rightarrow {}^6H_{5/2}(Z)$ fluorescence, are derived for the ground level $^6H_{5/2}$. The Stark components of the upper levels, $^4G_{5/2}$, $^4I_{9/2}$, $^4I_{11/2}$, $^4I_{13/2}$ and $^4F_{5/2}$, are derived by adding the energies of the absorption lines (from the excitation spectrum) to the ground level Stark components. The Stark components of $^6H_{7/2}$ and $^6H_{9/2}$ are derived from the fluorescence data. Transition assignments for all the lines in the excitation and fluorescence spectra are shown in figures 3.14 and 3.15 respectively. Table 3.5 lists the partial energy levels derived for Sm^{3+}: CaF_2.

From the difference tables constructed for each group in the excitation spectrum of centre A ($^6H_{5/2} \rightarrow {}^4G_{5/2}$, $^4I_{9/2}$, $^4I_{11/2}$, $^4I_{13/2}$ and $^4F_{5/2}$), the Stark components at 0, 48 and 70 cm^{-1} are derived for $^6H_{5/2}$. These values for the ground level Stark components are found to explain all groups in the excitation spectrum and the $^4G_{5/2} \rightarrow {}^6H_{5/2}$ fluorescence.

3.6.2 Transitions Involving Level $^4F_{5/2}(G)$

Excitation spectrum of this level of the A centre consists of six lines in the region from 4475 to 4520A

(figure 3.6). One line at 4491.1A is found to be very broad with a half width of ∿4A. Rest of the lines have half widths of ∿1.5A.

Stark components of this level are established from the $^6H_{5/2} \rightarrow {}^4F_{5/2}$ excitation spectrum. Three levels at 22185, 22203 and 22304 cm^{-1} explain all the lines in the A centre $^6H_{5/2}(Z) \rightarrow {}^6F_{5/2}(G)$ excitation spectrum.

Few weak lines of centre B are observed in the excitation spectrum in the region from 4500 to 4700A (figures 3.6 and 3.7). These lines belong to either $^6H_{5/2}(Z) \rightarrow {}^4F_{5/2}(G)$ transition or $^6H_{5/2}(Z) \rightarrow {}^4I_{13/2}(F)$ transition. Transition assignments for these lines is not made in the present studies. Most of these lines are found to be broad.

3.6.3 Transitions Involving Level $^4I_{13/2}(F)$

Absorption to this level is observed to be very strong and $^6H_{5/2}(Z) \rightarrow {}^4I_{13/2}(F)$ group (figure 3.7) in the excitation spectrum contains fourteen lines of centre A. All the lines are found to be very broad with a half width of ∿4A. Stark components at 21498, 21555, 21600, 21685, 21708, 21772 and 21801 cm^{-1} for $^4I_{13/2}$ explain all the A centre lines of this group.

3.6.4 Transitions Involving Levels $^4I_{11/2}$(E) and $^4I_{9/2}$(D)

Only seven weak A centre lines are observed in the region from 4750 to 4900A (figure 3.8) corresponding to the levels $^4I_{11/2}$ and $^4I_{9/2}$, mainly because of (1) very weak absorption to these levels and (2) very poor laser intensity in this region. Three lines on the lower wavelength side are assigned as due to $^6H_{5/2}(Z) \rightarrow {}^4I_{11/2}(E)$ transition and the rest to $^6H_{5/2}(Z) \rightarrow {}^4I_{9/2}(D)$ transition. All the A centre lines in this region are accounted for with a set of Stark levels at 20886, 20907 and 20944 cm^{-1} for $^4I_{11/2}$ and at 20422, 20453, 20562 and 20626 cm^{-1} for $^4I_{9/2}$.

No lines of B centre are observed in this region.

3.6.5 Transitions Involving Level $^4G_{5/2}$(A)

Excitation spectrum of $^4G_{5/2}$(A) of centre A in the region from 5470 to 5700A contains three weak and broad lines at 5481.9, 5496.2 and 5506.9A and separated far away from them, four intense and sharp lines. The three weak lines could not be due to the absorption into the lower Stark component of $^4F_{3/2}$ (B-18860 cm^{-1}), since the separation between $^4G_{5/2}$ (A-17990 cm^{-1}) and $^4F_{3/2}$(B) is $\sim$ 870 cm^{-1}, whereas the separation between the weak and intense lines (5496.2A and 5598.0A) is only 233 cm^{-1}. This leads to the conclusion of the existance of one of the Stark components of $^4G_{5/2}$

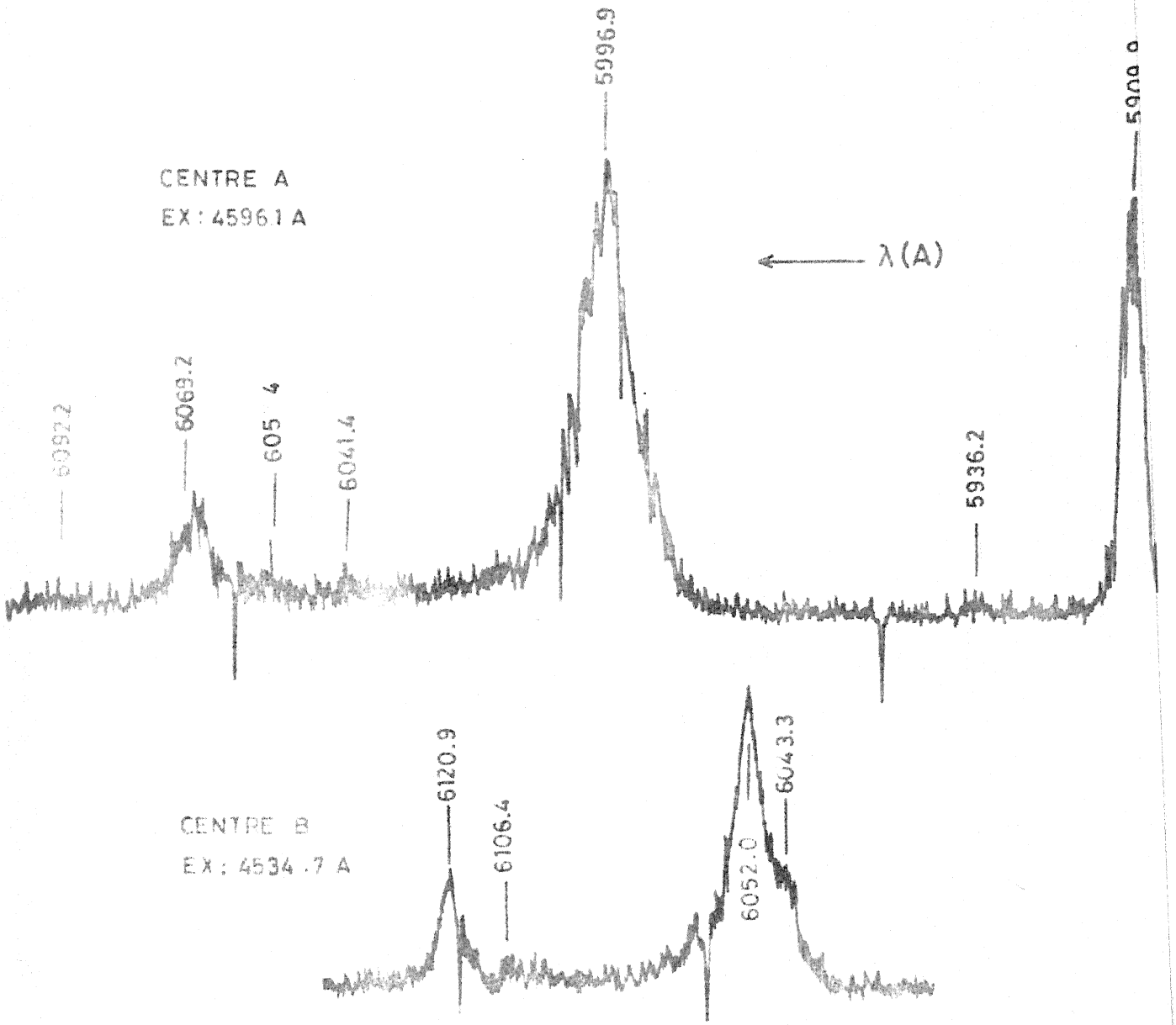

FIG. 3.11 FLUORESCENCE SPECTRUM OF Sm^{3+} : CaF_2 AT LNT ; $^4G_{5/2}(A)$ — $^6H_{7/2}(Y)$ GROUP .

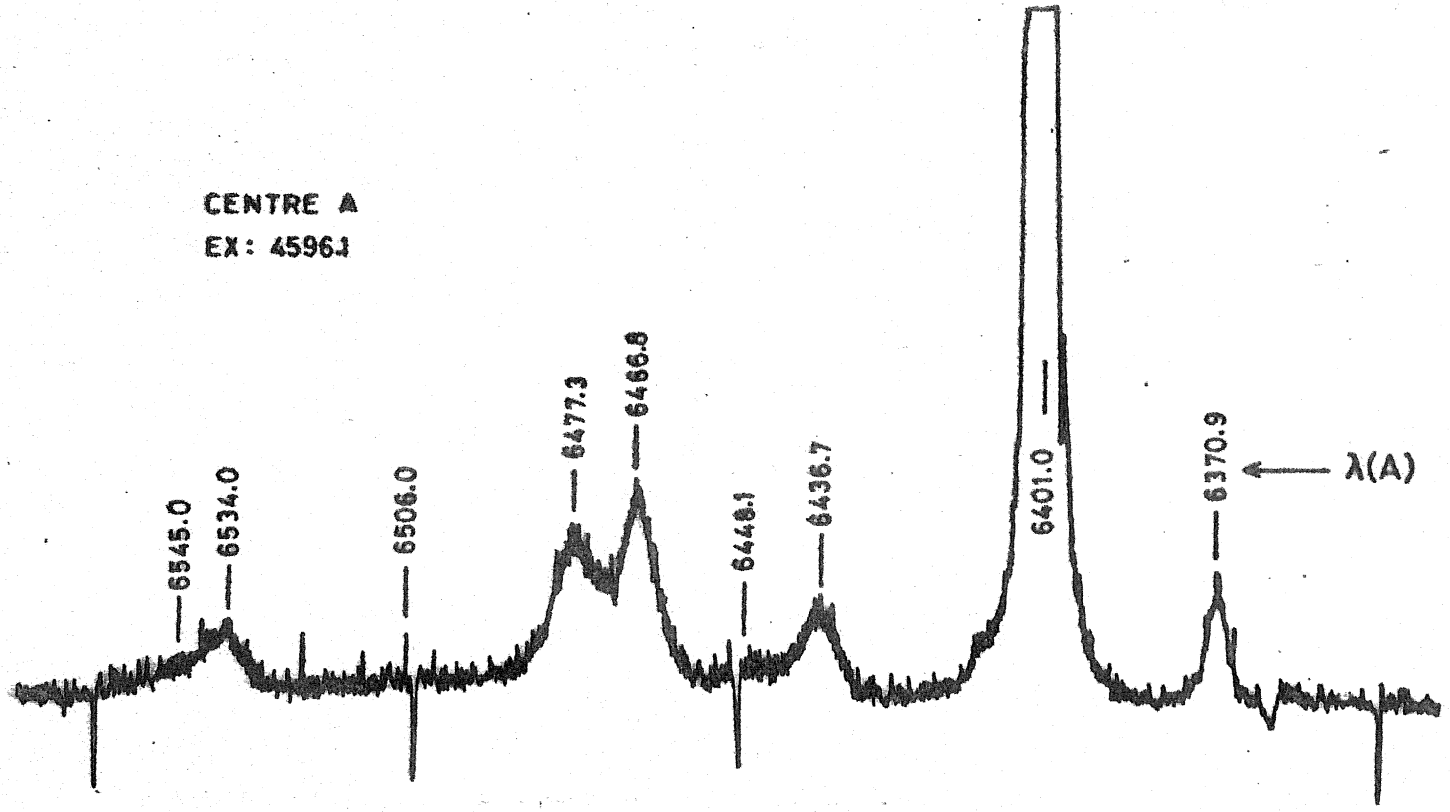

FIG. 3.12 FLUORESCENCE SPECTRUM OF Sm^{3+}: CaF_2 AT LNT; $^4G_{5/2}(A) \longrightarrow {}^6H_{9/2}(X)$ GROUP.

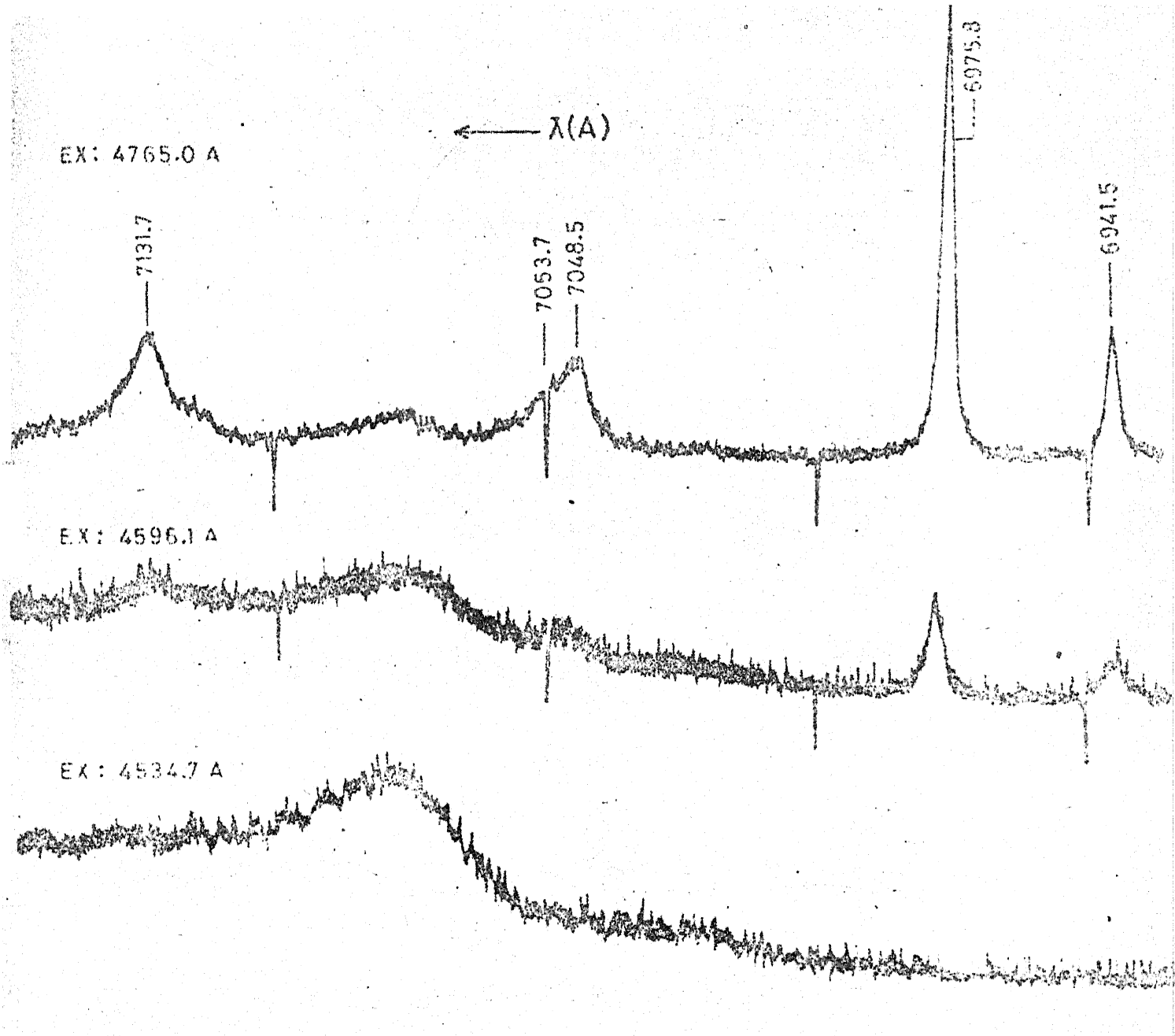

FIG. 3.13 FLUORESCENCE SPECTRUM OF $Sm^{3+}:CdF_2$ AT N.T. $^4G_{5/2}$ (A) — $^6H_{11/2}$ (W) GROUP.

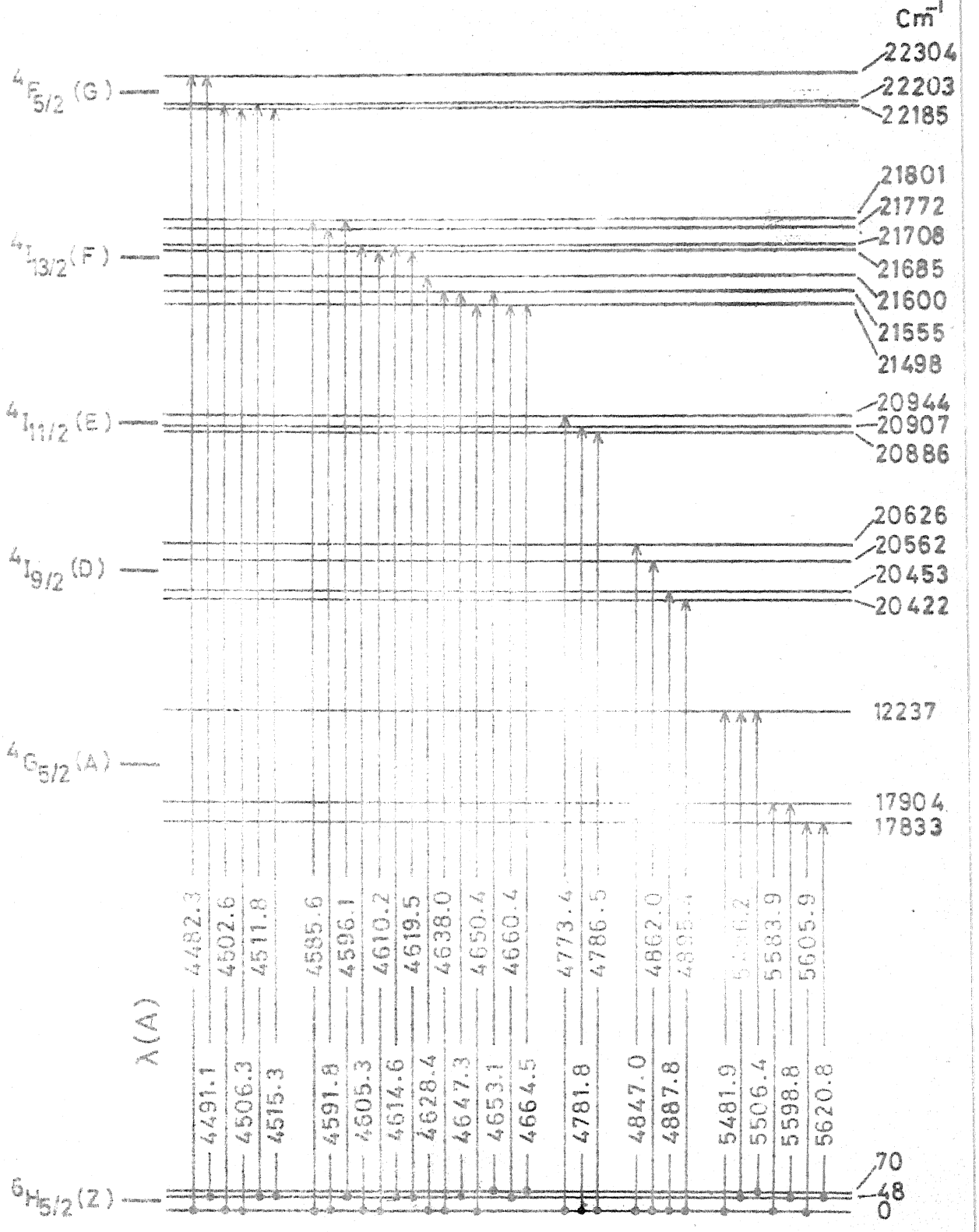

FIG. 3.14 PARTIAL ENERGY LEVEL DIAGRAM OF $Sm^{3+}:CaF_2$ SHOWING THE OBSERVED ABSORPTION LINES OF $^6H_{5/2} \longrightarrow {}^4F_{5/2}, {}^4I_{13/2}, {}^4I_{11/2}, {}^4I_{9/2}$ AND $^4G_{5/2}$ TRANSITIONS IN THE EXCITATION SPECTRUM OF CENTRE A AT LNT.

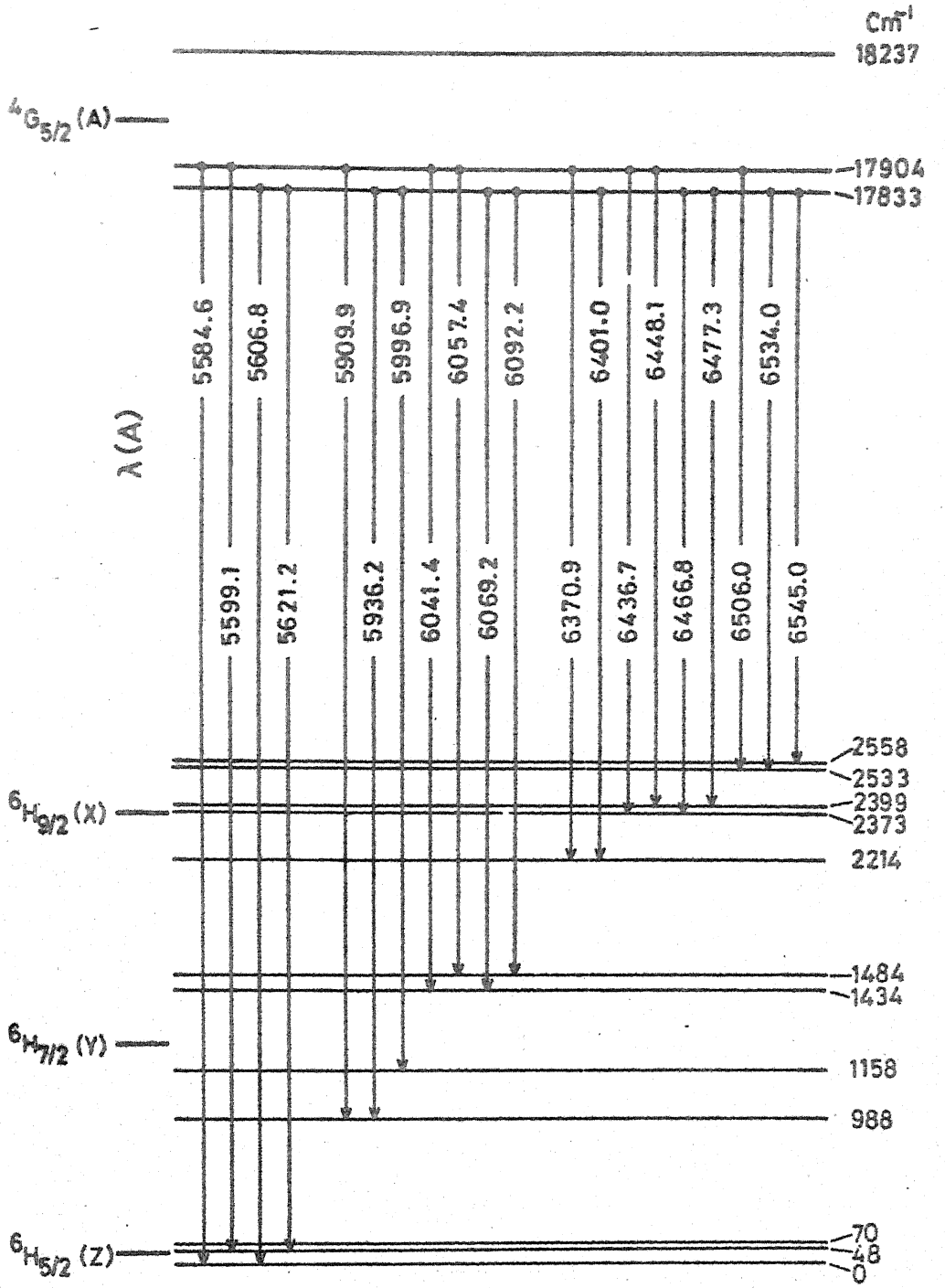

FIG. 3.15 PARTIAL ENERGY LEVEL DIAGRAM OF Sm^{3+}: CaF_2 SHOWING THE OBSERVED FLUORESCENCE LINES OF $^4G_{5/2} \longrightarrow {}^6H_{5/2}, {}^6H_{7/2}, {}^6H_{9/2}$ TRANSITIONS OF CENTRE A AT LNT.

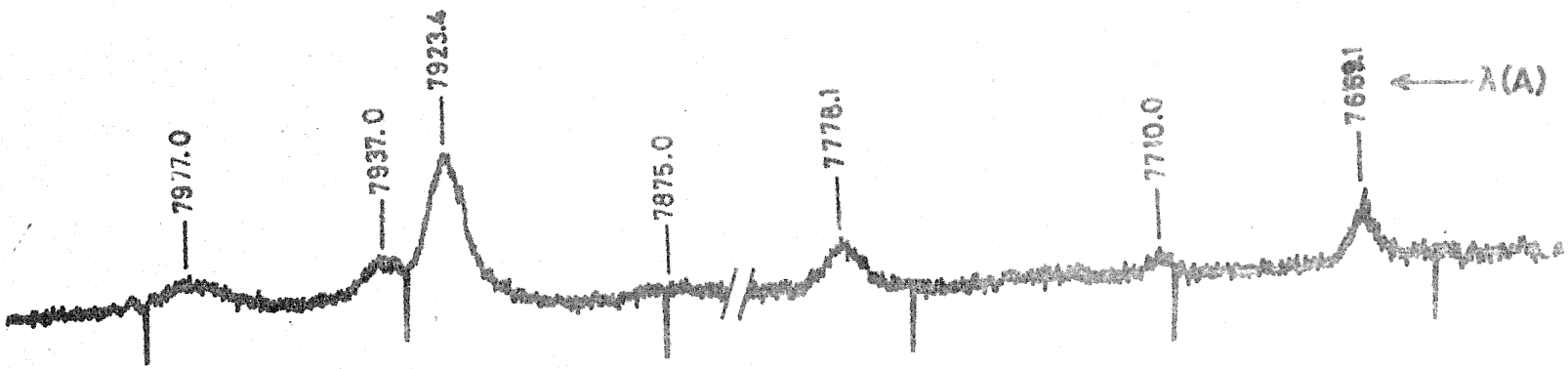

FIG. 3.16 FLUORESCENCE SPECTRUM OF $Sm^{3+}:CaF_2$ AT LNT; $^4G_{5/2}(A) \longrightarrow {}^6H_{13/2}(V)$ GROUP; EX: 4765A.

lying much above the remaining two. All the lines in the excitation spectrum of $^4G_{5/2}$ of centre A (except one weak line at 5576.2A) are very well explained with the Stark components of $^4G_{5/2}$ at 17833, 17904 and 18237 cm^{-1}.

Though the excitation wavelengths (4596.1A of centre A and 4534.7A of centre B) can pump the Sm^{3+} ions into the levels above $^4G_{7/2}$(C), fluorescence from $^4G_{5/2}$(A) alone is observed at LNT. The fluorescence spectrum in the region from 5500 to 7200A consists of four groups of lines, assigned as from $^4G_{5/2}$(A) to $^6H_{5/2}$(Z), $^6H_{7/2}$(Y), $^6H_{9/2}$(X) and $^6H_{11/2}$(W).

Fluorescence in the region from 5500 to 5670A is assigned as due to $^4G_{5/2}$(A) → $^6H_{5/2}$(Z) transition (figure 3.10). This region with A centre excitation consists of four sharp and intense lines and a weak line at 5666.0A which is very strong in the B centre fluorescence. Excitation spectra obtained by monitoring the line at 5666.0A clearly shows that it belongs to centre B and not centre A. This has also been verified by the study of decay times for all the lines in the group. A decay time of 5.5 ms is observed for 5666.0A line whereas that for all other lines in this group is 4.3 ms. But a weak line at this wavelength is also observed with all the excitations of A centre particularly when the absorption lines between 4400 and 4700A are excited. The presence of 5666.0A line in the fluorescence spectrum of A centre is

explained as due to (1) the presence of weak and broad absorption lines of centre B at the absorption lines of centre A (with full slits for the spectrophotometer it has been observed that there are large number of weak and broad fluorescence lines of centre B in the region from 4500 to 4700A), (2) a possible strong coupling of B centre levels with the lattice through phonons leading to a non-resonant excitation. Only one sharp and intense line at 5666.0A is observed in this region of the B centre spectrum. All the lines of the $^4G_{5/2}(A) \rightarrow {}^6H_{5/2}(Z)$ transition are explained with the Stark levels already derived from the excitation spectrum.

Fluorescence in the region from 5900 to 6070A (figure 3.11) due to $^4G_{5/2}(A) \rightarrow {}^6H_{7/2}(Y)$ transition contains seven lines of centre A with a sharp line at 5909.9A. Another strong and broad line with a half width of $\sim$8A is observed at 5996.9A. This group is observed to be the strongest in the fluorescence spectrum which is probably due to a large transition probability between these levels. Lifetime measurements show a decay time of 4.3 ms for all the lines except for the two lines at 6041.4A and 6057.4A close to the 6052A line which is due to the B centre. These two lines, when excited with N_2 laser, show a decay time of 4.78 ms, which is in between the decay times for A and B centres. Both the lines, however, show a decay time very close to 4.3 ms when

A centre lines are selectively excited using the dye laser. This indicates that these two lines belong to A centre only. Fluorescence of B centre in this region contains five lines including the strong line at 6052.0A.

6350-6550A group (figure 3.12) is assigned as due to the $^4G_{5/2}(A) \rightarrow {}^6H_{9/2}(X)$ transition. This group contains nine lines and all of them show a decay time of 4.3 $\pm$ 0.5 ms. 6401.0A line is found to be the only strong line in this group and is approximately ten times stronger than the rest of the lines in this group. No lines of centre B are observed in this region.

Only two lines of centre A could be identified in the region from 6900 to 7050A (figure 3.13) because of the continuum due to Sm^{2+}. These two lines are assigned as due to the $^4G_{5/2}(A) \rightarrow {}^6H_{11/2}(W)$ transition. Even in this region no lines of B centre are observed.

Using the positions of the Stark components of $^4G_{5/2}$ derived from the excitation spectrum, the Stark components of $^6H_{7/2}$ and $^6H_{9/2}$ of centre A are derived (by subtracting the energies of the fluorescence lines from the energies of the Stark components of $^4G_{5/2}$). The fluorescence from the Stark component at 18237 cm^{-1} of $^4G_{5/2}$ is likely to be very weak at LNT with any excitation, since the ions in this would relax very fast to the lower Stark components through

multiphonon processes. Also, at LNT, this Stark ~~level~~ component has very small population. The observed number of fluorescence lines are in good agreement with the number of lines expected with the energy level scheme developed for $^4G_{5/2}$ and $^4H_{5/2}$, $^6H_{7/2}$ and $^6H_{9/2}$. Stark components at 988, 1158, 1434 and 1484 cm^{-1} for $^6H_{7/2}$ and at 2214, 2373, 2399, 2533 and 2558 cm^{-1} for $^6H_{9/2}$ are derived from the fluorescence spectrum. Since only two lines of $^4G_{5/2} \rightarrow {}^6H_{11/2}$ are observed with dye laser excitation, the Stark components of $^6H_{11/2}$ could not be derived.

3.7 Steady State Fluorescence Spectrum of $Sm^{3+}:CaF_2$ Using 4765A Excitation of Ar^+ Laser

It is observed that 4765A excitation yields a pure A spectrum, all the lines of A centre being reproduced in position and relative intensities. This probably is due to 4765A excitation being very strongly coupled to A centre alone through phonon coupling. Remarkably, with this excitation, the intensities of both B centre and Sm^{2+} fluorescence are observed to be very weak.

This reduction in intensity of Sm^{2+} fluorescence (around 7050A) enabled the measurement of the A centre fluorescence lines due to $^4G_{5/2} \rightarrow {}^6H_{11/2}$ and $^4G_{5/2} \rightarrow {}^6H_{13/2}$ transitions, which otherwise are masked. The spectra of

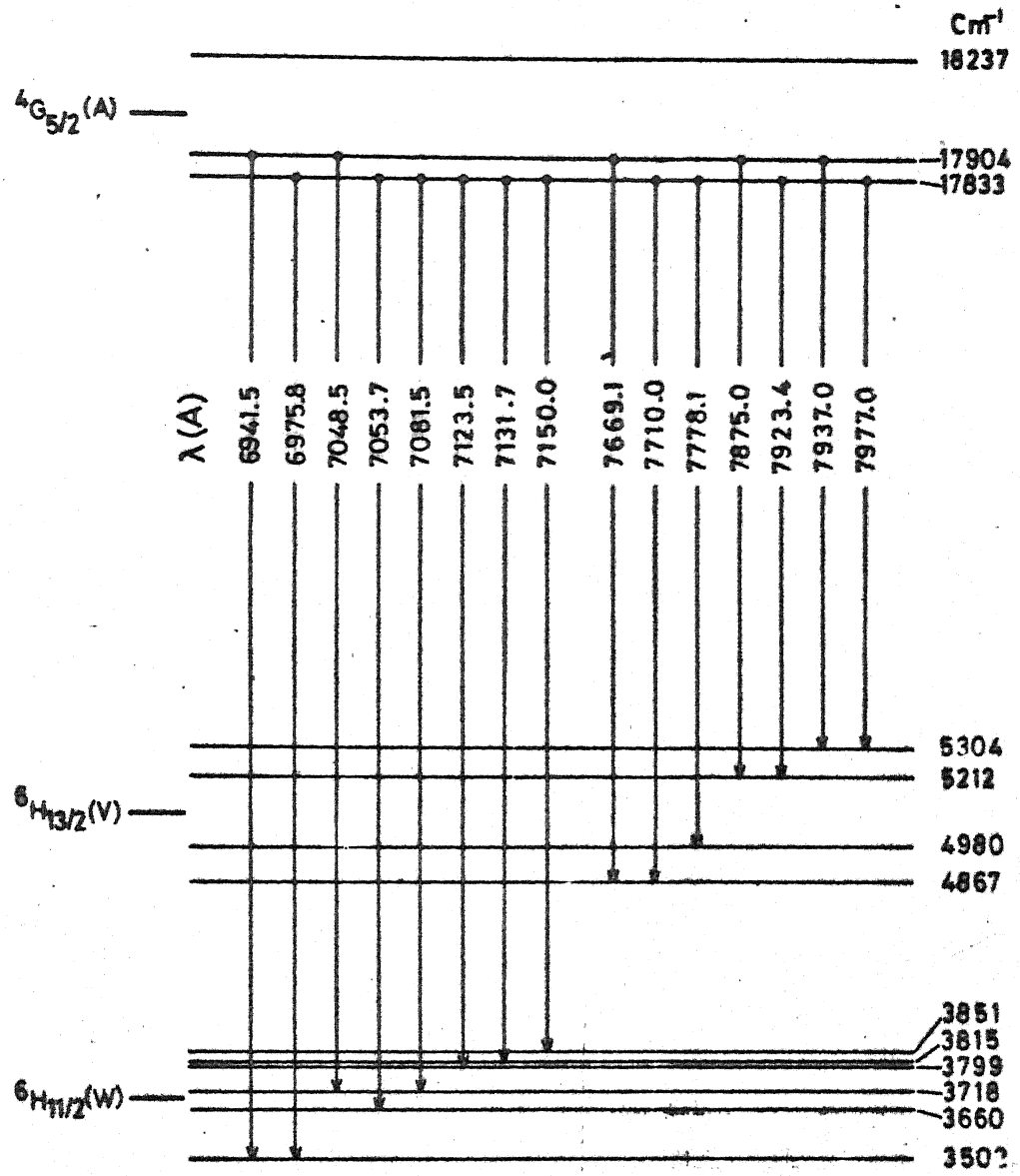

FIG. 3.17 PARTIAL ENERGY LEVEL DIAGRAM OF $Sm^{3+}:CaF_2$ SHOWING THE OBSERVED FLUORESCENCE LINES OF $^4G_{5/2} \longrightarrow {}^6H_{11/2}$ AND $^6H_{13/2}$ TRANSITIONS OF CENTRE A AT LNT EX: 4765 A OF Ar^+ LASER).

Table 3.5 : Fluorescence Spectrum of $Sm^{3+}:CaF_2$;
Excitation: 4765A; $^4G_{5/2}(A) \rightarrow {}^6H_{11/2}(W)$
and $^4G_{5/2}(A) \rightarrow {}^6H_{13/2}(V)$ Centre A

Wavelength A	Energy cm^{-1}	Intensity (arb.units)
	$^4G_{5/2}(A) \rightarrow {}^6H_{11/2}(W)$	
6941.5	14402	24
6975.8	14331	89
7048.5	14184	17
7053.7	14173	11
7081.5	14117	6
7123.5	14034	6
7131.7	14018	18
7150.0	13982	3
	$^4G_{5/2}(A) \rightarrow {}^6H_{13/2}(V)$	
7669.1	13036	11
7710.0	12967	5
7778.1	12853	10
7875.0	12695	3
7923.4	12617	25
7937.0	12596	8
7977.0	12533	5

these transitions are shown in figures 3.13 and 3.16. Table 3.5 lists the observed fluorescence lines with 4765A excitation.

$^4G_{5/2} \rightarrow {}^6H_{11/2}$ fluorescence group in the region from 6940 to 7150A (figure 3.13) contains eight lines out of which only two lines at 6941.5A and 6975.8A are found to be very sharp. The rest of the lines are broad and weak. $^4G_{5/2} \rightarrow {}^6H_{13/2}$ fluorescence group (7650 to 8000A) contains seven lines, all of which are observed to be very weak and broad. Both these groups contain much lesser number of fluorescence lines (8 and 7) than what are expected (12 and 14 respectively). Thus all the Stark components of these two levels could not be obtained. Figure 3.17 shows a possible partial energy level diagram which explains all the observed fluorescence lines in the $^4G_{5/2} \rightarrow {}^6H_{11/2}$ and $^4G_{5/2} \rightarrow {}^6H_{13/2}$ transitions. As in the case of $^6H_{7/2}$ and $^6H_{9/2}$, the Stark components of $^6H_{11/2}$ and $^6H_{13/2}$ are obtained by subtracting the energies of the fluorescence lines in these two regions from the energies of the Stark components of the originating level, $^4G_{5/2}$.

The Stark components at 3502, 3660, 3718, 3799, 3815 and 3851 cm^{-1} for $^6H_{11/2}$ and those at 4867, 4980, 5212 and 5304 cm^{-1} for $^6H_{13/2}$ explain the fluorescence groups terminating at $^6H_{11/2}$ and $^6H_{13/2}$.

3.8 Concentration Dependence of the Fluorescence

Fluorescence spectra are recorded using various excitations for different concentrations of Sm^{3+} in CaF_2. The spectra obtained with N_2 laser excitation are shown in figures 3.2 to 3.4. The spectra are also obtained by selectively exciting each centre of Sm^{3+} with the dye laser (not shown in figures). These spectra are found to be similar to the ones shown in figures 3.2 to 3.4 except for the disappearance of the lines due to the centre other than the one excited.

All the lines of centre A increase in intensity with the concentration and reach a maximum around 0.3 percent. Then the intensity of all the A lines decreases and becomes very weak in the 5 percent concentration crystal.
All the B centre lines show an increase in intensity with concentration and have maximum intensity at 1 percent concentration. In the 5 percent crystal, the intensity of even this centre reduces slightly, which is probably due to the ion-ion interactions at higher concentrations.

The relative intensities of all the lines in each centre however, are found to be the same for all concentrations (thereby confirming the analysis of the spectra). It is also observed that the intensity of the Sm^{2+} fluorescence increases slowly with the increase of concentration and has a maximum intensity in the 5 percent crystal.

3.9 High Temperature Fluorescence

Not much information is available in the literature about the energies of levels $^4F_{3/2}$(B) and $^4G_{7/2}$(C). Excitation spectra of these levels could not be obtained because of the nonavailability of a laser dye for this region. The energy separation between the free ion levels $^4F_{3/2}$ and $^4G_{5/2}$ is approximately 900 cm^{-1}. Because of this small gap, the multiphonon transition rate between $^4F_{3/2}$ and $^4G_{5/2}$ is very large and the ions in $^4F_{3/2}$ are drained away to the lower level. At higher temperatures however, thermalization between these levels could allow adequate population build-up in the $^4F_{3/2}$. The fluorescence from this level can thus be expected to increase with temperature T as

$$I_T = I_o \exp(-E/KT)$$

where E is the characteristic energy separation between the two levels and K is the Boltzman constant.

Thus, there is a good chance that if the experiment is carried out at higher temperatures, the fluorescence from $^4F_{3/2}$ may be observed. Earlier experiments of recording fluorescence at higher temperatures did yield fluorescence from thermally accessible levels [19].

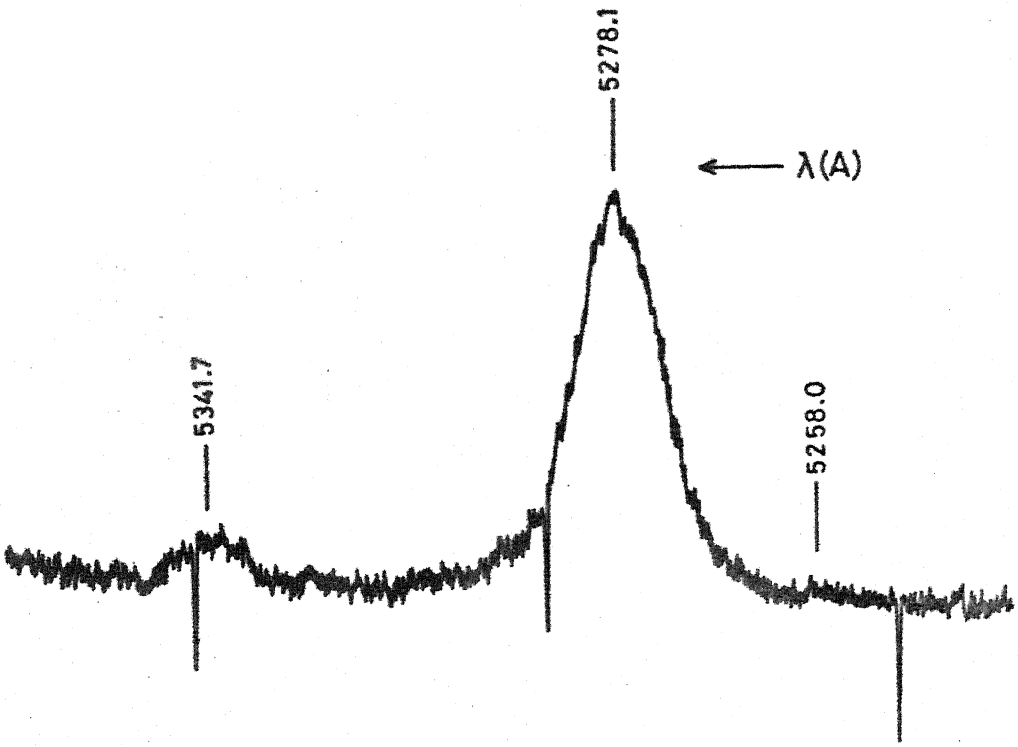

FIG. 3.18 FLUORESCENCE SPECTRUM OF Sm^{3+} : CaF_2 AT 300°K $^4F_{3/2} \longrightarrow {}^6H_{5/2}$; EX : 4880 A OF Ar^+ LASER .

However, even at a temperature of 550 K the $^4F_{3/2} \rightarrow {}^6H_{5/2}$ fluorescence could not be observed using dye laser because of its small average power (~10 mw). It could be recorded at room temperature with 4880A excitation of CW Ar^+ laser which has about 1300 mw of power output. With 4579A line which has only ~ 250 mw of power, this fluorescence could be recorded only at higher temperatures (~ 550 K).

Figure 3.18 shows $^4F_{3/2} \rightarrow {}^6H_{5/2}$ fluorescence at 300 K (RT) using 4880A line of Ar^+ laser. Three lines are observed at 5258.0A, 5278.1A and 5341.7A. Transition assignments between different Stark levels are made assuming that all these lines are because of A centre only. (It has been already seen that the fluorescence from centre B is very weak.) All the three lines can be explained with two Stark components of $^4F_{3/2}$ at 18715 and 19012 cm^{-1}.

CONCLUSIONS

Two different centres viz., A and B are identified for Sm^{3+} in CaF_2. All the observed transitions in the excitation and fluorescence spectra are identified as due to centres A and B. At low temperatures all the fluorescence emission is from the $^4G_{5/2}$(A) level. On the basis of these spectra, a partial energy level diagram is derived for the centre A of

Table 3.6 : Partial Energy Levels of Sm^{3+}:CaF_2 Derived from the Fluorescence and Excitation Spectra of Centre A

SLJ Level	Energies of Stark Components cm^{-1}	SLJ Level	Energies of Stark Components cm^{-1}
$^6H_{5/2}(Z)$	0	$^4I_{9/2}(D)$	20422
	48		20453
	70		20562
$^6H_{7/2}(Y)$	988		20626
	1158	$^4I_{11/2}(E)$	20886
	1434		20907
	1484		20944
$^6H_{9/2}(X)$	2214	$^4I_{13/2}(F)$	21498
	2373		21555
	2399		21600
	2533		21685
	2558		21708
$^6H_{11/2}(W)$	3502		21772
	3660		21801
	3718	$^4F_{5/2}(I)$	22185
	3799		22203
	3815		22304
	3851		
$^6H_{13/2}(V)$	4867		
	4980		
	5212		
	5304		
$^4G_{5/2}(A)$	17833		
	17904		
	18237		

$Sm^{3+}:CaF_2$. A list of the Stark components is given in table 3.6. Life times of the level $^4G_{5/2}$ for centres A and B are found to be 4.3 ms and 5.5 ms respectively. A study of the fluorescence with concentration series shows that the occurrence of centre B increases with increase of concentration. At very high concentrations, the fluorescence from both these centres becomes very weak and the intensity of Sm^{2+} fluorescence increases. Fluorescence from $^4F_{3/2}$(B) level is observed for the first time when the spectrum is recorded at higher temperatures (300 to 550 K).

REFERENCES

1. P.P. Sorokin and M.J. Stevenson, IBM J. Research and Development 5, 56 (1961).

2. W. Kaiser, C.G.B. Garrett and D.L. Wood, Phys. Rev. 123, 766 (1961);
D.L. Wood and W. Kaiser, Phys. Rev. 126, 2079 (1962).

3. A.S.M. Mahbub'ul Alam and Baldassare Di Bartolo, J. Chem. Phys. 47, 3791 (1967).

4. F.G. Spedding and R.S. Bear, Phys. Rev. 39, 948 (1932); 44, 2897 (1933); 46, 308 (1934).

5. H. Lämmermann et al., Z. Physik, 150, 551 (1958); 160, 355 (1960);
A. Friedrich, K.H. Hellwege and H. Lämmermann, ibid 159, 524 (1960).

6. M.S. Magno, Dissertation, The Johns Hopkins University, 1958.

7. M.S. Magno and G.H. Dieke, J. Chem. Phys. 37, 2354 (1962).

8. B.G. Wybourne, J. Chem. Phys. 36, 2301 (1962b).

9. J.D. Axe and G.H. Dieke, J. Chem. Phys. 37, 2364 (1962).

10. H.E. Rast, J.L. Fry and H.H. Caspers, J. Chem. Phys. 46, 1460 (1967).

11. G.H. Dieke, H.M. Crosswhite and B. Dunn, J. Opt. Soc. Am. 51, 826 (1961).

12. Norman Rabbiner, Phys. Rev. 130, 502 (1963).

13. Norman Rabbiner, J. Opt. Soc. Am. 57, 1376 (1967).

14. T.V. Babkina, V.F. Zolin and L.N. Muravey, Opt. Spectrosc. 32, 613 (1972).

15. 'Spectra and Energy Levels of Rare Earth Ions in Crystals' by G.H. Dieke, Interscience Publishers (1968).

16. Yu.K. Voronko, V.V. Osiko and M.M. Fursikov, 'Growth of Crystals', Vol. 5B, Edited by N.N. Sheftal', 171 (1968).

17. T.F. Ewanizky, P.J. Caplan and J.R. Postore, J. Chem. Phys. 43, 4351 (1965).

18. G.K. Miner, et al., J. Chem. Phys. 57, 1263 (1972);
W. Low, Phys. Rev. 109, 265 (1958);
D.R. Tallant and J.C. Wright, J. Chem. Phys. 63, 2074 (1975).

CHAPTER 4

ABSORPTION AND FLUORESCENCE SPECTRA OF $Ho^{3+}:CaF_2$

ABSTRACT

Absorption, fluorescence and excitation spectra of $Ho^{3+}:CaF_2$ are recorded at LNT. The absorption spectrum is photographed using a 1 percent concentration crystal. The fluorescence spectrum is recorded using several laser excitations, and for different concentrations of Ho^{3+} in CaF_2. From the steady state fluorescence, and the excitation spectrum, all the lines in the optical spectrum are classified under two centres. Decay times of all the fluorescence lines are measured to confirm this classification. Two groups around 6500A and 7500A in the fluorescence spectrum, which are observed to be due to overlapping transitions, are analysed and the fluorescence lines belonging to different parent levels are identified. A partial energy level diagram is proposed for both the centres of Ho^{3+} in CaF_2. A variation in the fluorescence intensity of both these centres with concentration of Ho^{3+} in CaF_2 is studied by selectively exciting each centre.

4.1 Introduction

Holmium is the eleventh element in the Lanthanide series and in its trivalent state, has the lowest configuration as $4f^{10}$. This configuration consists of 47 multiplets which through spin orbit interaction give rise to 107 SLJ states with $^5I_8$ as the ground state. Gobrecht [1] was the first to report on the optical spectrum of holmium, by photographing the absorption spectrum of $Ho_2(SO_4)_3$ in borax beads at 77 K, in the spectral range 7500 to 12000A. Machen and Nutting [2] were able to construct the energy level diagram in the range 3500-7000A by photographing the absorption spectrum of $Ho_2(SO_4)_3.5H_2O$ at various temperatures between 4 K and the room temperature. Khale [3] photographed the absorption spectrum of $HoCl_3.6H_2O$ and (Ho + Yb)Cl_3 while Singh [4] studied the absorption spectrum of $HoCl_3.9H_2O$ and Ho_2O_3. The first interpretation of the spectra of Ho^{3+} in solids was given by Crozier and Runciman [5] and Hufner in 1961. Later in 1964 Dieke and Pandey [6] have studied the absorption and fluorescence spectra of Ho^{3+} in $LaCl_3$, which yielded a virtually complete energy level diagram upto about 40,000 cm^{-1}. More comprehensive theoretical interpretation of the Ho^{3+} energy levels was given by Crozier and Runciman. Caspers et al [7], with the help of absorption and fluorescence data, established the complete Stark splittings of the levels of Ho^{3+} in LaF_3 below 26000 cm^{-1}. Some of the other hosts in which the optical spectra of Ho^{3+} has been studied are:

YPO_4 [8], $CaWO_4$ [9], YGaG [10], YIG [10], $YAlO_3$ [11] and MeF_2 [12] (Me = Ca, Ba, Sr) and some glasses [13].

Voronko [14] et al observed the stimulated emission at 5512A in Ho^{3+}:CaF_2 at 77 K using optical pumping. They concluded that this emission corresponds to the $^5S_2$ to $^5I_8$ transition. However, they have not given any details about the absorption or fluorescence spectra. Johnson [15] observed the laser action at 2.092 μ in Ho^{3+}:CaF_2 at 77 K, on a $^5I_7$ to $^5I_8$ transition.

Several studies have been performed to ascertain the site of holmium ions doped in CaF_2. Thermoluminescence spectrum of the transition $^5S_2$ to $^5I_8$ in the region 5365 to 5598A has been reported by Merz and Pershan [16]. They concluded that the Ho^{3+} ions responsible for the observed spectra, are located in sites of cubic symmetry. Schlesinger and Whippy [17] also studied the thermoluminescence spectrum and they attributed the relative change in the intensities of emission lines as due to the mobility of Ho^{3+} ions at higher temperatures. They further concluded that at low temperatures the spectrum is due to the presence of more than one centre of Ho^{3+} (Merz and Pershan reported cubic sites only). They have used a 0.5 percent concentration crystal by adding HoF_3 to pure CaF_2. Verber et al [18], have observed the fluorescence around 6500A using pulsed infrared excitation.

EPR studies of Ho^{3+}:CaF_2, by Korienko and Rybaltovskii [19] showed that the Ho^{3+} ions are in a crystal field of tetragonal symmetry. The crystals were synthesized by the Stockberger process in graphite crucibles and fluorine atmosphere with 0.1 percent HoF_3 being added to the mixture. Linear Stark [20]effect studies showed that there are two types of trigonal centres. Recently Bansilal [21] using Ar^+ laser as the excitation source and a concentration series of Ho^{3+} in CaF_2 (from 0.01 to 0.1%) reported the fluorescence spectra in the range from 4800 to 7600A. From the variation of line intensities with concentration, he attributed the spectrum to more than one centre. However, he did not analyse the fluorescence spectrum completely.

Because of their complexity, much work has not so far been done to analyse the fluorescence and absorption spectra of Ho^{3+}:CaF_2. This chapter presents the work done to identify and characterise the optical spectra due to the various kinds of centres of holmium in CaF_2 crystal.

4.2 Experimental Details

Experimental set-ups used for recording the absorption and fluorescence spectra are discussed in Chapter 2. Seven crystals of CaF_2 with different concentrations of Ho^{3+} are grown (0.01, 0.03, 0.09, 0.3, 0.65, 1, 5 percent by

weight of HoF_3 in CaF_2) in a vacuum furnace, also described in Chapter 2. Absorption spectra are recorded using 5 percent and 1 percent concentration crystals. Ar^+ laser and N_2 laser pumped dye laser are used for recording the fluorescence spectra. A synchronous signal averager is used to study the signals with decay times more than 100 μs and faster signals ($\sim$15 μs) are measured using a boxcar integrator.

4.3 The Optical Absorption Spectrum

The optical absorption spectrum of Ho^{3+}:CaF_2 recorded at LNT consists of seven groups of lines in the region from 3500 to 6500A. Densitometer traces of the absorption spectra, recorded using 1 percent concentration crystal are shown in figure 4.1 and table 4.1 lists the absorption lines. One absorption group in the region from 4600 to 4750A is found to be very weak in the 1 percent concentration crystal. The data presented in table 4.1 for this group are taken from the spectrum recorded with 5 percent concentration crystal. There is an over-absorption in all other groups in the case of 5 percent crystal and hence the lines of these groups could not be measured at LNT. Absorption in all other crystals of the concentration series is too weak to record.

A comparison of the observed spectrum with that of Ho^{3+} in LaF_3 and $LaCl_3$ lead to the following transition assignments.

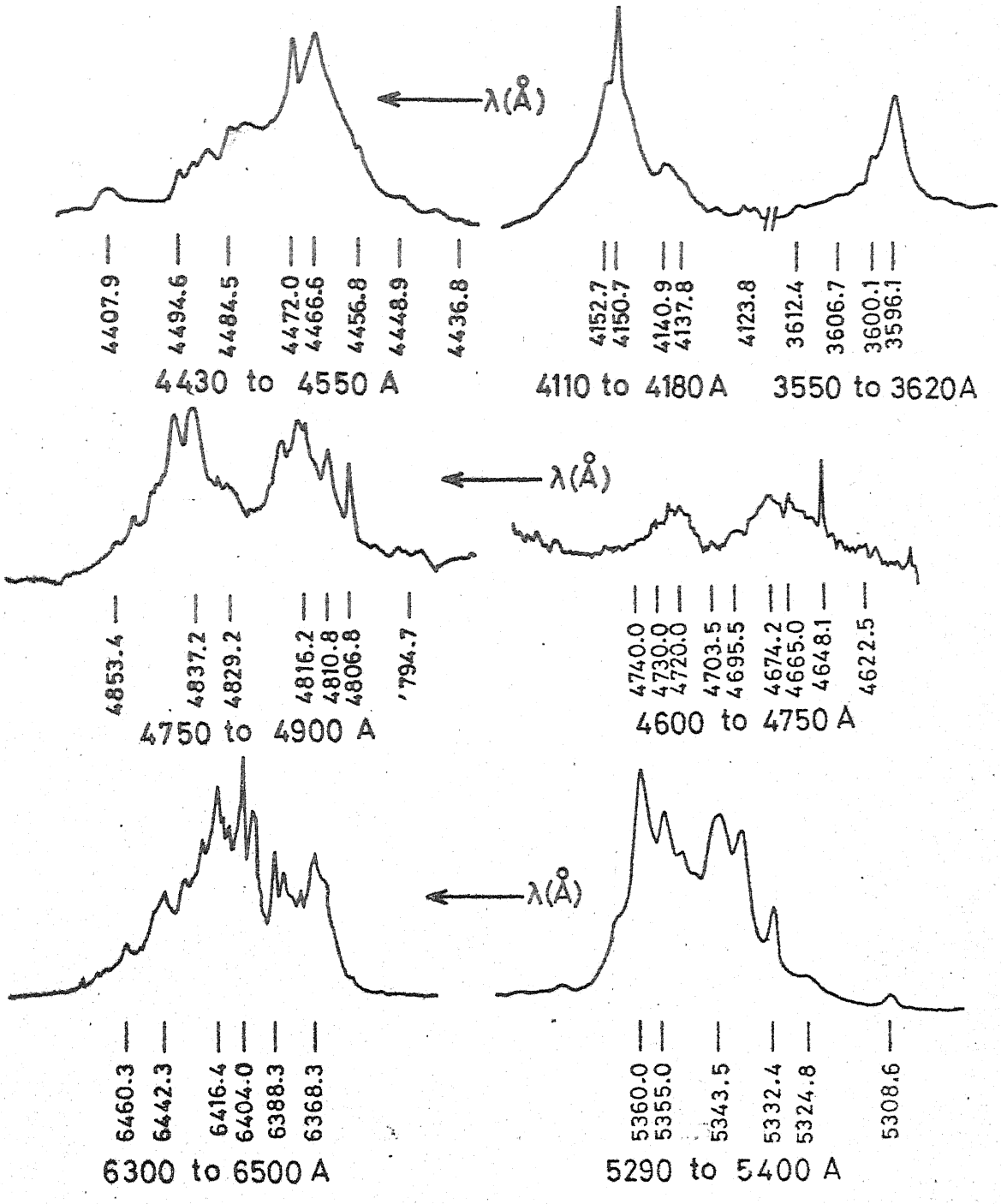

Fig. 4.1 Ho^{3+}: CaF_2 absorption at LNT, 1%. Conc.

Absorption Group	Transition Assignment
3590-3620A	$^5I_8(Z) \rightarrow {}^5G'_5(H)$
4120-4160A	$^5I_8(Z) \rightarrow {}^5G_5(J)$
4430-4520A	$^5I_8(Z) \rightarrow {}^5G_6 + {}^5F_1\ (I)^+$
4620-4750A	$^5I_8(Z) \rightarrow {}^3K_8(H) + {}^5F_2\ (G)$
4780-4860A	$^5I_8(Z) \rightarrow {}^5F_3(F)$
5290-5410A	$^5I_8(Z) \rightarrow {}^5F_4 + {}^5S_2\ (E)^+$
6350-6500A	$^5I_8(Z) \rightarrow {}^5F_5(D)$

Absorption to the levels $^5G_4(K)$ and $^3K_7(L)$ which is expected to be in the region between 3620 to 4120A, is not observed even in the 5 percent concentration crystal. Most of the lines in the absorption spectrum of 1 percent crystal are found to be approximately 2A broad (full width at half maximum). It is not possible to obtain the crystal field splittings of the levels from the absorption data alone because of the presence of more than one centre of Ho^{3+} ion in CaF_2 which is confirmed from the fluorescence studies of the concentration series. However, the absorption data recorded with the tungsten lamp has been used as a verification that there are no extra lines in the absorption spectrum other than the ones classified under different centres from the selective excitation data.

+ The notations I and E correspond to the mixtures of the SLJ levels $^5G_6$ and $^5F_1$ and $^5F_4$ and $^5S_2$ respectively.

Table 4.1 : Absorption Spectrum of Ho^{3+}:CaF_2 at LNT

Wavelength A	Energy cm^{-1}
$^5I_8(Z) \rightarrow {}^5G_5(H)$	
3596.1	27800
3600.1	27765
3606.7	27718
3612.4	27675
$^5I_8(Z) \rightarrow {}^5G_5(J)$	
4123.8	24243
4137.8	24161
4140.0	24148
4149.1	24095
4150.7	24086
4152.7	24074
$^5I_8(Z) \rightarrow {}^5G_6 + {}^5F_1(I)$	
4436.8	22533
4442.1	22506
4448.9	22471
4456.8	22431
4466.6	22382
4472.0	22355
4481.2	22309
4484.5	22293
4488.5	22273
4491.5	22258
4494.6	22243
4498.8	22223
4504.2	22195
4507.9	22177
4515.5	22140
$^5I_8(Z) \rightarrow {}^3K_8(H) + {}^5F_2(G)$	
4622.5	21627
4648.1	21508
4653.0	21486
4658.1	21462
4665.0	21430
4670.3	21406
4674.2	21388
4680.2	21361
4695.5	21291
4703.5	21255
4709.3	21229
4714.3	21206
4720.7	21177
4730.0	21135
4740.0	21091
$^5I_8(Z) \rightarrow {}^5F_3(F)$	
4781.9	20906
4794.7	20851
4806.4	20800
4810.8	20781
4816.2	20758

Table 4.1 : (Continued)

Wavelength A	Energy cm^{-1}
4819.7	20742
4829.6	20700
4832.8	20686
4837.2	20667
4841.2	20650
4845.7	20631
4853.4	20598
$^5I_8(Z) \rightarrow {}^5F_4 + {}^5S_2$ (E)	
5291.7	18892
5308.6	18832
5318.9	18796
5324.8	18775
5332.4	18748
5339.0	18725
5343.5	18709
5351.7	18681
5855.0	18669
5360.0	18652
5364.8	18635
5375.0	18600
5384.0	18568
5391.0	18544
5400.1	18513
$^5I_8(Z) \rightarrow {}^5F_5(D)$	
6358.8	15722
6363.6	18710

Wavelength A	Energy cm^{-1}
6368.3	15699
6370.7	15693
6375.9	15680
6380.6	15668
6379.2	15672
6382.6	15663
6383.8	15660
6388.3	15649
6395.2	15632
6397.9	15626
6399.3	15622
6400.7	15619
6404.0	15611
6406.0	15606
6407.3	15603
6411.0	15594
6414.0	15587
6416.4	15581
6418.0	15577
6420.8	15570
6424.6	15561
6429.4	15549
6432.6	15542
6442.7	15517
6447.2	15506
6451.2	15497
6460.3	15475
6469.5	15453
6474.0	15442
6479.5	15429
6485.7	15414

4.4 Steady State Fluorescence Spectra of the Concentration Series of Ho^{3+} in CaF_2 using Ar^+ Laser

Steady state fluorescence spectra of CaF_2 with different concentrations of Ho are recorded at LNT in the range from 4800 to 7600A using 4765A excitation of the Ar^+ laser. This excitation is nonresonant (as can be seen from the absorption data that there is no absorption line at this energy) and leads to the pumping of Ho^{3+} ions into different excited states of all the centres through phonon coupling as in the case of 'broad band' excitation. Figures 4.2 to 4.5 illustrate the observed spectrum with this excitation, in the range from 4800 to 7600A as the concentration of Ho is varied from 0.01 percent to 5 percent.

Four groups of fluorescence lines are observed and the following transition assignments are made after a comparison of the observed spectra with the Ho^{3+} in other lattices.

Fluorescence Group	Transition Assignment
4800-4980A	$^5F_3(F) \rightarrow {}^5I_8(Z)$
5250-5550A	$^5F_4 + {}^5S_2(E) \rightarrow {}^5I_8(Z)$
6350-6650A	$^5F_3(F) \rightarrow {}^5I_7(Y)$
	$^5F_5(D) \rightarrow {}^5I_8(Z)$
7400-7600A	$^5F_4 + {}^5S_2(E) \rightarrow {}^5I_7(Y)$
	$^5I_4(C) \rightarrow {}^5I_8(Z)$

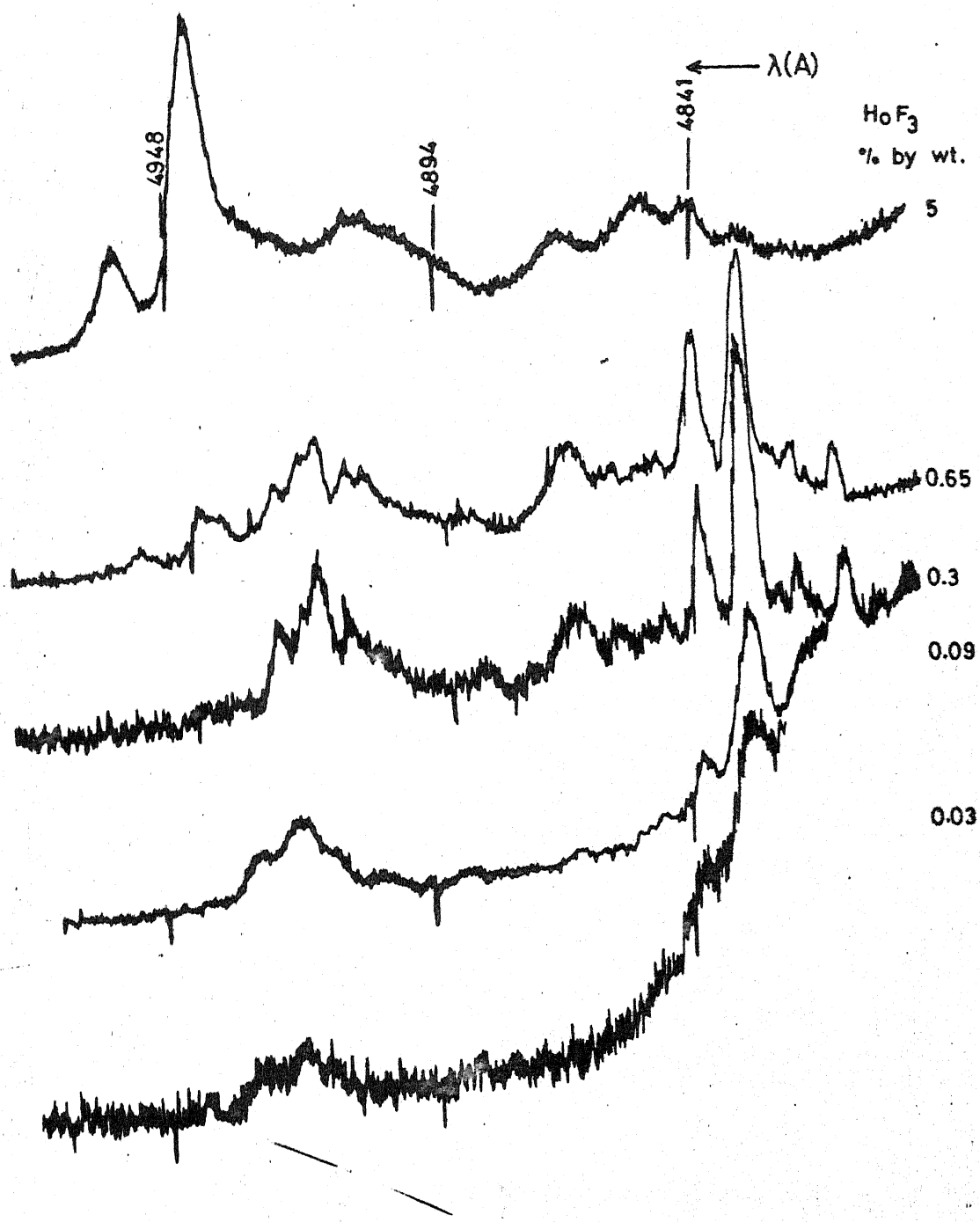

FIG. 4.2 FLUORESCENCE SPECTRUM OF $Ho^{3+}:CaF_2$ AT LNT; CONCENTRATION SERIES $^5F_3(F) \longrightarrow {}^5I_8(Z)$; EX:4765A

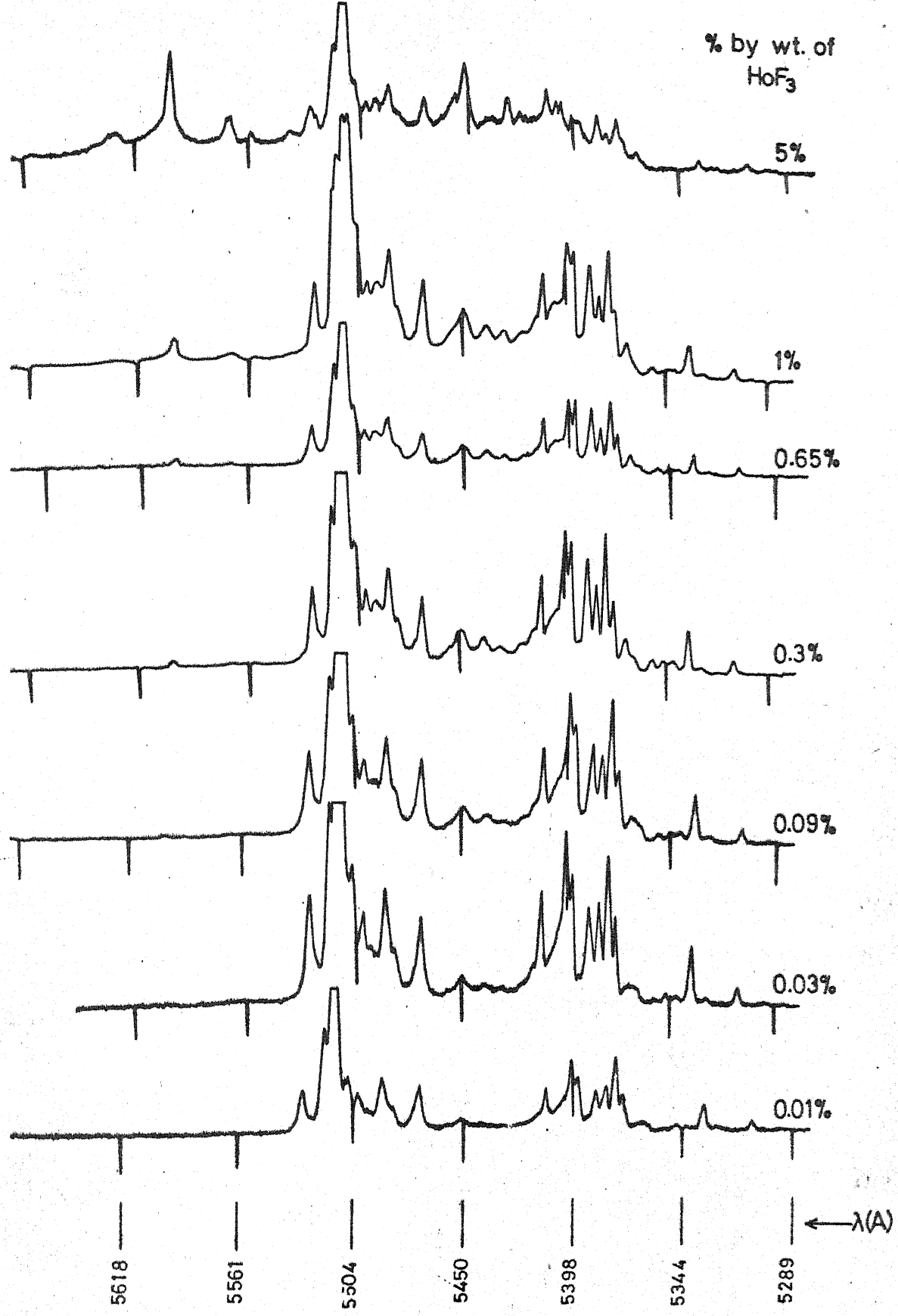

Fig. 4.3 Ho^{3+} : CaF_2 concentration series; fluorescence at LNT
$^5F_4 + {}^5S_2$ (E) ⟶ $^5I_8$ (Z) ; EX: 4765A.

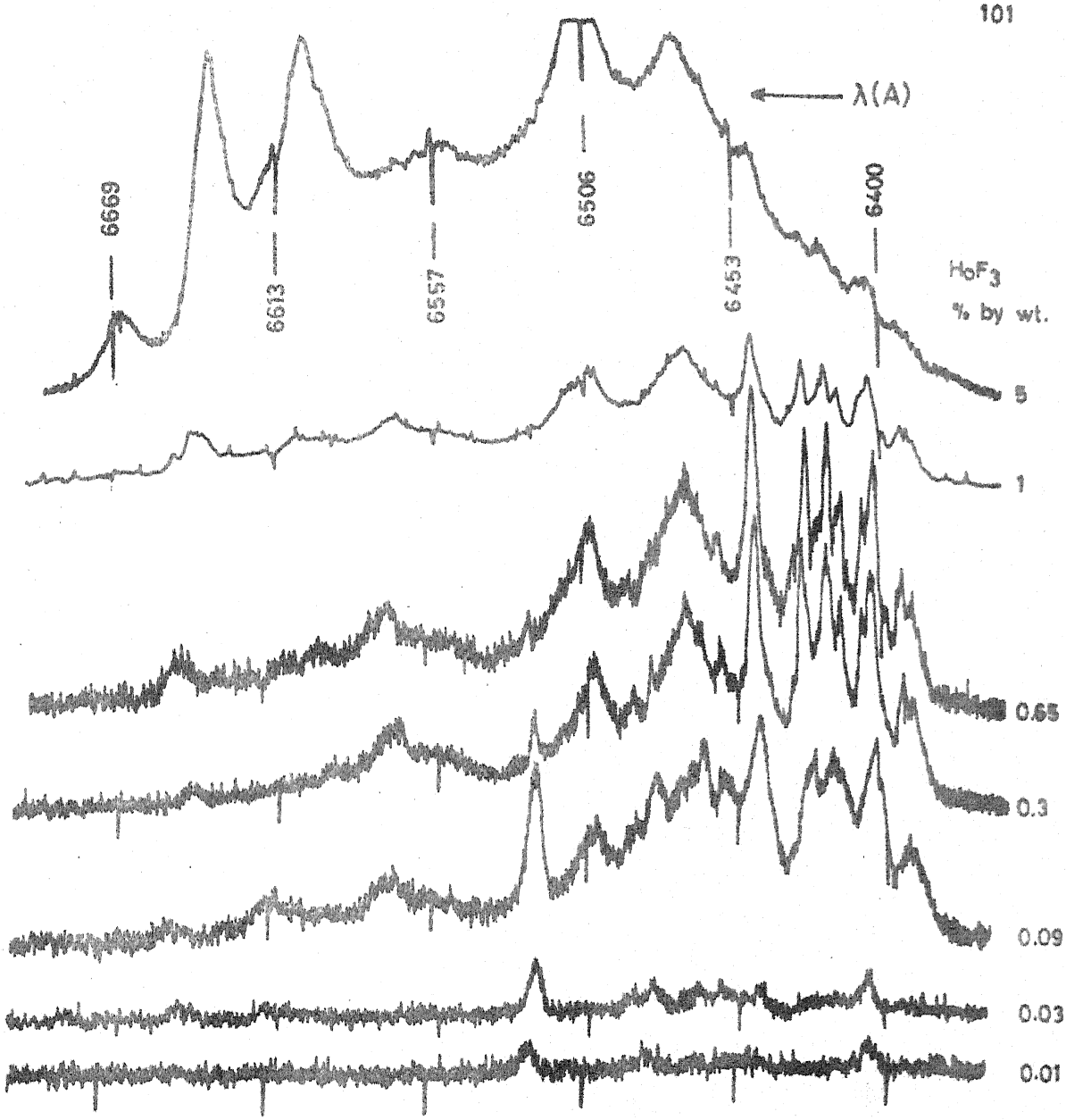

FIG. 4.4 FLUORESCENCE SPECTRUM OF Ho^{3+}: CaF_2 AT LNT; CONCEN-TRATION SERIES $^5F_5$ (D) $\longrightarrow$ $^5I_8$ (Z) & $^5F_3$ (F) $\longrightarrow$ $^5I_7$ (Y); EX 4765 A.

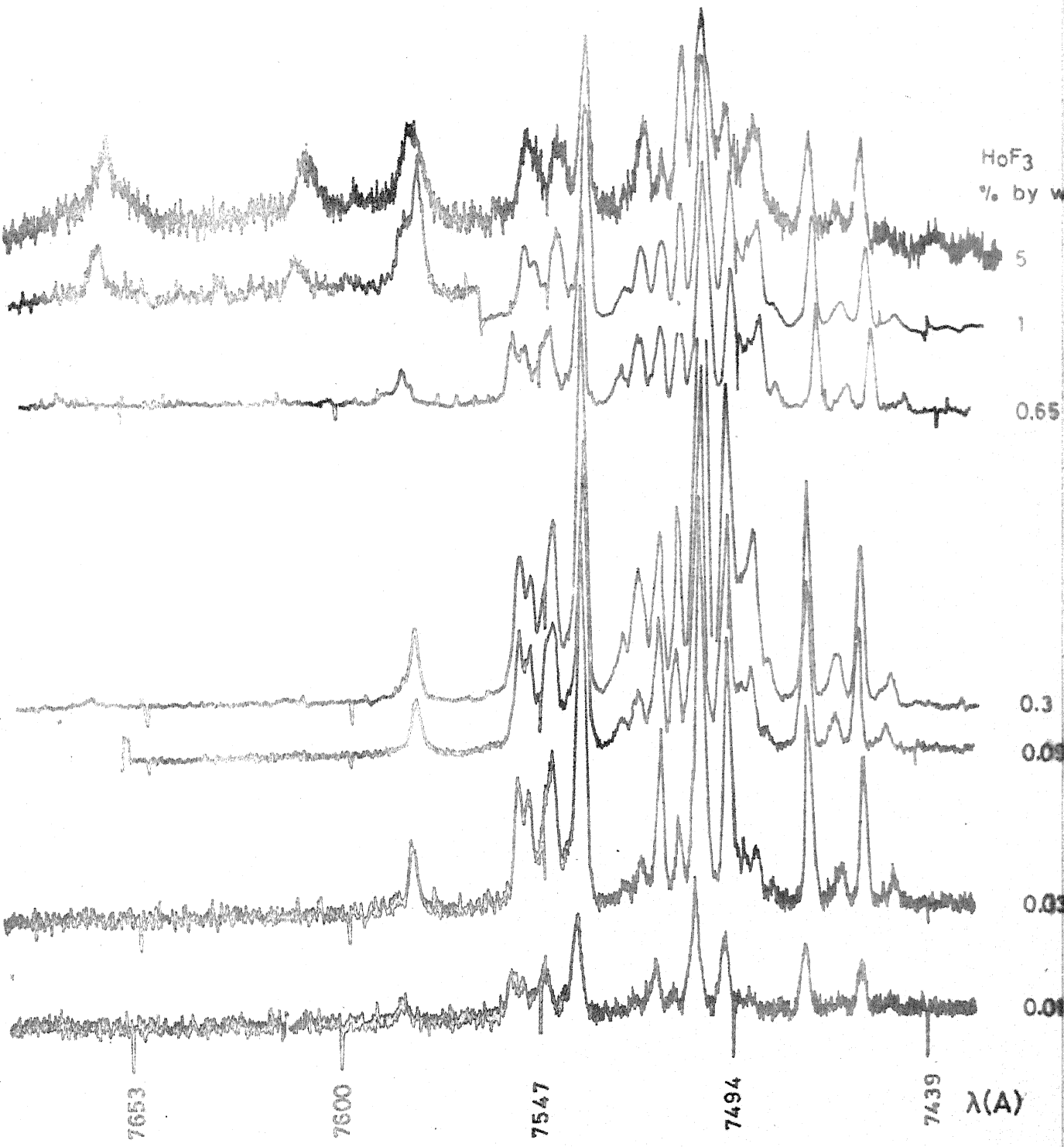

FIG. 4.5 FLUORESCENCE SPECTRUM OF Ho^{3+}: CaF_2 AT LNT; CONCENTRATION SERIES. $^5F_4 + {}^5S_2(E) \longrightarrow {}^5I_7(Y)$; EX: 4765 A

As in the case of $Sm^{3+}:CaF_2$, the spectrum is seen to contain two sets of lines, the relative intensity of these two sets showing a change with concentration. This indicates the presence of at least two centres, each giving rise to one set of lines in the fluorescence spectrum. The fluorescence lines whose relative intensity increases with increase of Ho concentration are referred to as B set of B centre lines. The remaining lines are referred to as A set or A centre lines.

4.5 Fluorescence and Excitation Spectra of $Ho^{3+}:CaF_2$ using N_2 Laser Pumped Dye Laser

A detailed study of the absorption and fluorescence spectra has been carried out by recording the excitation spectrum and the selectively excited fluorescence at LNT using N_2 laser pumped dye laser. A 0.65 percent concentration crystal is chosen for these studies as the intensities of the fluorescence lines of both the sets are comparable at this concentration.

Unlike $Sm^{3+}:CaF_2$, $Ho^{3+}:CaF_2$ presented numerous problems because of the large J values of the ground level (J = 8) as well as the upper fluorescing levels (J = 3 to 6) and consequently a large number of Stark components are expected for each level even under the highest site symmetry (cubic).

As a result, the fluorescence from (or excitation to) these levels contain a large number of lines. Since fluorescence from the corresponding levels of different centres fall in the same regions, it is expected that many of the lines due to different centres may overlap with each other (which is observed to be the case in all the groups). The following procedure is adopted to identify the lines due to different centres of Ho^{3+} in CaF_2.

The excitation spectra are recorded by monitoring each fluorescence line in the 5300A group recorded with Ar^+ laser excitation. The fluorescence spectra are recorded by selectively exciting each absorption line recorded in the absorption spectrum taken on the Jarrell-Ash spectrograph. As a next step, each absorption line recorded in the excitation spectrum is selectively excited and the fluorescence spectra in the region from 4800 to 7600A are recorded. The fluorescence spectrum thus resulted, is again monitored and the excitation spectra are recorded. This procedure is repeated till identical spectra (lines being reproduced in intensity and position) are obtained with at least three excitations of each centre in the case of fluorescence. Similarly, excitation spectra are also reproduced by monitoring at least three fluorescence lines. The selective excitation on many lines of the excitation spectrum has lead to the fluorescence from either centre A or centre B exclusively. In case of

the overlapping absorption (or fluorescence) lines, the resulting fluorescence (or excitation) spectrum contained lines from both the centres. Figures 4.6 through 4.15 compare the excitation and fluorescence spectra of A and B centres.

From the excitation and fluorescence spectra shown in figures 4.6 through 4.15, it can be seen that there is a weak 'background' through out the region of each group and all the spectral lines are superposed over this 'background'. This weak 'background' can be attributed as due to the tails of each line extending over a long region. Hence if an A centre fluorescence line is monitored, the resulting excitation spectrum invariably contains some lines which are very strong in the B spectrum, due to the weak fluorescence 'background' of B centre at this wavelength. Similarly when B centre lines are monitored, the resulting excitation spectrum contained some of the very strong A centre lines. The selectively excited fluorescence spectra contained lines from the other centre for this reason. Thus the weak 'background' due to one centre is reflected in the spectra due to the other centre in the form of a weak line. This can be easily visualised with the following example. In figure 4.8, the two lines at 4778.6A and 4796.7A in the excitation spectrum obtained monitoring 5437.8A (centre B) line, are due to centre A, the intensities at these wavelengths being equal to the intensities of the 'background' fluorescence of

centre A at 5437.8A when excited by 4778.6 and 4796.7A respectively. These problems are due to the present limitations of cooling the crystal to LNT only. (At liquid helium temperature, it is expected that there will be more number of well isolated lines in the spectra, which will lead to pure excitation and fluorescence spectra). Thus in the present experiments it was impossible to record hundred percent pure A and B spectra except in the case of 4778.6A and 4796.7A excitations of A centre where the fluorescence spectra are found to be free from all B centre lines.

Further confirmation of the classification of the lines in the fluorescence and excitation spectra is obtained by recording the spectra in crystals with Ho^{3+} concentration between 0.01 and 5 percent. The intensity of all the A centre lines reaches a maximum at 0.3 percent and does not vary much with further increase in Ho^{3+} concentration. Intensity of the B centre lines increases with increase of concentration. It is also observed that the relative intensities of the fluorescence lines of each centre remain unchanged with the variation of the concentration. The fluorescence spectra recorded for different concentrations with selective dye laser excitation are not shown in figures. In the concentration range from 0.01 to 1 percent, the abundance of centres other than A and B is either very low to produce any detectable fluorescence or they are completely

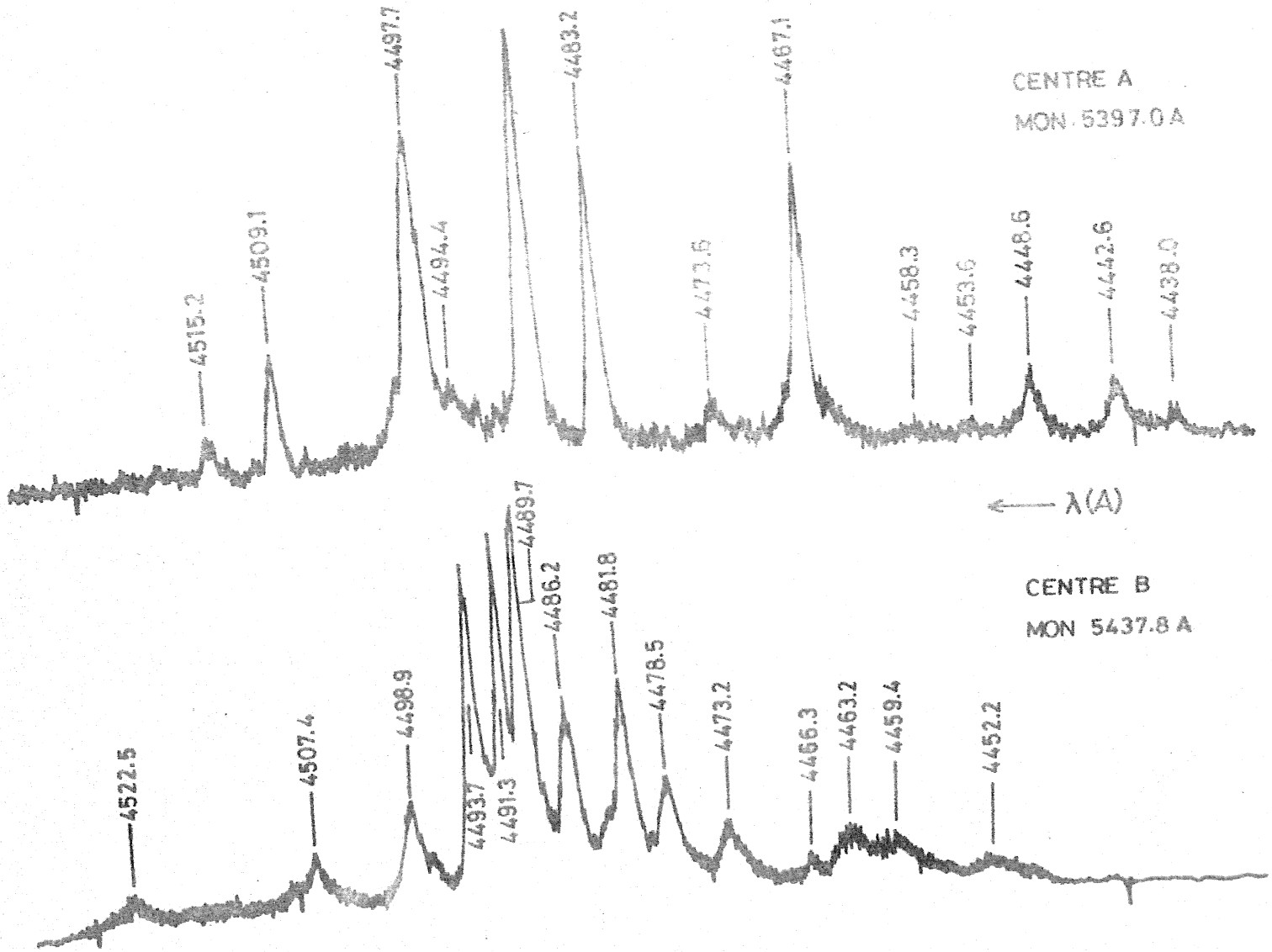

FIG. 4.6 $^5I_8 (Z) \longrightarrow {}^5G_6 + {}^5F_1 (I)$ EXCITATION SPECTRUM OF $Ho^{3+}:CaF_2$ AT LNT.

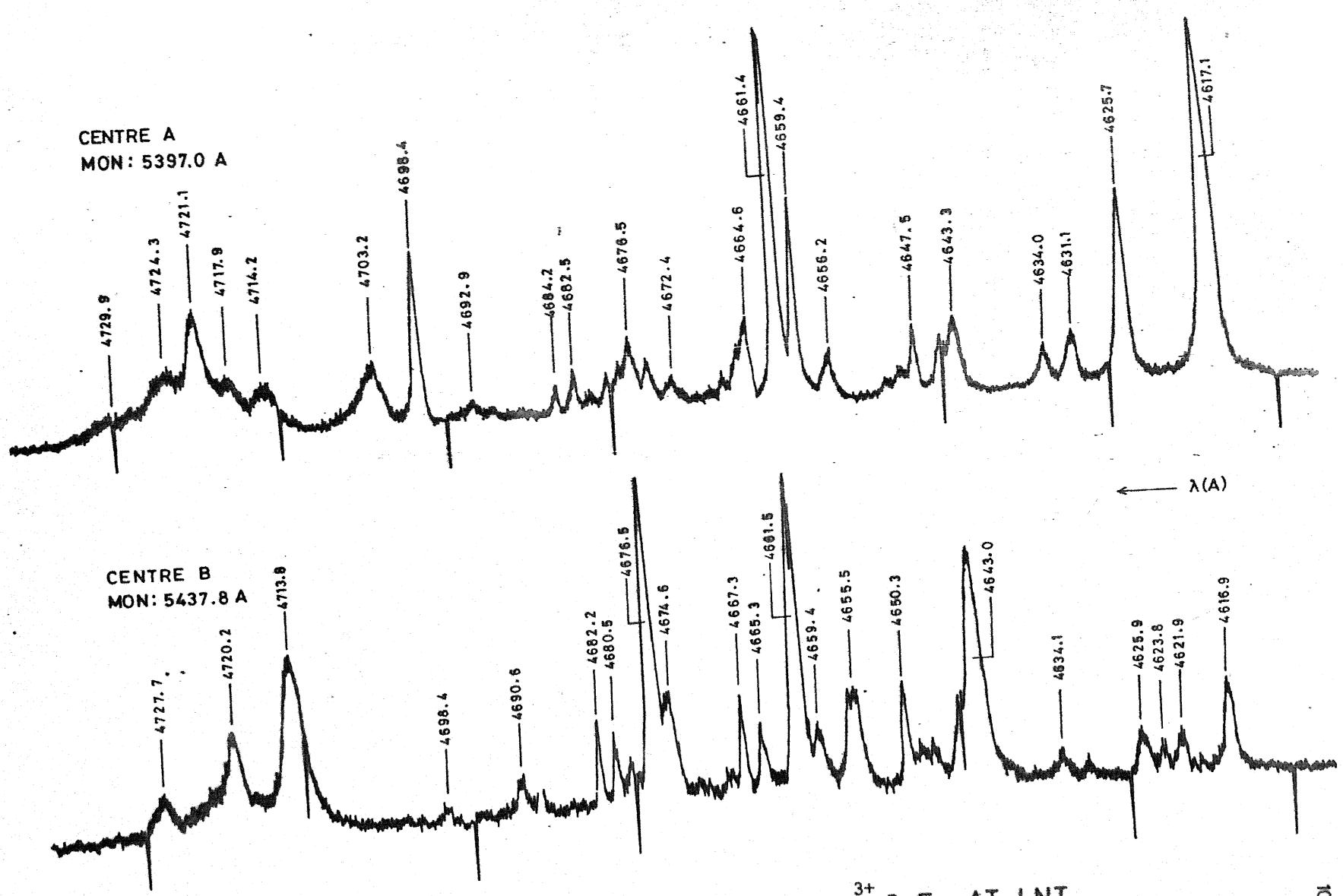

FIG.4.7 $^5I_8(Z) \longrightarrow {}^3K_8 + {}^5F_2$ (H+G) EXCITATION SPECTRUM OF Ho^{3+}:CaF_2 AT LNT.

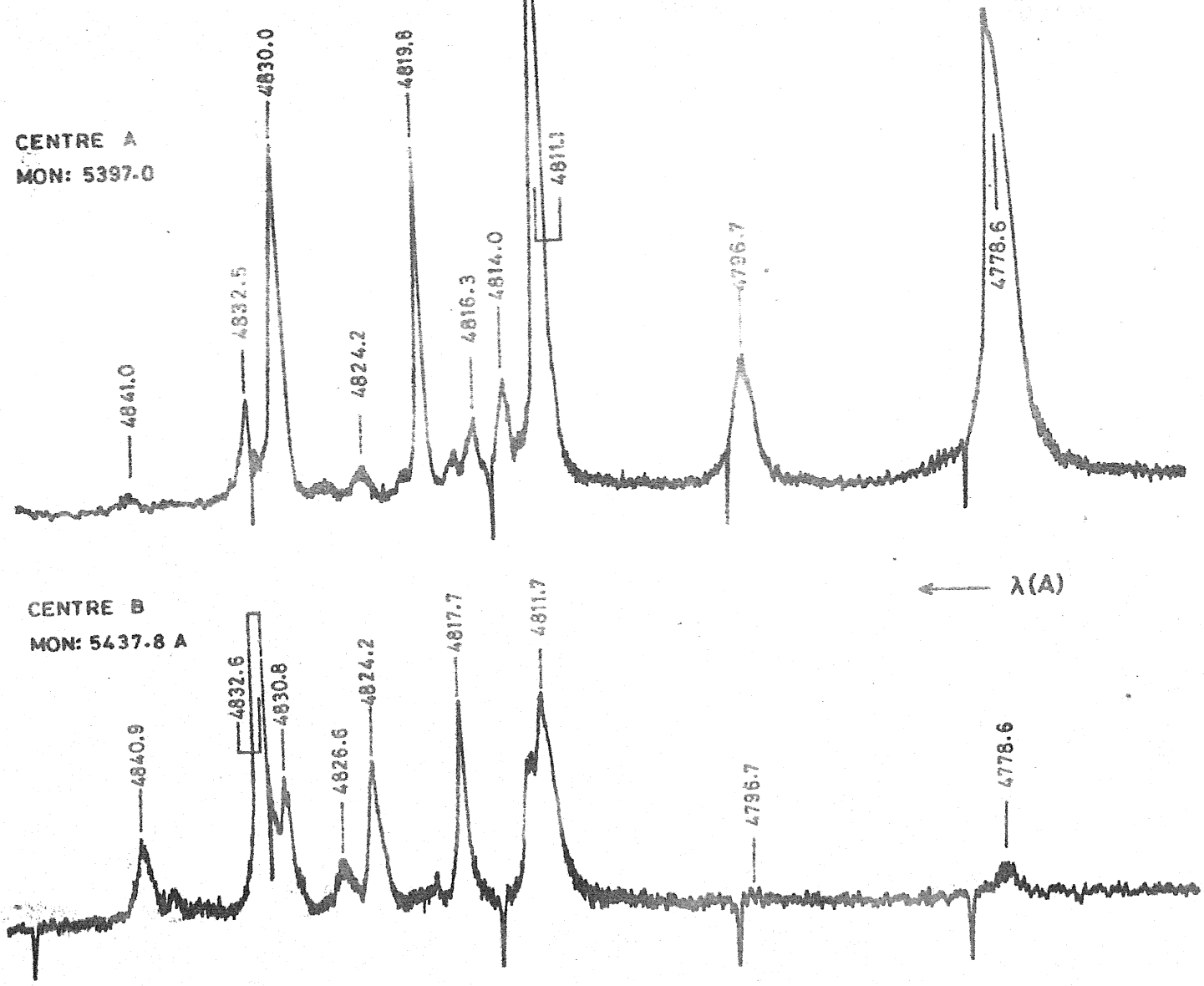

FIG. 4.8 $^5I_8$ (Z) ⟶ $^5F_3$ (F) EXCITATION SPECTRUM OF Ho^{3+}: CaF_2 AT LNT.

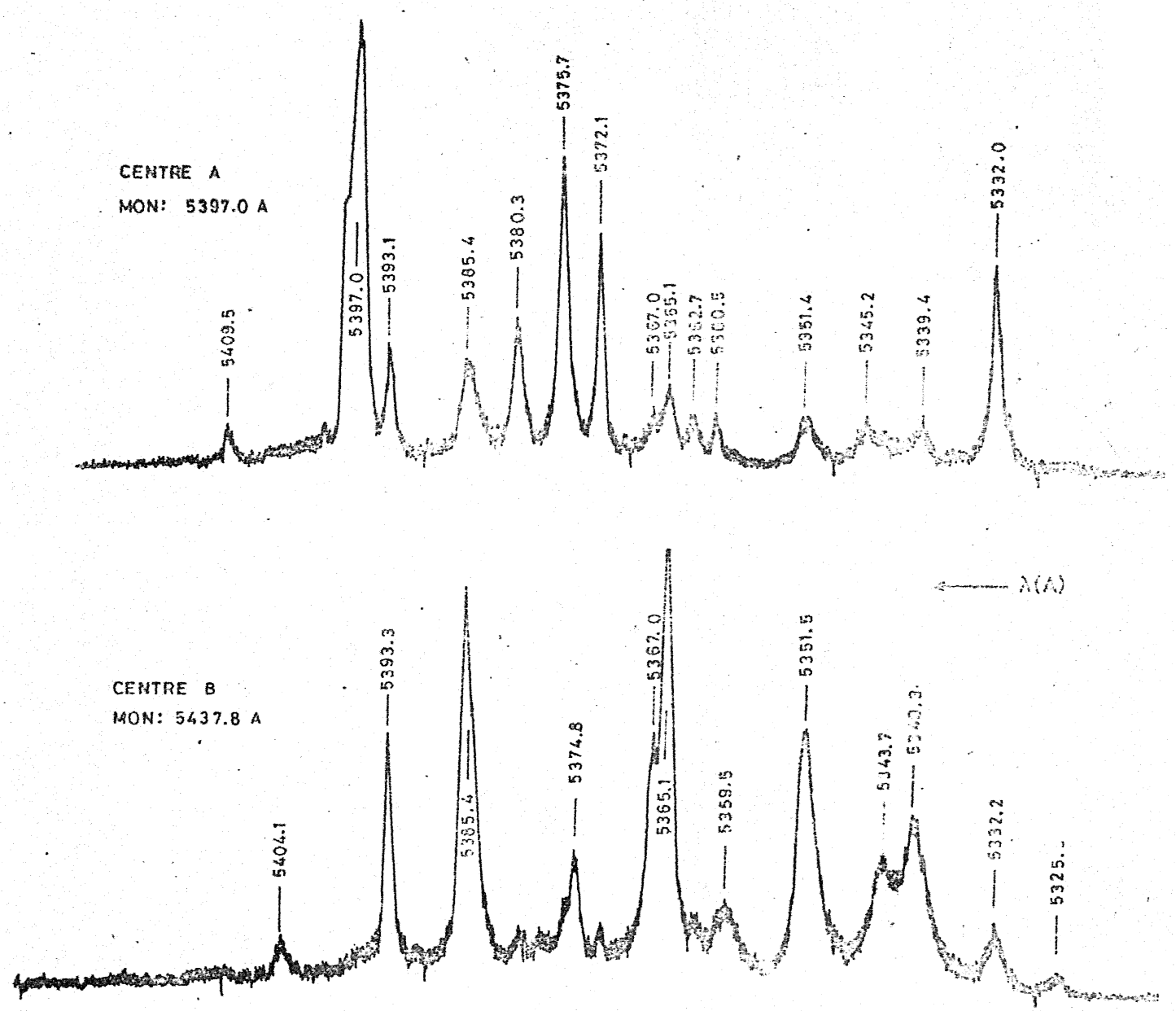

FIG. 4.9 $^5I_8$ (Z) $\longrightarrow$ $^5F_4$ + $^5S_2$ (E) EXCITATION SPECTRUM OF Ho^{3+}:CaF_2 AT LNT.

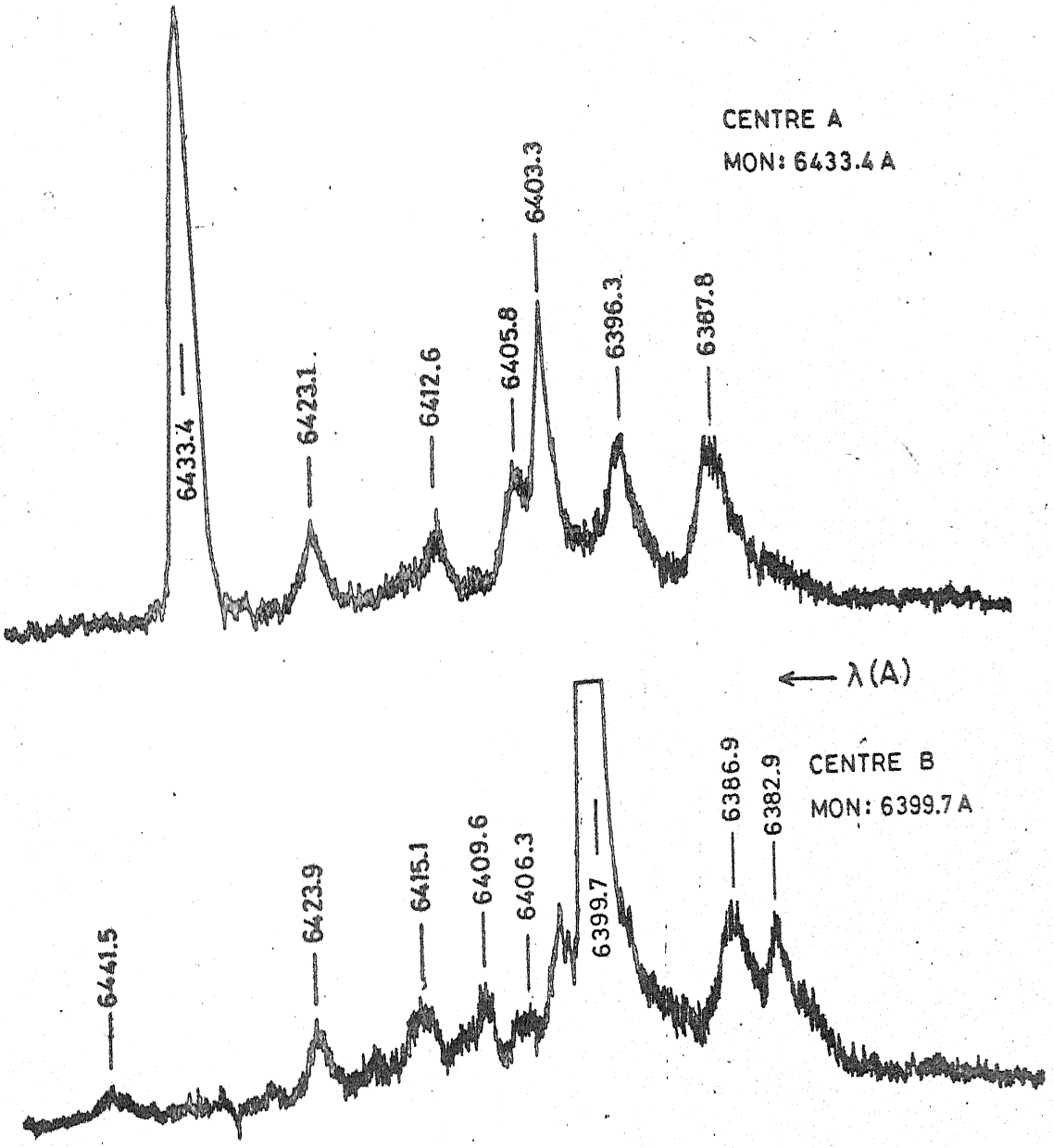

FIG.4.10 $^5I_8(Z) \longrightarrow {}^5F_5(D)$ EXCITATION SPECTRUM OF $Ho^{3+}:CaF_2$ AT LNT.

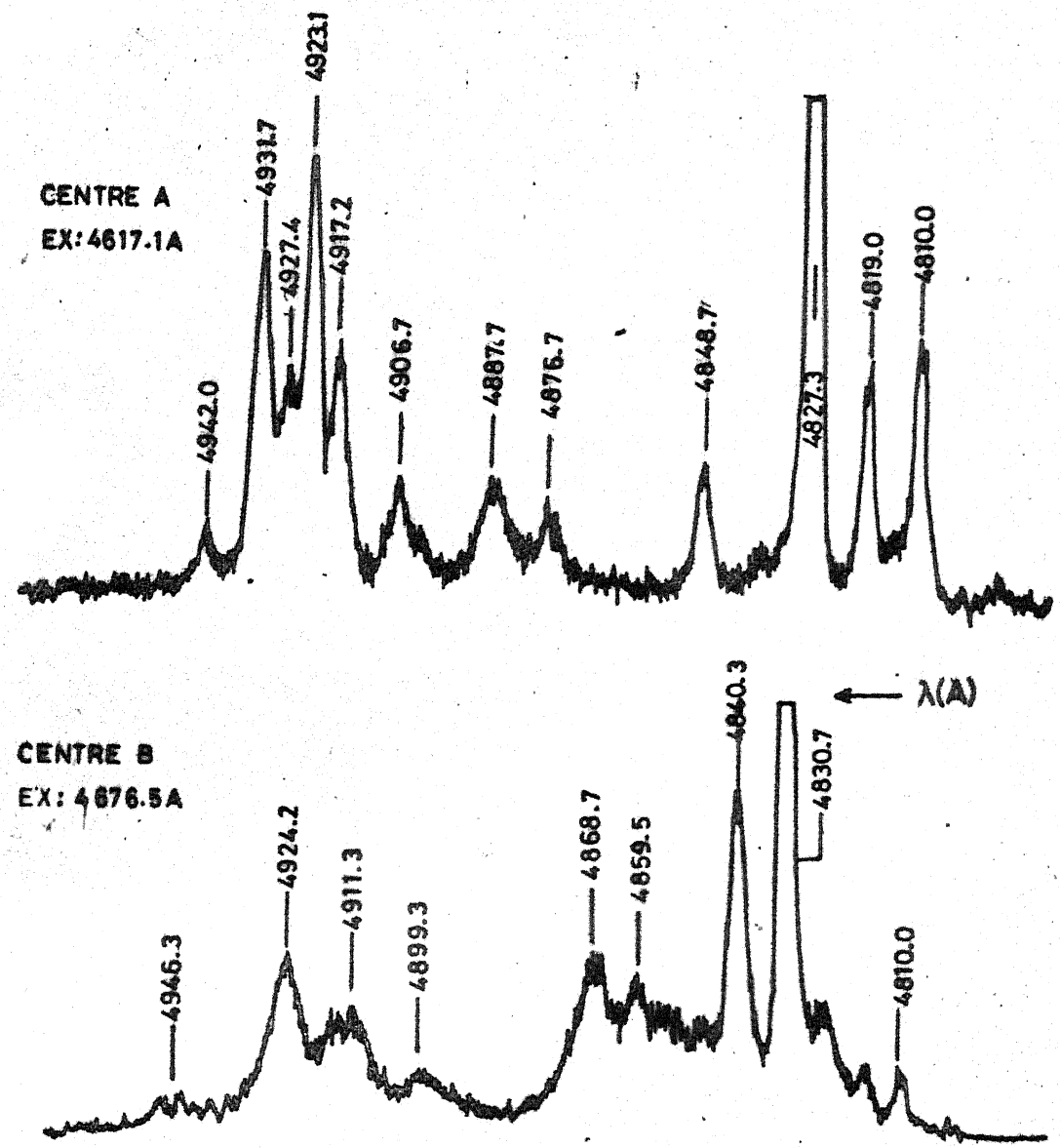

FIG. 4.11 FLUORESCENCE SPECTRUM OF Ho^{3+}: CaF_2 AT LNT; $^5F_3$ (F) $\longrightarrow$ $^5I_8$ (Z) GROUP.

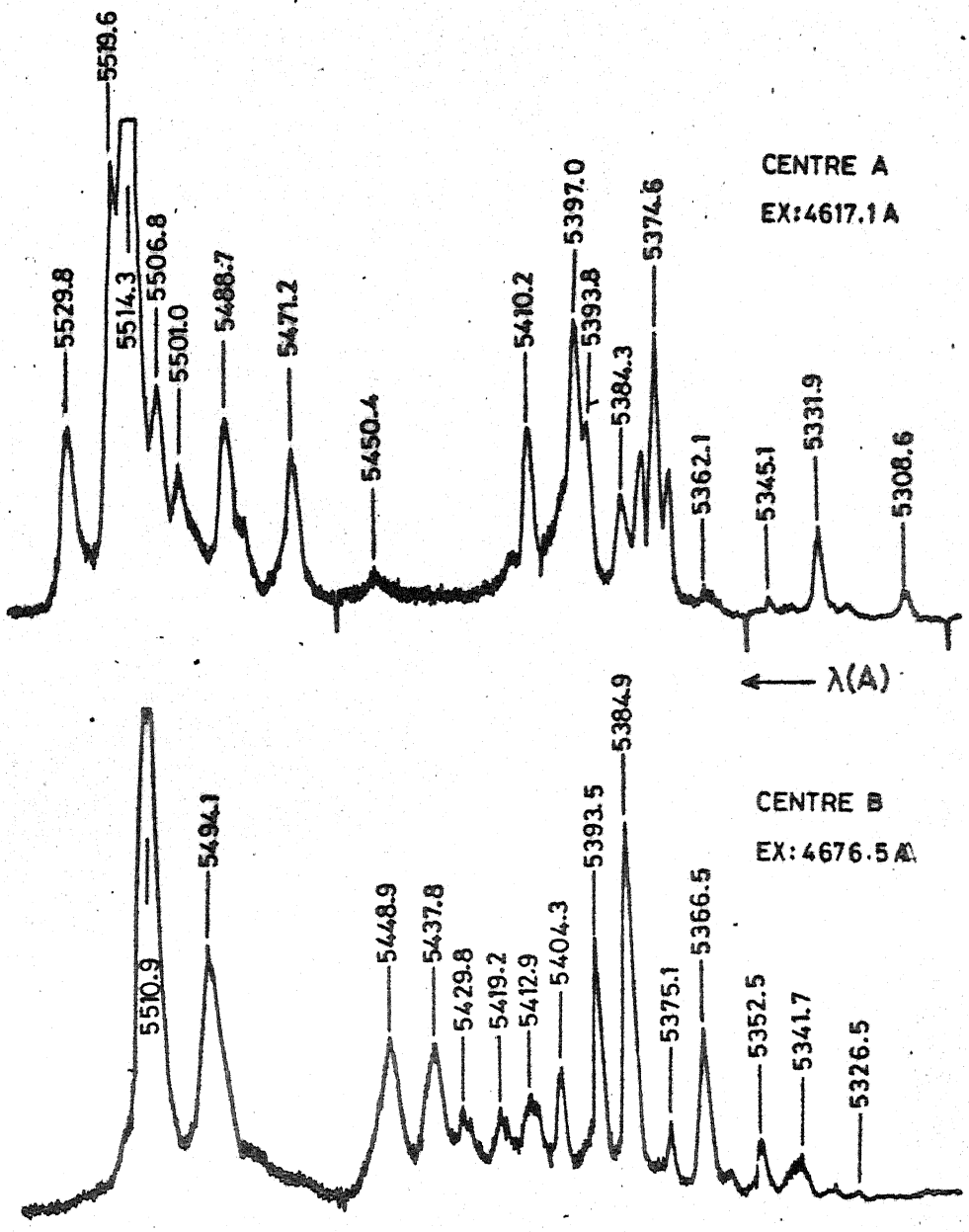

FIG. 4.12 FLUORESCENCE SPECTRUM OF Ho^{3+} : CaF_2 AT LNT; $^5F_4 + ^5S_2(E) \longrightarrow {}^5I_8(Z)$ GROUP.

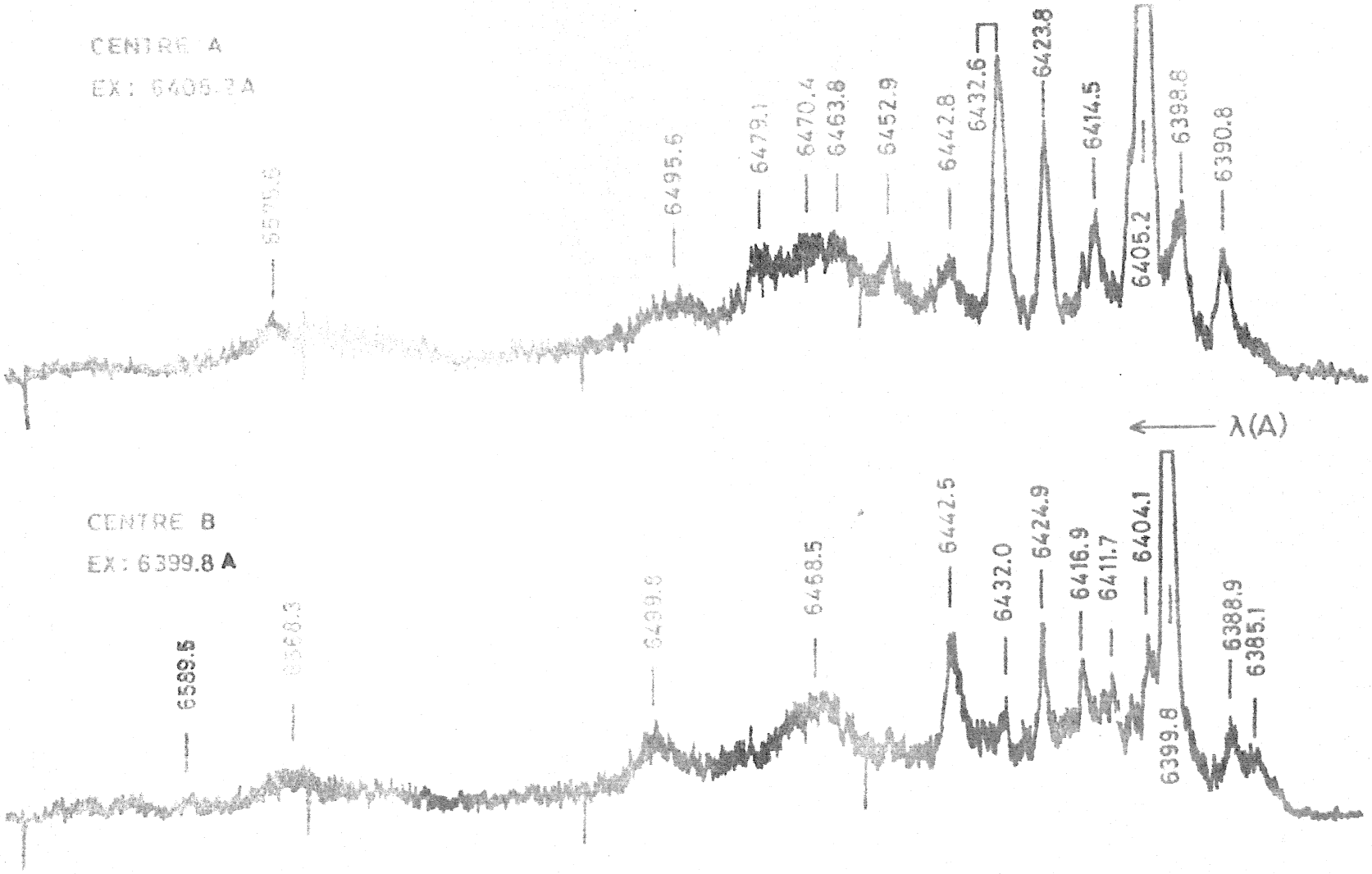

FIG. 4.13 FLUORESCENCE SPECTRUM OF Ho^{3+} CaF_2 AT LNT; $^5F_5$ (D) ⟶ $^5I_8$ (Z) GROUP.

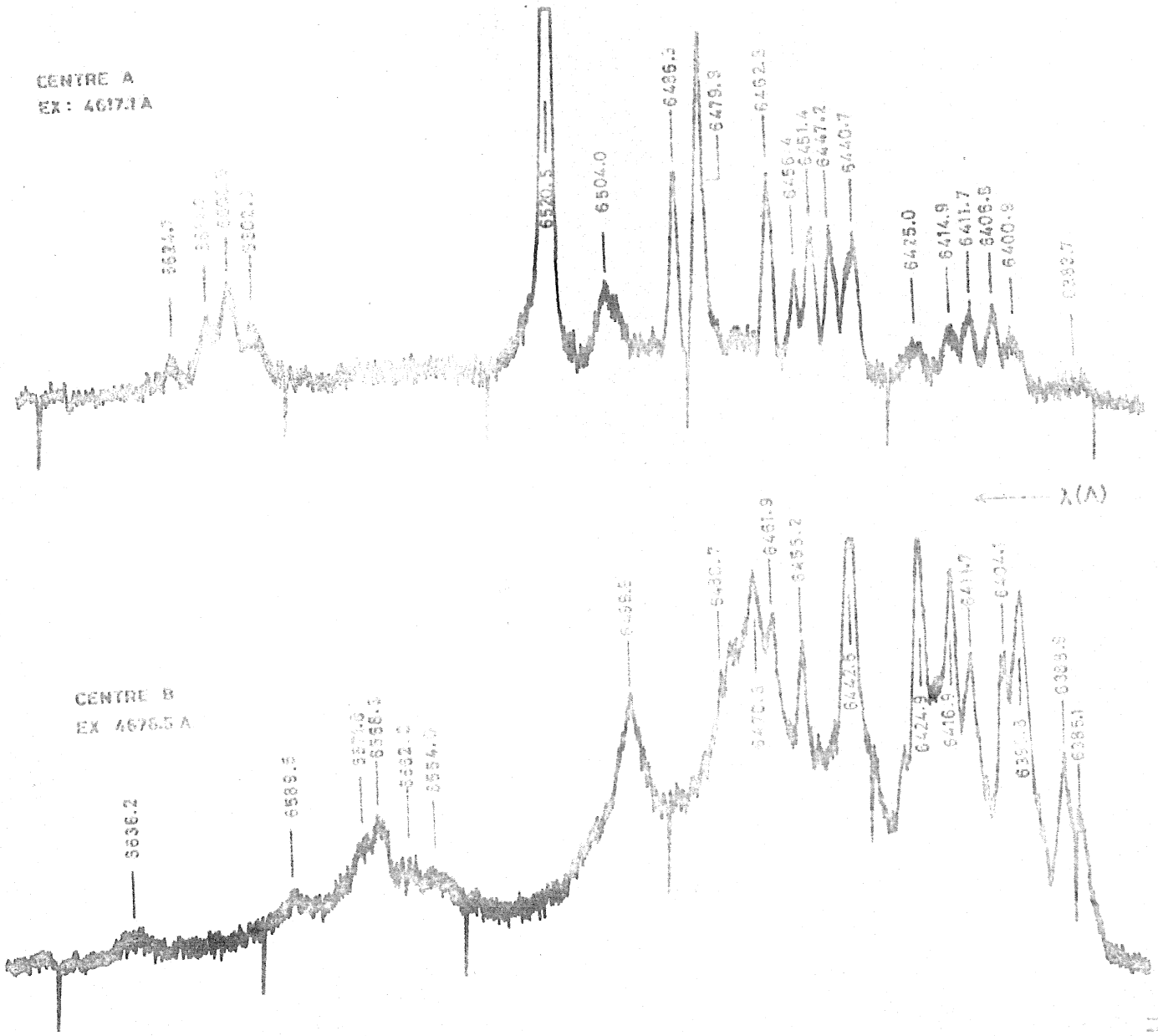

FIG . 4.14 FLUORESCENCE SPECTRUM OF $Ho^{3+}:CaF_2$ AT LNT ; 6500 A GROUP

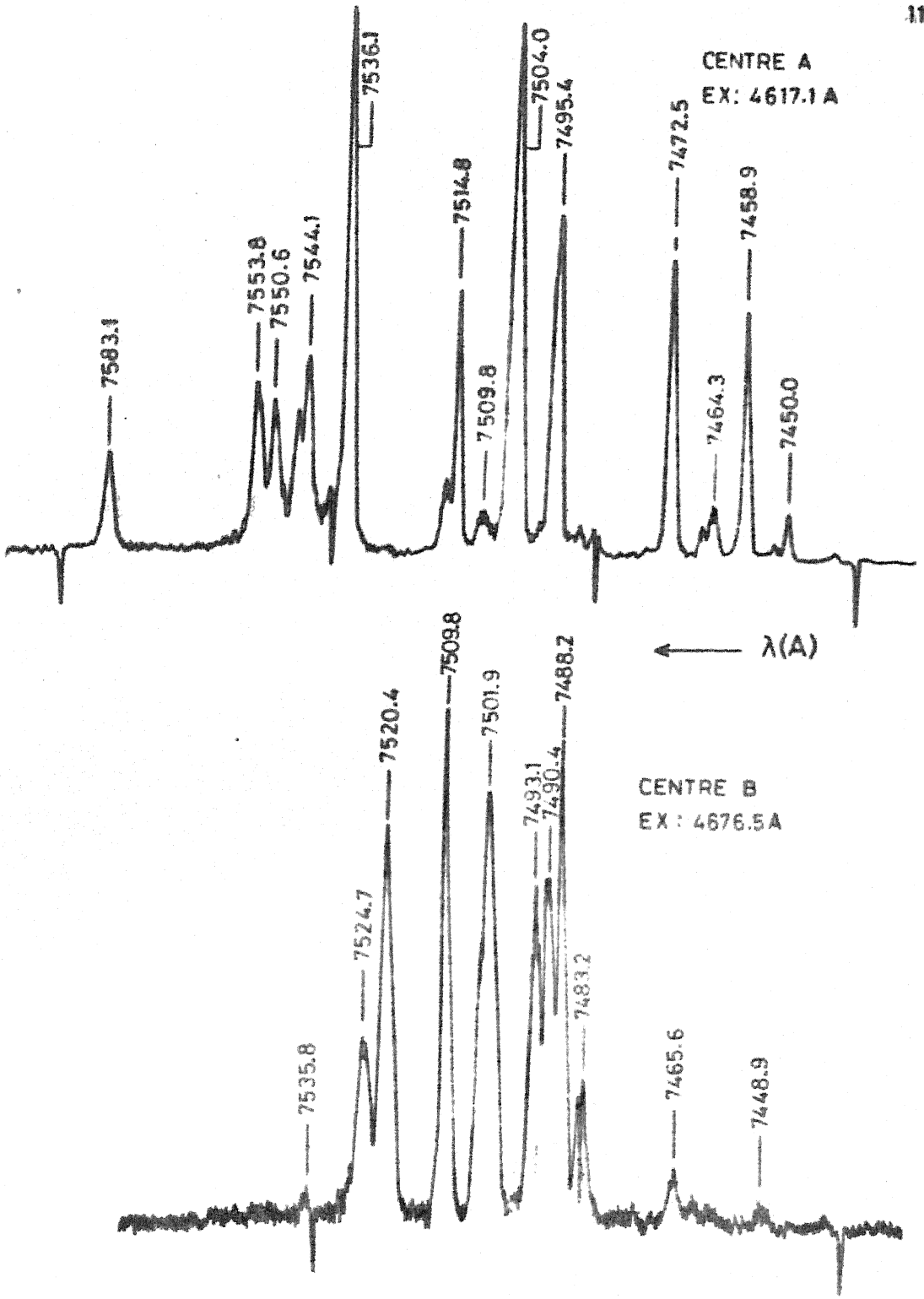

FIG. 4.15 FLUORESCENCE SPECTRUM OF $Ho^{3+}:CaF_2$ AT LNT, $^5F_4 + {}^5S_2(E) \longrightarrow {}^5I_{7,8}$ GROUP.

Table 4.2 : Excitation Spectrum of $Ho^{3+}:CaF_2$ at LNT

Centre A			Centre B		
Wavelength A	Energy cm^{-1}	Intensity (arb.units)	Wavelength A	Energy cm^{-1}	Intensity (arb.units)
		$^5I_8(Z) \rightarrow {}^5G_6 + {}^5F_1$ (I)			
4438.0	22526	7	4422.0	22608	1
4442.6	22503	17	4448.9	22471	4
4448.6	22473	20	4452.2	22455	8
4453.6	22447	6	4459.4	22418	14
4458.3	22424	8	4463.2	22399	16
4467.1	22380	66	4466.3	22384	10
4473.6	22347	13	4473.2	22349	20
4478.6	22322	9	4478.5	22323	32
4483.2	22299	73	4481.8	22306	58
4488.6	22272	100	4486.2	22284	54
4494.4	22244	20	4489.7	22267	105
4497.7	22227	80	4491.3	22259	96
4509.1	22171	30	4493.7	22248	93
4515.2	22141	10	4496.7	22232	16
			4498.9	22221	28
			4503.0	22201	8
			4507.4	22180	18
			4508.9	22172	11
			4513.2	22151	7
			4518.0	22128	6
			4522.5	22106	9
		$^5I_8(Z) \rightarrow {}^3K_8(H) + {}^5F_2(G)$			
4617.1	21653	108	4616.9	21639	30
4620.5	21637	1	4621.9	21630	12

Table 4.2 : (Continued)

Centre A			Centre B		
Wavelength A	Energy cm^{-1}	Intensity (arb.units)	Wavelength A	Energy cm^{-1}	Intensity (arb.units)
			4623.8	21621	10
4625.7	21612	58	4625.9	21611	14
4631.1	21587	16	4631.4	21586	6
4634.0	21574	11	4634 1	21573	9
4643.3	21530	21	4637.2	21559	2
4644.8	21523	14	4643.0	21532	77
4647.5	21511	20	4644.5	21525	14
4648.8	21505	6	4647.5	21511	14
4650.5	21498	3	4648.7	21505	14
4656.2	21471	12	4650.3	21498	34
4659.4	21456	50	4655.5	21474	32
4661.4	21447	115	4656.4	21470	32
4664.6	21432	24	4659.4	21456	22
4665.6	21427	16	4661.5	21446	104
4672.4	21396	7	4665.3	21429	24
4674.7	21386	14	4667.3	21420	32
4677.8	21372	13	4668.8	21413	9
4679.0	21366	10	4670.7	21404	7
4680.6	21359	4	4671.9	21399	7
4682.5	21350	13	4674.6	21386	35
4684.2	21342	7	4676.5	21378	108
4687.8	21326	1	4678.9	21367	16
4691.0	21311	2	4680.5	21359	21
4692.9	21303	4	4682.2	21352	28
4698.4	21278	52	4688.6	21322	10
4703.2	21256	18	4690.6	21313	11
4705.6	21245	12	4698.4	21278	5

Table 4.2 : (Continued)

Centre A			Centre B		
Wavelength A	Energy cm^{-1}	Intensity (arb.units)	Wavelength A	Energy cm^{-1}	Intensity (arb.units)
4714.2	21207	13	4702.8	21258	3
4717.9	21190	16	4713.8	21208	56
4719.0	21185	20	4718.0	21190	13
4721.2	21176	36	4720.2	21180	31
4724.3	21161	19	4727.7	21146	14
4729.9	21136	6			
		$^5I_8(Z) \rightarrow {}^5F_3(F)$			
4778.6	20921	91	4811.7	20777	57
4796.7	20842	22	4812.6	20773	39
4811.1	20780	130	4817.7	20751	47
4814.0	20767	20	4819.8	20742	7
4816.3	20757	11	4821.2	20736	3
4817.9	20750	5	4824.2	20723	38
4819.8	20742	65	4826.6	20713	14
			4830.8	20695	37
4821.3	20736	5	4832.6	20687	160
4824.2	20723	7			
4826.8	20712	3	4836.2	20672	2
4830.0	20698	70	4837.3	20667	2
4832.5	20687	19	4838.8	20661	6
4833.7	20682	3	4840.9	20652	17
4841.0	20651	2			
		$^5I_8(Z) \rightarrow {}^5F_4 + {}^5S_2(E)$			
5332.0	18750	47	5325.3	18773	6
5339.4	18724	10	5332.2	18749	18

Table 4.2 : (Continued)

Centre A			Centre B		
Wavelength A	Energy cm^{-1}	Intensity (arb.units)	Wavelength A	Energy cm^{-1}	Intensity (arb.units)
5345.2	18703	10	5340.3	18720	51
5360.5	18650	14	5343.7	18708	37
5362.7	18642	12	5351.5	18681	75
5372.1	18610	52	5359.5	18653	24
5375.7	18597	70	5362.3	18644	20
5380.3	18581	35	5363.2	18640	20
5385.4	18564	27	5365.1	18634	125
5393.1	18537	26	5366.8	18628	68
5397.0	18524	- [α]	5372.0	18610	18
5399.8	18514	9	5374.8	18600	40
5409.5	18481	8	5378.2	18588	15
			5380.4	18581	15
			5385.4	18564	110
			5393.3	18536	70
			5404.1	18499	14
		$^5I_8(Z) \rightarrow {}^5F_5(D)$			
6387.8	15651	29	6382.9	15663	30
6396.3	15630	29	6386.9	15653	32
6403.3	15613	50	6399.7	15621	~ 60
6405.8	15607	24	6403.0	15613	29
6409.3	15598	8	6406.3	15605	15
6412.6	15590	14	6409.6	15597	18
6423.1	15565	15	6411.8	15592	13
			6415.1	15584	18
			6419.1	15574	9
			6423.9	15563	13
			6427.6	15554	5
			6432.2	15543	4
			6434.2	15538	3
			6441.5	15520	5

[α] These positions correspond to the laser excitation wavelengths and hence the actual intensities of the lines cannot be estimated.

Table 4.3 : Fluorescence Spectrum of Ho^{3+}:CaF_2 at LNT

Centre A			Centre B		
Wavelength A	Energy cm^{-1}	Intensity (arb.units)	Wavelength A	Energy cm^{-1}	Intensity (arb.units)
		$^5F_3(F) \rightarrow {}^5I_8(Z)$			
4810.0	20784	44	4810.0	20784	9
4819.0	20745	40	4816.9	20754	10
4827.3	20710	150	4823.3	20727	19
4848.7	20618	23	4830.7	20695	109
4876.7	20500	15	4840.3	20654	55
4887.7	20454	20	4853.5	20598	18
4906.7	20375	19	4859.5	20573	23
4917.2	20331	40	4868.7	20534	27
4923.1	20307	73	4886.2	20460	4
4927.4	20289	37	4899.3	20405	8
4931.7	20271	57	4911.3	20356	17
4942.0	20229	10	4914.8	20341	17
			4924.2	20302	27
			4946.3	20212	6
			4961.9	20148	2
		$^5F_4 + {}^5S_2$ (E) $\rightarrow {}^5I_8(A)$			
5293.2+	18887	1	5326.5	18769	2
5308.6+	18832	6	5333.0	18746	4
5323.9+	18787	3	5341.7	18715	9
5331.9	18750	21	5344.9	18704	9
5338.8	18726	3	5352.5	18678	15
5345.1	18704	4	5366.5	18628	42
5360.5	18650	8	5375.1	18599	19
5362.1	18644	8	5384.9	18565	93
5371.6	18611	36	5393.5	18536	65

Table 4.3 : (Continued)

Centre A			Centre B		
Wavelength A	Energy cm^{-1}	Intensity (arb.units)	Wavelength A	Energy cm^{-1}	Intensity (arb.units)
5374.6	18601	67	5404.3	18499	34
5379.0	18586	40	5412.9	18469	27
5384.3	18567	30	5419.2	18448	23
5393.8	18535	47	5429.8	18412	24
5397.0	18524	72	5437.8	18385	40
5410.2	18479	46	5448.9	18347	42
5450.4	18342	13	5471.3	18272	9
5471.2	18272	41	5494.1	18196	64
5483.9	18230	25	5510.9	18141	~125
5488.7	18214	49			
5501.0	18176	37			
5506.8	18154	56			
5514.3	18130	~150			
5519.6	18112	110			
5529.8	18079	46			
		$^5F_5(D) \rightarrow {}^5I_8(Z)$			
6390.8	15643	41	6382.3	15664	11
6398.8	15624	59	6385.1	15657	16
6405.2	15608	- [α]	6388.9	15648	22
6414.5	15585	35	6399.8	15621	- [α]
6423.8	15563	58	6407.9	15601	31
6432.6	15542	76	6411.7	15592	35
6452.9	15493	22	6416.9	15580	42
6463.8	15467	30	6420.7	15570	30
6470.4	15451	30	6424.9	15560	47
6475.6	15438	11	6442.5	15518	47
6479.1	15430	26	6468.5	15455	34

Table 4.3 : (Continued)

Centre A			Centre B		
Wavelength A	Energy cm^{-1}	Intensity (arb.units)	Wavelength A	Energy cm^{-1}	Intensity (arb.units)
6495.6	15391	15	6488.7	15407	19
			6499.8	15381	23
			6557.5	15246	12
			6568.3	15220	14
			6589.5	15171	13
			6636.2	15065	4
		$^5F_3(F) \rightarrow {}^5I_7(Y)$			
6383.7	15661	8	6451.6	15496	62
6400.9	15619	18	6455.2	15487	62
6406.8	15604	25	6461.9	15471	83
6411.7	15592	22			
6414.9	15584	19			
6425.0	15560	15			
6440.7	15522	40			
6447.2	15506	44			
6451.5	15496	45			
6456.4	15484	35			
6462.8	15469	57			
6470.9	15450	18			
6479.9	15428	94			
6486.3	15413	58			
6493.9	15395	17			
6504.0	15371	29			
6520.5	15332	180			
6554.4	15253	11			
6572.2	15211	10			

Table 4.3 : (continued)

Centre A			Centre B		
Wavelength A	Energy cm^{-1}	Intensity (arb.units)	Wavelength A	Energy cm^{-1}	Intensity (arb.units)
6602.3+	15142	17			
6608.5+	15128	28			
6614.7+	15114	19			
6624.7+	15091	10			
	$^5F_4 + {}^5S_2$ (E) → $^5I_7$(Y)				
7441.0	13435	1	7436.2	13444	2
7450.0	13419	7	7448.9	13421	4
7452.0	13416	2	7458.5	13404	4
7458.9	13403	44	7461.5	13398	5
7464.3	13393	9	7465.6	13391	11
7466.2	13390	5	7469.0	13385	3
7472.5	13379	59	7475.7	13373	3
7495.4	13338	65	7483.2	13360	25
7497.8	13334	5	7488.2	13351	91
7504.0	13323	99	7490.4	13347	64
7514.8	13303	49	7493.1	13342	62
7517.0	13300	14	7501.9	13326	82
7526.9	13282	2	7509.8	13312	97
7536.1	13266	101	7515.1	13303	3
7539.3	13260	13	7520.4	13294	75
7544.1	13252	36	7524.7	13286	34
7546.3	13248	26	7535.8	13266	6
7550.6	13240	29			
7553.8	13235	32			
7583.1	13184	18			

α These positions correspond to the laser excitation wavelengths and hence the actual intensities of the lines cannot be estimated.

\+ The transition assignments for these lines are not shown in the figures 4.19 and 4.20.

absent. However the 5 percent concentration crystal shows an entirely different type of spectrum which is discussed in section 4.7.

As discussed in Chapter 3, by selectively exciting each absorption line of both the centres, the decay time (decay times) of each fluorescence line is studied to confirm the classification of the lines made through the steady state spectra.

Lines in the excitation spectra, are classified by measuring the decay times of two representative lines, 5397.0A of centre A and 5437.8A of centre B. Similarly the decay times of all the fluorescence lines are measured by choosing two excitations for each centre (4617.1 A and 4778.6A of centre A and 4676.5A and 4826.8A of centre B). The decay times, thus measured, agreed with each other within the experimental errors. The decay times of the different fluorescing levels are summarised in table 4.4. Decay times which are intermediate between those of centres A and B are observed in the case of overlapping fluorescence lines.

Transient behaviour of 5393.6A line of $^5F_4 + {}^5S_2 \rightarrow {}^5I_8$ transition which is present in both the centres is also studied by selectively exciting with each absorption line recorded in the excitation spectrum. A variation of decay times from 460 μs to 1100 μs is observed when excited with

different A centre lines. An excitation of B centre lines resulted in a variation of decay times from 330 μs to 600 μs. In all the cases the decay curves are found to fit to single exponentials. The variation in the decay times over such a range initially lead to the supposition that several centres of holmium are present in CaF_2.

Table 4.4 : Decay Times of Different Fluorescing Levels of $Ho^{3+}:CaF_2$

Fluorescing Level	Centre A	Centre B
$^5F_3(F)$	10 μs	18 μs
$^5F_4 + {}^5S_2(E)$	1100 μs	330 μs
$^5F_5(D)$	118 μs	145 μs

To identify whether these variations are due to the presence of different centres or due to simultaneous presence of two exponentials with decay times 330 μs and 1100 μs of centres B and A respectively (since the spectra always contained only two sets of lines), curves f(t) of the type

$$f(t) = x\, e^{-t/330} + y\, e^{-t/1100}$$

are drawn for different values of x and y ranging between x = 1.0, y = 0.2; and x = 0.05 and y = 1.0. They all seem to have shapes that differ very little (within experimental errors) from single exponentials with apparent characteristic times lying between 330 μs and 1100 μs, the exact value depending on x/y. That there are in fact only two centres is confirmed by the fact that the fluorescence lines which have no overlap show decay times of either 330 μs or 1100 μs only when excited on any one of the lines present in the respective excitation spectra.

Tables 4.2 and 4.3 list the excitation and fluorescence lines classified into different centres. Variation of dye laser power with wavelength is not taken into account in giving the intensities of the lines in table 4.2.

4.6 Results and Discussion

Two different schemes for the Stark components of the levels $^5I_8$, $^5I_7$, $^5F_5$, $^5F_4 + {}^5S_2$, $^5F_3$, $^3K_8 + {}^5F_2$ and $^5G_6$ are derived from the observed fluorescence and excitation spectra of the two centres. Partial energy level diagrams of $Ho^{3+}:CaF_2$ showing the fluorescence and excitation spectra of different groups of both these centres are shown in figures 4.16 through 4.21. Since the experiments are done at LNT, several Stark components of the participating levels could

be populated as indicated earlier and contribute to fluorescence or absorption. This complicates the analysis significantly.

To arrive at a set of Stark components the following procedure is adopted.

It is assumed that the strong lines in the spectra are due to the lower Stark components of the originating level. The assumption could have been checked by looking at the intensities of these lines in the spectra recorded at higher temperatures. This could however lead to erroneous conclusion in the present case for the following reason. The J values of all the participating levels are large and at high temperature the number of thermally accessible levels increases. This leads to a large increase in the number of lines and probability of overlaps between lines of different centres, that would make intensity comparisons unreliable. Difference tables are constructed for each group of the excitation spectrum. From these tables a set of numbers are arrived at, for the ground level (taking care that all these differences appear in all the tables). Similarly difference tables are constructed for all the fluorescence groups terminating at $^5I_8$ (the ground level), and the upper Stark components are derived from them.

The Stark components of the excited levels are obtained by adding the energies of the absorption lines (from the excitation spectrum) to the ground level Stark components and a minimum number of Stark components which explain all the transitions are chosen. As a cross check, it has been varified that the energy differences between the Stark components of each group are present in the difference table for the corresponding fluorescence group. In other words both the fluorescence and absorption are taken into account to arrive at the Stark splittings for the upper levels. The set of energy levels (table 4.5) derived for $Ho^{3+}:CaF_2$ are one possible set which explains all the fluorescence and absorption lines observed in the present experiments.

4.6.1 The Ground Level, $^5I_8(Z)$

From the difference tables constructed for each group of the excitation spectrum of centre A, one set of Stark components at 0, 7, 33, 75, 100 and 141 cm^{-1} of the ground level are seen to explain the excitation spectra of different SLJ levels. With a choice of Stark ~~levels~~ components other than the particular set mentioned above, all the absorption lines and the relative intensities in the excitation spectra could not be explained. Most of the weak absorption lines are attributed as due to the Stark components above 75 cm^{-1}.

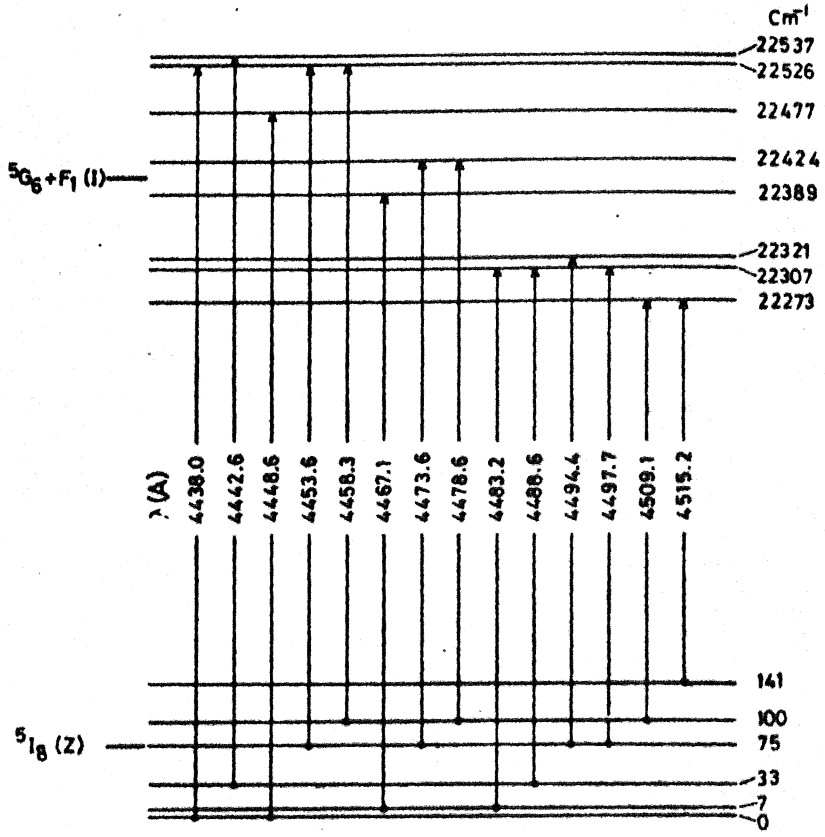

FIG.4.16a PARTIAL ENERGY LEVEL DIAGRAM OF Ho^{3+} : CaF_2 SHOWING THE OBSERVED ABSORPTION LINES OF $^5I_8 \longrightarrow {}^5G_6 + {}^5F_1$ TRANSITION IN THE EXCITATION SPECTRUM OF CENTRE A AT LNT.

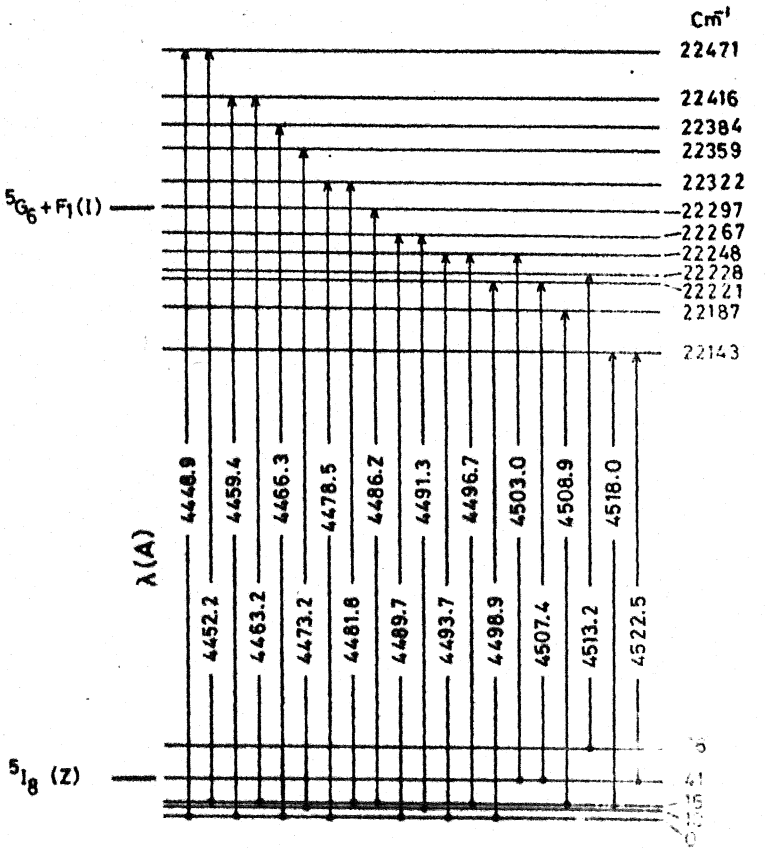

FIG.4.16b PARTIAL ENERGY LEVEL DIAGRAM OF Ho^{3+} : CaF_2 SHOWING THE OBSERVED ABSORPTION LINES OF $^5I_8 \longrightarrow {}^5G_6 + {}^5F_1$ TRANSITION IN THE EXCITATION SPECTRUM OF CENTRE B AT LNT.

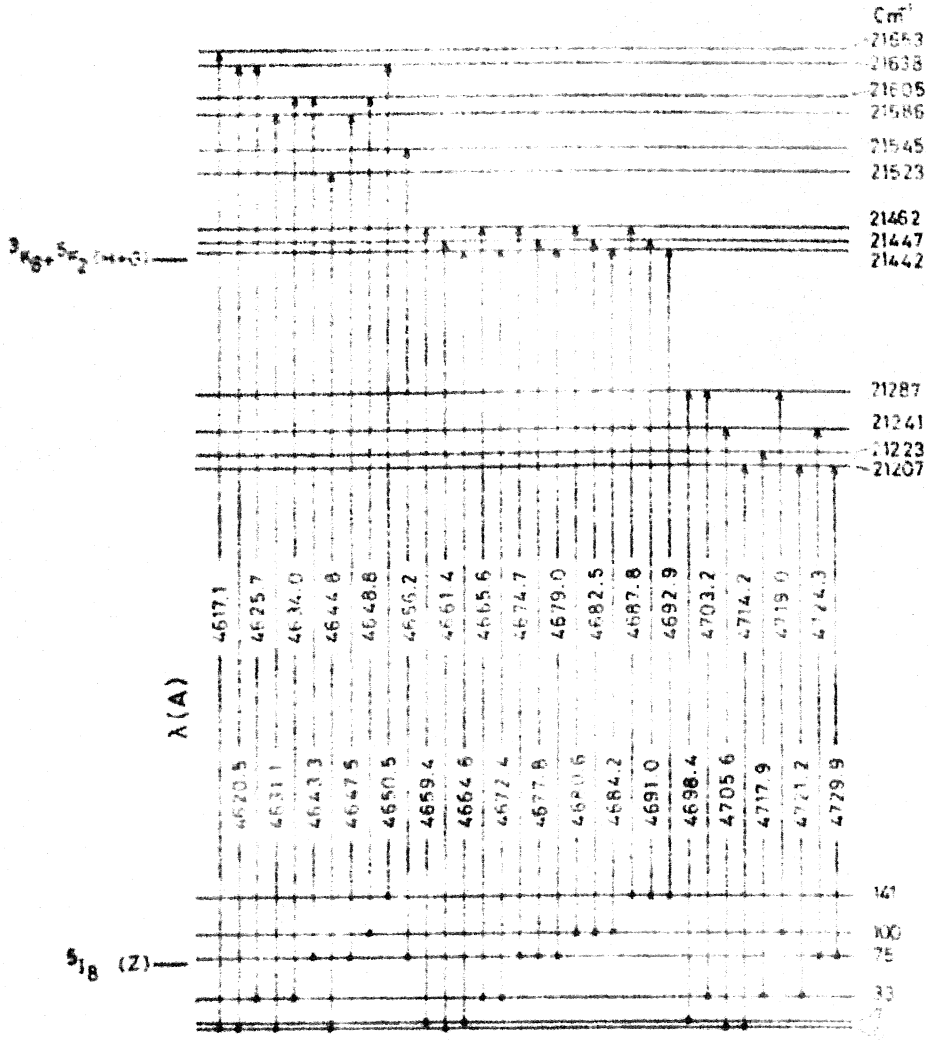

FIG.4.17a PARTIAL ENERGY LEVEL DIAGRAM OF $Ho^{3+}:CaF_2$ SHOWING THE OBSERVED ABSORPTION LINES OF $^5I_8 \longrightarrow {}^3K_8 + {}^5F_2$ TRANSITION IN THE EXCITATION SPECTRUM OF CENTRE A AT LNT.

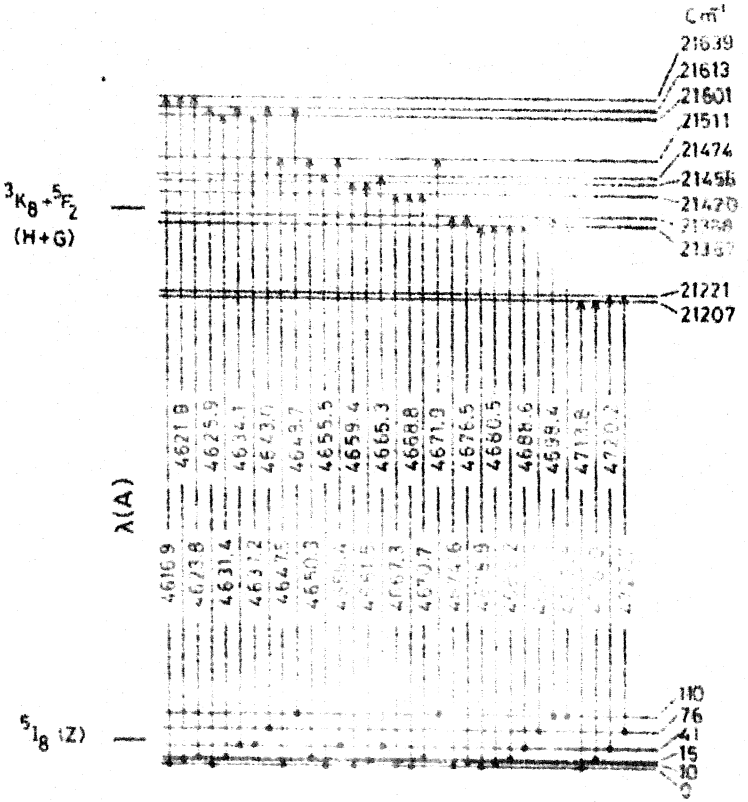

FIG 4.17b PARTIAL ENERGY LEVEL DIAGRAM OF $Ho^{3+}:CaF_2$ SHOWING THE OBSERVED ABSORPTION LINES OF $^5I_8 \longrightarrow {}^3K_8 + {}^5F_2$ TRANSITION IN THE EXCITATION SPECTRUM OF CENTRE B AT LNT

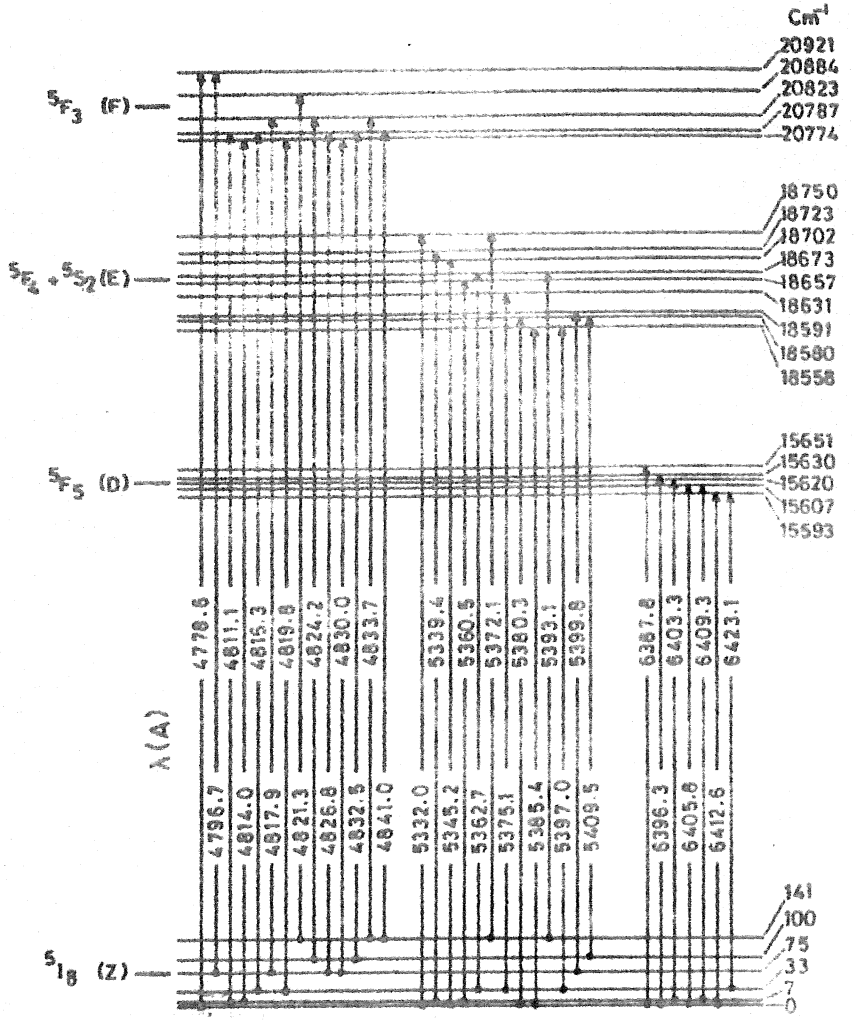

FIG. 4.18a PARTIAL ENERGY LEVEL DIAGRAM OF Ho^{3+}: CaF_2 SHOWING THE OBSERVED ABSORPTION LINES OF $^5I_8 \longrightarrow {}^5F_3, {}^5F_4 + {}^5S_2$ AND $^5F_5$ TRANSITIONS IN THE EXCITATION SPECTRUM OF CENTRE A AT LNT.

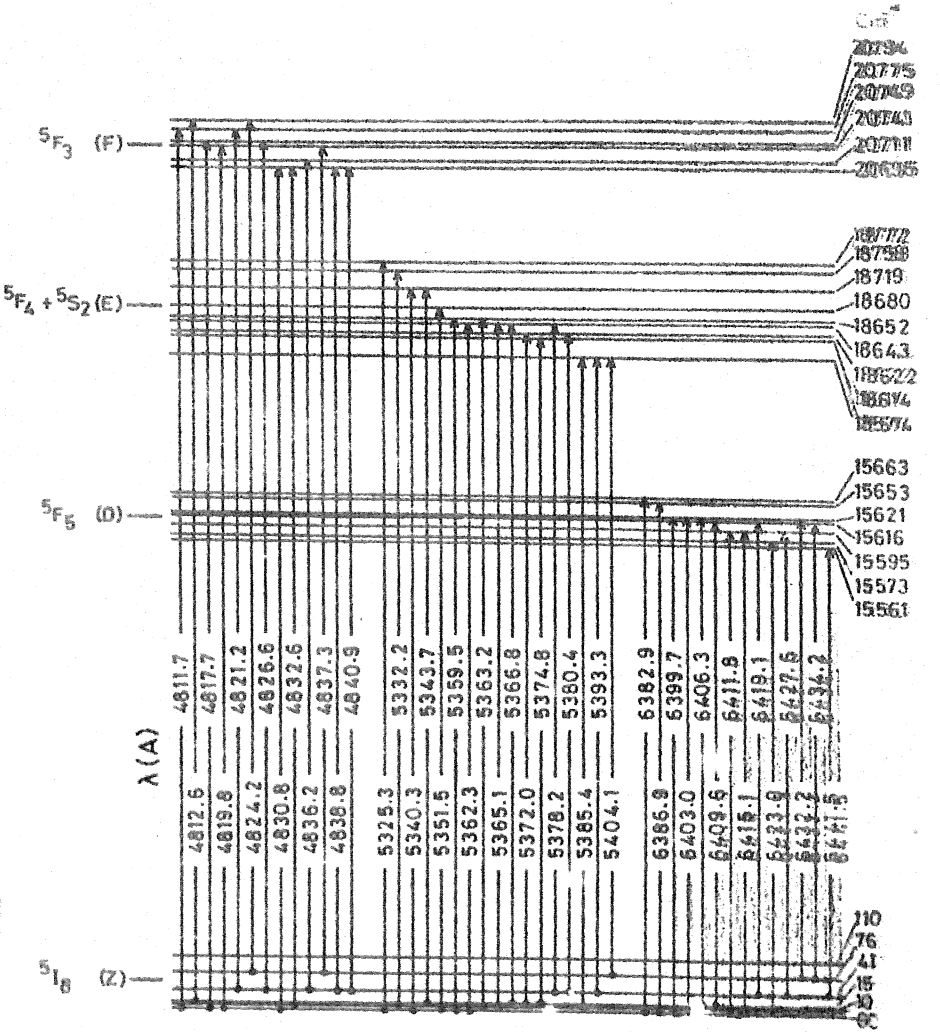

FIG. 4.18b PARTIAL ENERGY LEVEL DIAGRAM OF Ho^{3+}: CaF_2 SHOWING THE OBSERVED ABSORPTION LINES OF $^5I_8 \longrightarrow {}^5F_3, {}^5F_4 + {}^5S_2$ AND $^5F_5$ TRANSITIONS IN THE EXCITATION SPECTRUM OF CENTRE B AT LNT.

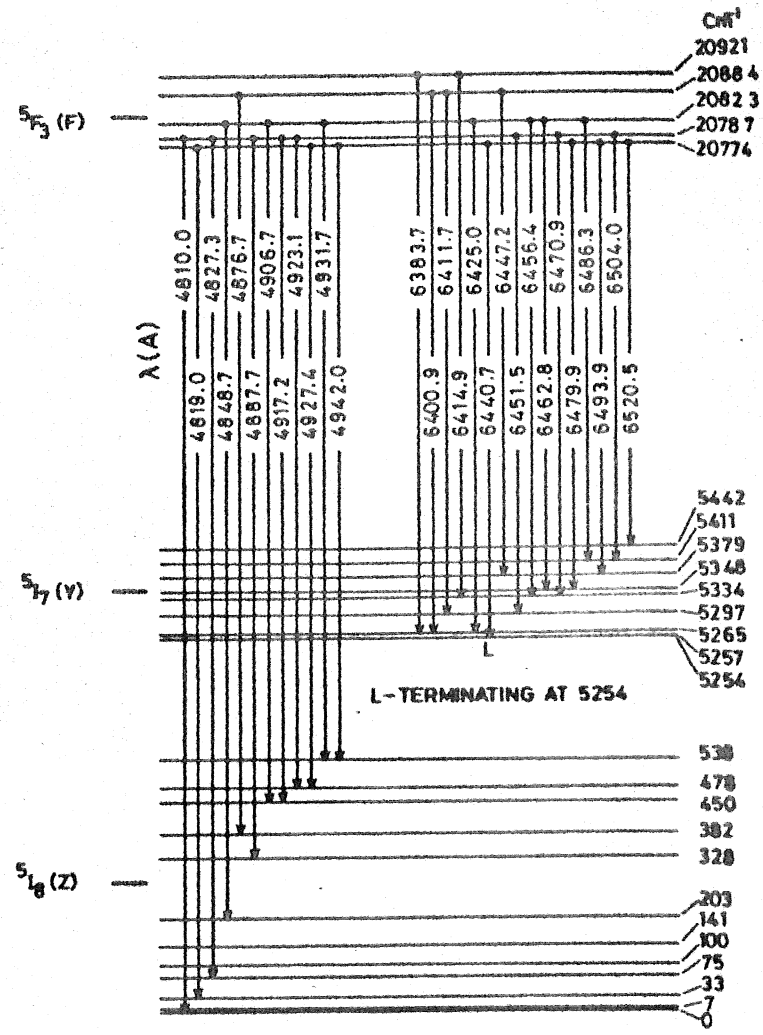

FIG.4.19a PARTIAL ENERGY LEVEL DIAGRAM OF Ho^{3+}: CaF_2 SHOWING THE OBSERVED FLUORESCENCE LINES OF $^5F_3 \longrightarrow {}^5I_8$ & $^5I_7$ TRANSITIONS OF CENTRE A AT LNT.

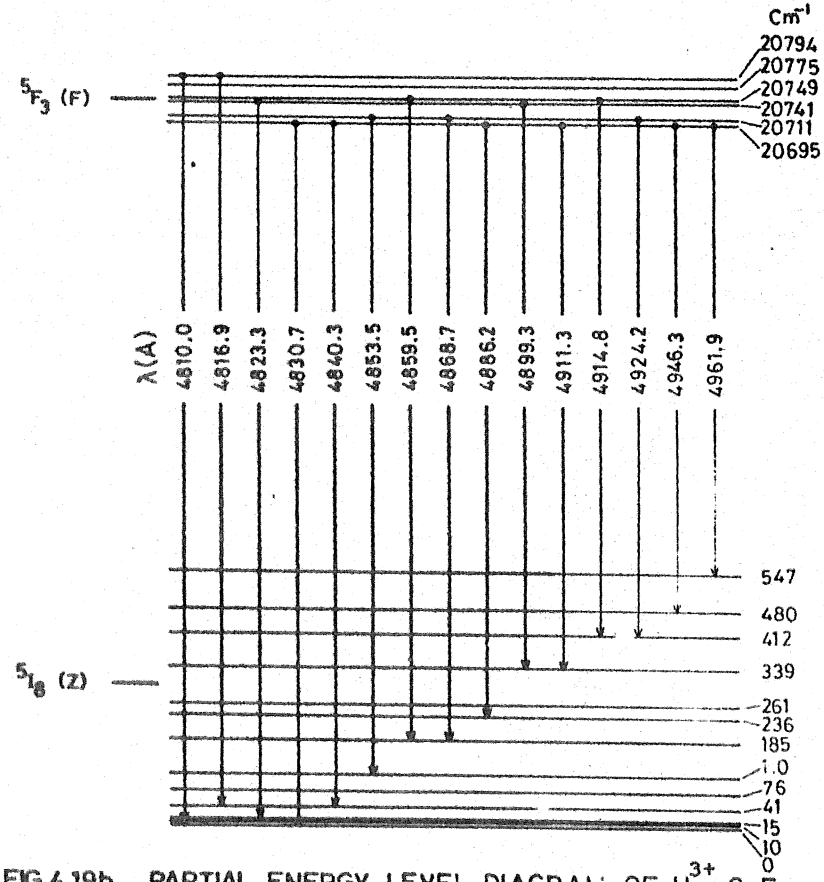

FIG.4.19b PARTIAL ENERGY LEVEL DIAGRAM OF Ho^{3+}: CaF_2 SHOWING THE OBSERVED FLUORESCENCE LINES OF $^5F_3 \longrightarrow {}^5I_8$ TRANSITION OF CENTRE B AT LNT.

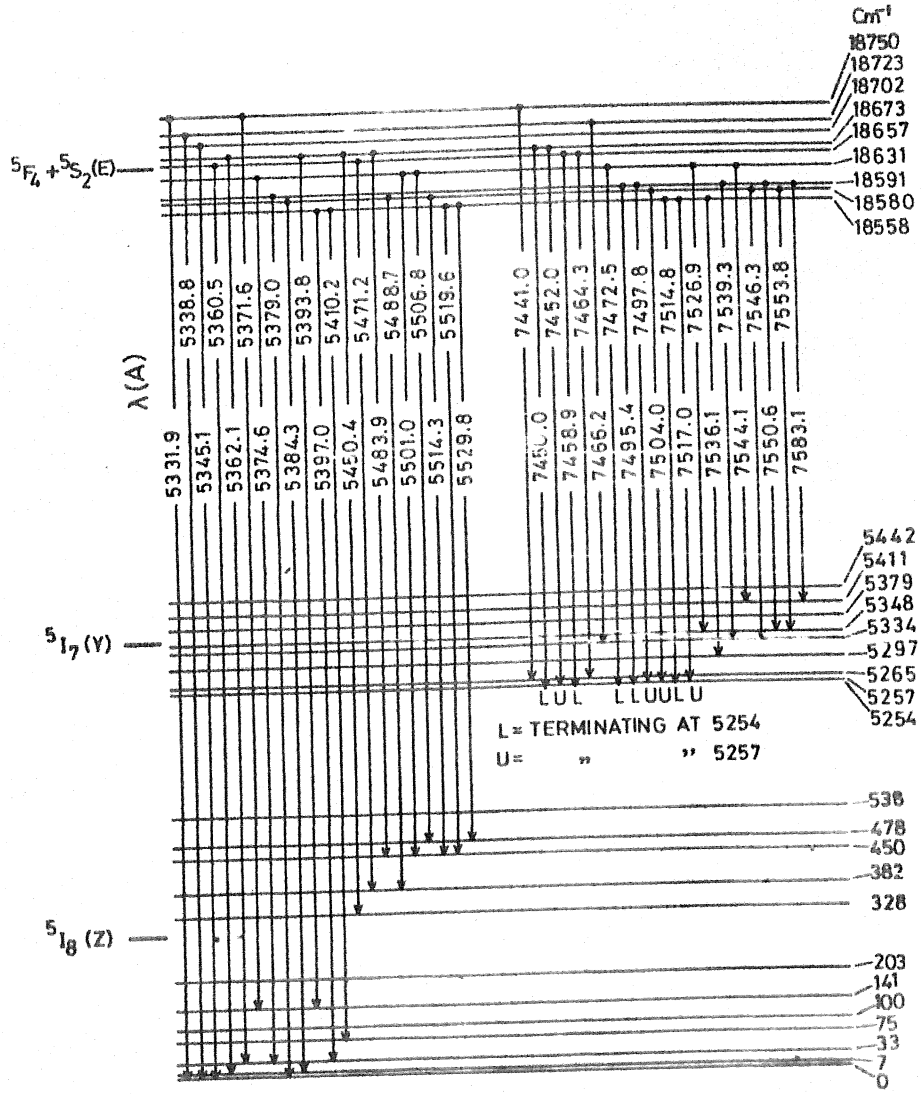

FIG.4.20a PARTIAL ENERGY LEVEL DIAGRAM OF Ho^{3+}: CaF_2 SHOWING THE FLUORESCENCE LINES OF $^5F_4 + ^5S_2 \longrightarrow ^5I_8$ and $^5I_7$ TRANSITIONS OF CENTRE A AT LNT.

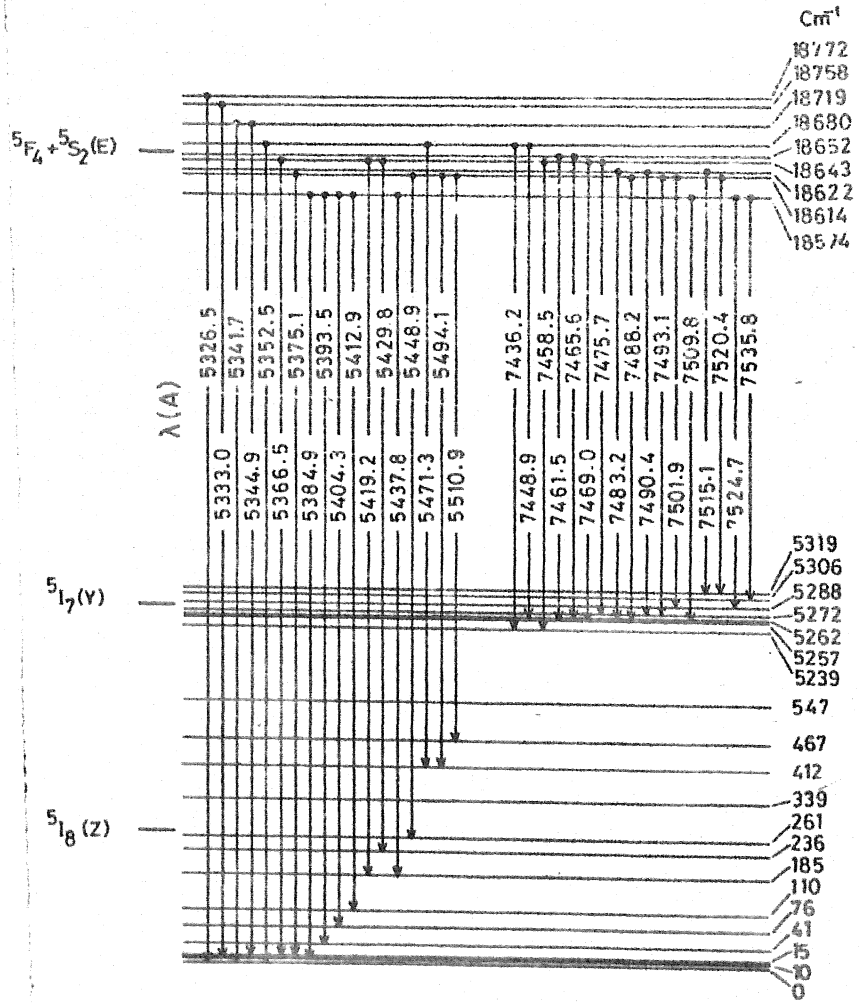

PARTIAL ENERGY LEVEL DIAGRAM OF Ho^{3+}: CaF_2 SHOWING THE OBSERVED FLUORESCENCE LINES OF $^5F_4 + ^5S_2 \longrightarrow ^5I_8$ AND $^5I_7$ TRANSITION OF CENTRE B AT LNT.

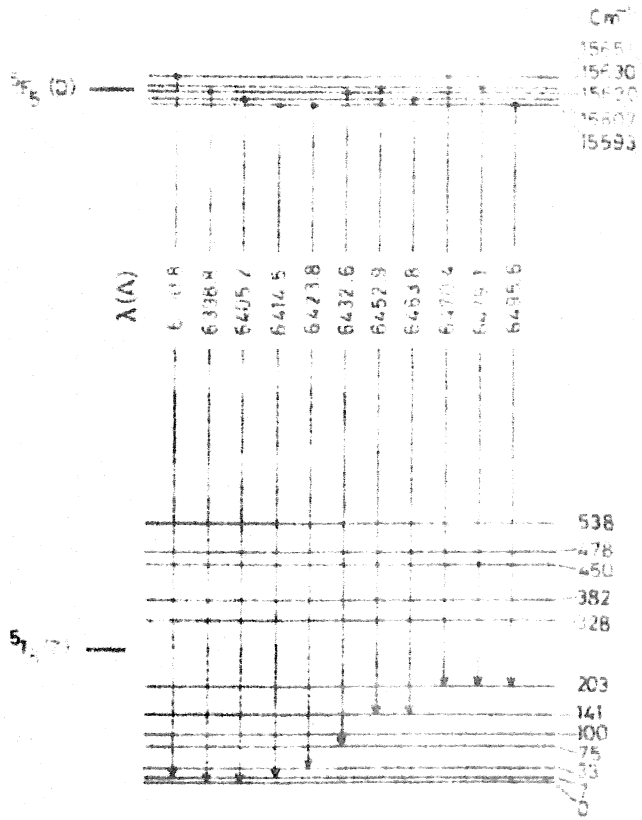

FIG.4.21a PARTIAL ENERGY LEVEL DIAGRAM OF $Ho^{3+}:CaF_2$ SHOWING THE OBSERVED FLUORESCENCE LINES OF $^5F_5 \longrightarrow {}^5I_8$ TRANSITION OF CENTRE A AT LNT.

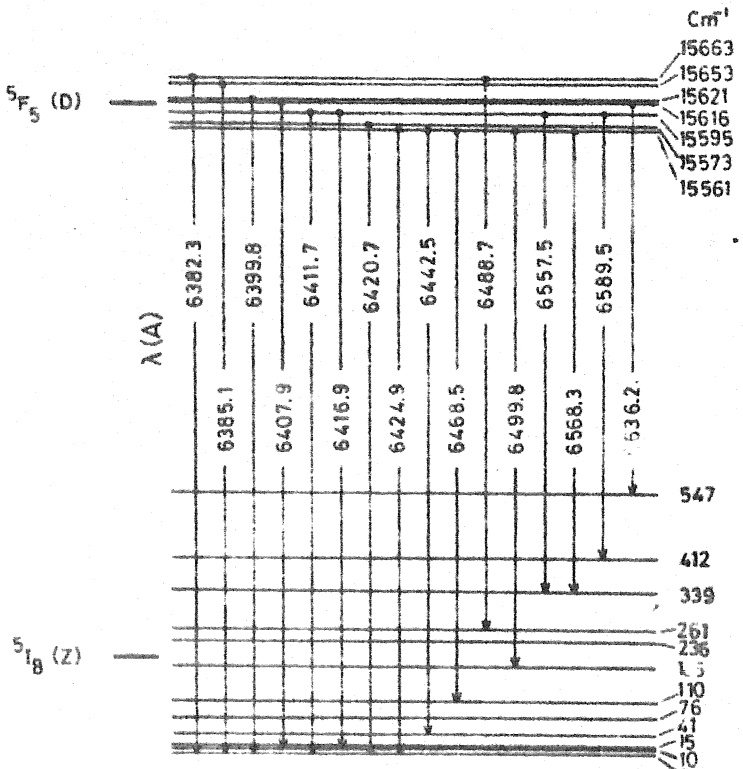

FIG.4.21b PARTIAL ENERGY LEVEL DIAGRAM OF $Ho^{3+}:CaF_2$ SHOWING THE OBSERVED FLUORESCENCE LINES OF $^5F_5 \longrightarrow {}^5I_8$ TRANSITION OF CENTRE B AT LNT.

Table 4.5 : Partial Energy Levels of Ho^{3+}:CaF_2 Derived from the Excitation and Fluorescence Spectra

SLJ Level	Energies of Stark Components (cm^{-1})	
	Centre A	Centre B
$^5I_8(Z)$	0	0
	7	10
	33	15
	75	41
	100	76
	141	110
	203	185
	328	236
	382	261
	450	239
	478	412
	538	547
$^5I_7(Y)$	5254	5239
	5257	5257
	5265	5262
	5297	5272
	5334	5288
	5348	5306
	5379	5319
	5411	
	5442	
$^5F_4+^5S_2$ (E)		
	18558	18574
	18580	18614
	18591	18622
	18631	18643
	18657	18652
	18673	18680
	18702	18719
	18723	18758
	18750	18772
$^5F_5(D)$	15593	15561
	15607	15573
	15620	15595
	15630	15616
	15651	15621
		15653
		15663
$^5F_3(F)$	20774	20695
	20787	20711
	20823	20741
	20884	20749
	20921	20775
		20794
$^3K_8(H) + ^5F_2(G)$		
	21207	21207
	21223	21221
	21241	21367
	21287	21388
	21442	21420
	21447	21456
	21462	21474

Table 4.5 : (Continued)

SLJ Level	Energies of Stark Components (cm^{-1})	
	Centre A	Centre B
	21523	21511
	21545	21601
	21586	21613
	21605	
	21638	
	21653	
$^5G_6 + {}^5F_1$ (I)		
	22273	22143
	22307	22187
	22321	22221
	22389	22228

SLJ Level	Energies of Stark Components (cm^{-1})	
	Centre A	Centre B
	22424	22248
	22477	22267
	22526	22297
	22537	22322
		22359
		22384
		22416
		22471

A set of Stark components at 0, 10, 15, 41, 76 and 110 cm^{-1} are arrived at in the above manner for the ground level, $^5I_8$ of centre B to explain the B excitation spectrum.

Higher Stark components of the ground level of both the centres are established through the fluorescence from $^5F_3$, $^5F_4 + {}^5S_2$ and $^5F_5$ to $^5I_8$. They are at 203, 328, 382, 450, 478 and 538 cm^{-1} for the centre A and 185, 236, 261, 339, 412, 467 cm^{-1} for the centre B.

4.6.2 Transitions Involving the Levels $^5G_5$(M) and $^5G_5$(J)

Information about these levels could be obtained only through the absorption data, since the availability of the laser dyes is limited to the region from 4400 to 7000A. Attempts to separate the lines due to different centres in the region from 3600 to 4200A, using the concentration series method, were not successful as the absorption to these levels could be recorded with only one concentration (section 4.3). Barycentres of M and J levels are around 27740 cm^{-1} and 24130 cm^{-1} respectively.

4.6.3 Transitions Involving Levels $^5G_6 + {}^5F_1$ (I) and $^3K_8$(H) + $^5F_2$(G)

Though levels $^5G_6 + {}^5F_1$ and $^3K_8 + {}^5F_2$ are excited, fluorescence from $^5F_3$, $^5F_4 + {}^5S_2$ and $^5F_5$ only is observed

in the present study. Ho^{3+} ions in these levels cascade nonradiatively to $^5F_3$ through the emission of phonons, since these levels lie quite close to each other. The positions of the Stark components of these levels are established only through the excitation spectrum, shown in figure 4.6. The spectra contain fourteen A centre lines and twenty one B centre lines. Centre A has few and well separated lines in this region, whereas most of the B centre lines are broad (except for the few lines around 4890A), which may probably be due to the presence of several close lines. Excitation with most of the A lines in this region resulted in a fluorescence spectrum containing B lines also. In contrast, excitation with most of the B lines resulted in a pure B fluorescence spectrum which is also confirmed through the decay times measurement.

Eight Stark components at 22273, 22307, 22321, 22389, 22424, 22477, 22526 and 22537 cm^{-1} explain the absorption lines in the A centre excitation spectrum of $^5G_6 + {}^5F_1$ (figure 4.16). With this set all the lines except 4515.2A are explained with maximum error of $\pm$ 3 cm^{-1}. The 4515.2A line is very weak and is assigned as due to the transition from the Stark component at 141 cm^{-1} to 22273 cm^{-1}. The inaccuracy in this assignment is 9 cm^{-1} which corresponds to 2A.

B excitation spectrum is explained (with a maximum inaccuracy of ± 5 cm^{-1}) with twelve Stark components (figure 4.16) at 22143, 22187, 22221, 22228, 22248, 22267, 22297, 22322, 22359, 22384, 22416 and 22471 cm^{-1}.

It has been experimentally observed in many other hosts [6,7] that the Stark components of $^3K_8$ and $^5F_2$ overlap each other because of the very small energy gap between them. Hence the absorption lines of the excitation spectrum in the region of 4600A are assigned as due to both the levels $^3K_8$ and $^5F_2$. The spectrum in this region contains thirty four A centre lines and thirty B centre lines. Two lines at 4667.3A and 4668.6A present in the A spectrum are found to be due to centre B. Absorption lines of both the centres in this region are sharp with half widths of 1A.

Excitation spectra in this region are explained with the Stark components of $^3K_8 + {}^5F_2$ at 21207, 21223, 21241, 21287, 21442, 21447, 21462, 21523, 21545, 21586, 21605, 21638, and 21653 cm^{-1} for the centre A and 21207, 21221, 21367, 21388, 21420, 21456, 21474, 21511, 21601 and 21613 cm^{-1} for the centre B. With these sets of Stark components, transition assignments (figure 4.17) for all the lines in this region are made with a maximum error of ± 5 cm^{-1}.

4.6.4 Transitions Involving the Level $^5F_3$(F)

Excitation spectra of this level obtained by monitoring 5397.0A and 5437.8A of centres A and B respectively are shown in figure 4.8. All the A lines (except for the two lines at 4887.7 and 4906.0A) are sharper than the B lines in this region. In this region the spectrum contains thirteen B lines and fourteen A lines.

This level gives rise to fluorescence in the 4800A and 6500A regions, due to the transitions $^5F_3 \rightarrow {}^5I_8$ and $^5F_3 \rightarrow {}^5I_7$ respectively.

$^5F_3 \rightarrow {}^5I_8$ fluorescence spectrum is illustrated in figure 4.11. A total of twenty seven lines are observed in this region. Centre A has twelve well isolated lines, and centre B which has fourteen lines superposed on a broad background. This has reflected in the observation that, the excitation spectral lines of B could never be avoided, whatever be the monitoring wavelength (in this region). Decay times of all the lines in this group are measured with A and B excitations and average values of 10.0 μs and 18 μs are observed for $^5F_3$ of centre A and B respectively.

Stark components of this level for both the centres are obtained from the $^5I_8 \rightarrow {}^5F_3$ excitation spectrum and $^5F_3 \rightarrow {}^5I_8$ fluorescence spectrum. Figures 4.18 and 4.19

show the transition assignments for the lines in the different groups involving this level. All the lines in the excitation spectra and fluorescence spectra are accounted for with a set of Stark components for $^5F_3$ at 20774, 20787, 20823, 20884, 20921 cm^{-1} for the centre A and at 20695, 20711, 20741, 20749, 20775 and 20794 cm^{-1} for the centre B.

$^5F_3 \rightarrow {}^5I_7$ transition will be discussed in section 4.6.6.

4.6.5 Transitions Involving the Levels $^5F_4 + {}^5S_2$ (B)

The free ion energies of these levels are separated by less than 100 cm^{-1} and since at LHT, transitions are possible even from a Stark component at 141 cm^{-1}, the excitation and the fluorescence spectra in the 5300A region consists of lines due to the Stark components of both the levels F_4 and S_2, and they cannot be separated out.

The excitation spectrum of these levels is obtained by monitoring the fluorescence from the same levels. It contains thirteen lines from the centre A and seventeen lines from the centre B. From the measurement of the decay times it is identified that the three lines at 5351.4, 5365.1 and 5367.0A in the A spectrum are due to the B centre. Similarly the line at 5396.0A in the B spectrum is due to the A centre. All the lines are found to have half widths of ~2A. Figure

4.9 compares the excitation spectra of centres A and B in this region.

It has been observed in several other crystals containing Ho^{3+} that both the levels $^5F_4 + {}^5S_2$ and $^5I_4$ fluoresce and lead to fluorescence in the region 7500A, in addition to the 5300A group due to $^5F_4 + {}^5S_2 \rightarrow {}^5I_8$ transition. In the present experiments it has been confirmed from the decay times measurement and from the excitation spectra of all the lines in the 7500A group, that the lines of this group are due to the transition $^5F_4 + {}^5S_2 \rightarrow {}^5I_7$ only and not due to $^5I_4 \rightarrow {}^5I_8$. $^5I_4 \rightarrow {}^5I_8$ fluorescence is not observed even when $^5F_5$ (which lies in between $^5F_4 + {}^5S_2$ and $^5I_4$) is selectively excited. (It has been observed in $Ho^{3+}:YAlO_3$ [23] that the branching ratios for the emission from the higher excited levels $^5F_4$, $^5S_2$ and $^5F_5$ to $^5I_4$ are much smaller than the ratios obtained for the transitions from these levels to the other lower levels. Further $^5I_4 \rightarrow {}^5I_8$ fluorescence is found to be much weaker than the $^5I_4 \rightarrow {}^5I_7$, $^5I_6$, $^5I_5$ fluorescence). The $^5I_4$ level could not be selectively excited, because of the lack of a dye for this region. The 5300A and 7500A fluorescence groups are shown in figures 4.12 and 4.15.

The $^5F_4 + {}^5S_2 \rightarrow {}^5I_8$ transition is observed to be the strongest in the observed fluorescence. Unlike the 4800A

group, larger number of lines are observed in the 5300A and 7600A groups corresponding to centre A than to centre B. The centres A and B give rise to 24 and 18 lines respectively in the 5300A group. Except for the two lines at 5384.9A and 5393.5A, all the lines in the B centre fluorescence spectrum of 5300A are broad with half widths around 4A. Lines corresponding to the centre A in this region have a maximum half width of 3A. The line appearing at 5413.9A in the A spectrum is identified as due to the B centre. Similarly 5309.8, 5410.8, 5471.3 and 5529.8A lines in the B spectrum are attributed as due to the A centre.

All the fluorescence and excitation spectral lines are explained with the following sets of Stark components: 18558, 18580, 18591, 18631, 18657, 18673, 18702, 18723 and 18757 cm^{-1} for centre A; and 18574, 18614, 18622, 18643, 18652, 18680, 18719, 18758 and 18772 cm^{-1} for centre B (figures 18 and 20).

The 7500A group contains a total of thirty seven lines, twenty of which belong to the A centre and the others to B centre. Lines in this region due to both the centres are sharp. The 7510.0A line in the A spectrum and the 7472.8A and 7504.0A lines in the B spectrum are identified to be as due to the B and A centres respectively. The positions of the Stark components of the level $^5I_7$ are obtained

by subtracting the energies of the lines in the 7500A group, from the energies of the originating Stark components of $^5F_4 + {}^5S_2$ (account is also taken of the $^5F_3 \rightarrow {}^5I_7$ fluorescence in deriving the Stark manifold of I_7). The Stark components of $^5I_7$ are identified to be at 5254, 5257, 5265, 5297, 5334, 5348, 5379, 5411 and 5442 cm^{-1} for centre A and at 5239, 5257, 5262, 5272, 5288, 5306 and 5319 cm^{-1} for centre B. Transition assignments for the lines involving $^5I_7$ and $^5F_4 + {}^5S_2$ levels are shown in figure 4.20.

4.6.6 Transitions Involving the Level $^5F_5$ and the $^5F_3 \rightarrow {}^5I_7$ Transition

Fluorescence in the 6500A region has not been analysed by the earlier workers probably because of the complexity of this group due to the overlapping transitions, $^5F_3 \rightarrow {}^5I_7$ and $^5F_5 \rightarrow {}^5I_8$. In the present study, different excitations are used to record the steady state and transient spectra to resolve this complexity. Since $^5F_5$ is the lower level, fluorescence from this level alone is recorded by exciting with the 6328A line of a 0.5 mW (Spectra Physics model 130) He-Ne laser. As this is a nonresonant excitation, it lead to fluorescence from both the centres A and B. Fluorescence from the level $^5F_5$ to the ground state only is within the detector band width, and monitoring each of these lines, $^5I_8 \rightarrow {}^5F_5$

excitation spectra are obtained. Using the procedure which was described earlier, fluorescence and excitation spectra are recorded to obtain pure A and B spectra. $^5F_5 \rightarrow {}^5I_8$ fluorescence spectrum, shown in figure 4.13 consists of several partially resolved lines. Only two sharp lines, one from centre A at 6433.4A and one from centre B at 6399.7A could be chosen for monitoring, since at all other positions, there is an overlap of A and B lines. The excitation spectra are shown in figure 4.10. It is confirmed that these two lines belong to the centres A and B respectively by recording the excitation spectra of $^5F_4 + {}^5S_2$ while monitoring these two lines. However, the spectrum shown in figure 4.10 could not be confirmed by monitoring other lines (no other well separated lines could be located), and thus the separation of the two excitation (and similarly the fluorescence spectra shown in figure 4.13) spectra is some what tentative.

The excitation spectrum contains seven lines for A and fourteen lines for B. The observed number of lines is quite small in view of the large J values of the two participating levels. The two strong lines at 6433.4 and 6399.7A in the A and B spectra respectively are due to the laser scattering. However, there are two absorption lines at these wavelengths, the presence of which is confirmed by monitoring other fluorescence lines. Following are the Stark components of $^5F_5$ arrived at from the difference tables for the

$^5F_5 \rightarrow {}^5I_8$ fluorescence groups and $^5I_8 \rightarrow {}^5F_5$ excitation spectra: 15593, 15607, 15620, 15630 and 15651 cm^{-1} for centre A and 15561, 15573, 15593, 15616, 15621, 15653 and 15663 cm^{-1} for centre B. Figures 4.19 and 4.21 show the transition assignments for all the lines in the 6500A region of the optical spectrum.

Average values of decay times of fluorescence lines from $^5F_5$ of centre A and centre B are found to be 118 μs and 145 μs respectively.

As a second step towards the understanding of the 6500A group, the steady state fluorescence in this region is recorded by exciting into $^3K_8 + {}^5F_2$ at 4617.1A for centre A and 4676.5A for centre B (figure 4.14). With the former excitation, the fluorescence spectrum in the 6500A region is found to contain very sharp lines with a decay time of ~10 μs which is exactly the same as that of $^5F_3$ corresponding to centre A. $^5F_5 \rightarrow {}^5I_8$ fluorescence of centre A was found to be very weak with this excitation. Excitation into the same manifold with 4676.5A, resulted in $^5F_5 \rightarrow {}^5I_8$ fluorescence of centre B only. The difference in the fluorescence intensities of the 6500A group of centre B in figures 4.13 and 4.14 is due to the laser powers at the excitation wavelengths. Only few lines at 6451.6, 6455.2 and 6461.9A could be identified to be as due to $^5F_3 \rightarrow {}^5I_7$ transition of centre B from

their very sharp initial decay, characteristic of the $^5F_3$ level of centre B. Broad 'background' fluorescence at these wavelengths is reflected in the tail of the decay curve which has a decay time around 140 μs approximately (characteristic of $^5F_5$). Measurement of the decay times could not be made for the very weak lines on the higher wavelength side, to identify if there are any more lines due to $^5F_3 \rightarrow {}^5I_7$ transition.

Transition assignments for all the lines in the $^5F_3 \rightarrow {}^5I_7$ fluorescence group could be made using the Stark splittings of the participating levels already derived from the other groups.

4.7 Steady State and Transient Fluorescence Spectra of the Concentration Series

Fluorescence spectra are recorded for all the crystals of the concentration series using 4617.1A of centre A and 4676.5A of centre B excitations.

Centre A:

It has been found that the relative intensity of the fluorescence lines in each group is unaffected with the increase of concentration from 0.01 to 5 percent. The intensity of the A centre lines increases with concentration and reaches a maximum value around 0.3 percent and does not

increase with further increase of concentration. However, the decay times of the fluorescence signals from F_3, $F_4 + S_2$ and F_5 decrease gradually with the increase of concentration.

Centre B:

Fluorescence from the centre B also increases with the increase of concentration from 0.01 to 1 percent, except that in the 5 percent concentration crystal the relative intensities of the lines show a drastic change from that of the other concentrations. The intensities of the lines on the higher wavelength side of each group show an increase relative to the lines on the shorter wavelength side. The decay times however, are found to be the same for all lines in each group. Proper explanation for the variation of the intensities at higher concentrations could not be given because of the insufficient data on hand at present. This variation is possibly due to increased ion-ion interactions at these concentrations.

CONCLUSIONS

From the fluorescence and excitation spectra, it is concluded that there are two prominent centres A and B for Ho^{3+} in CaF_2 in the concentration region below 1 percent. The spectrum becomes complicated in the 5 percent concentration crystal and could not be analysed. All the lines in

the observed fluorescence and excitation spectra could be classified under centres A and B. Two groups around 6500A and 7500A are found to be due to overlapping transitions. All the lines belonging to different parent levels are identified through selective excitation studies and the decay time measurements. The Stark components of $^5I_8$, $^5I_7$, $^5F_5$, $^5F_4 + {}^5S_2$, $^5F_3$, $^3K_8 + {}^5F_2$ and $^5G_6 + {}^5F_1$ are derived for both the centres A and B from the observed spectra.

REFERENCES

1. H. Gobrecht, Ann. Physik 28, 673 (1937); 31, 755 (1938).

2. E.J. Mechan and G.C. Nutting, J. Chem. Phys. 7, 1002 (1939).

3. H.G. Khale, Z. Physik 145, 345 (1956).

4. S. Singh, Ph.D. Dissertation (1957), The Johns Hopkins University, U.S.A.

5. M.H. Crozier and W.A. Runciman, J. Chem. Phys. 35, 1392 (1961); ibid 36, 1088 (1962).

6. G.H. Dieke and B. Pandey, J. Chem. Phys. 41, 1952 (1964).

7. H.H. Caspers, H.E. Rast and J.L. Fry, J. Chem. Phys. 53, 3208 (1970).

8. P.J. Becker, Physica Status Solidi B43, 583 (1971).

9. D.E. Wortman and D. Sanders, J. Chem. Phys. 53, 1247 (1970).

10. D.E. Wortman, C.A. Morrison and R.T. Farrar, J. Opt. Soc. Am. 62, 1329 (1973).

11. L.F. Jhonson, J.F. Dillon and J.P. Rameika, J. Appl. Phys. 40, 1499 (1969).

12. J.L. Merz and P.S. Pershan, Phys. Rev. 162, 235 (1967);
D.R. Tallant and J.C. Wright, J. Chem. Phys. 63, 2074 (1975);
M.D. Kurz and J.C. Wright, J. Luminescence 15, 169 (1977).

13. R. Reisfeld and J. Hormadaly, J. Phys. Chem. 64, 3207 (1976).

14. Yu.K. Voronko, A.A. Kaminskii, V.V. Osiko and A.M. Prokhorov, JETP Letters 1, 3 (1965).

15. L.F. Johnson, J. Appl. Phys. 34, 897 (1963).

16. J.L. Merz and P.S. Pershan, Phys. Rev. 162, 217 (1967).

17. M. Schlesinger and P.W. Whippey, Phys. Rev. 177, 563 (1969).

18. C.M. Verber, D.R. Grieser and W.H. Jones, J. Appl. Phys. 42, 2767 (1971).

19. L.S. Kornienko and A.O. Rybaltovskii, Sov. Phys. Solid State 13, 1785 (1972).

20. A.A. Kaplaskii, Opt. Spectrosc. 39, 437 (1975).

21. Bansilal, Ph.D. Dissertation (1977), I.I.T. Kanpur, India.

CHAPTER 5

FLUORESCENCE AND EXCITATION SPECTRA OF $Ho^{3+}:BaF_2$

ABSTRACT

Three groups of lines in the region from 5200 to 7700A, assigned as due to the transitions from $^5F_3$, $^5F_4 + {}^5S_2$ and $^5F_5$, are observed in the fluorescence spectrum of $Ho^{3+}:BaF_2$. Excitation spectra are recorded by monitoring most of the intense lines in the fluorescence spectrum. From the study of the excitation and fluorescence spectra, all the lines in the observed spectrum are classified under one centre. Decay times are also measured to confirm the analysis. Partial energy level scheme could be derived for some of the levels involved in the observed spectra.

5.1 Introduction

The investigation on the optical spectra due to different centres of Ho^{3+} is also extended to another host viz., BaF_2. The $Ho^{3+}:BaF_2$ crystal has been obtained from the Semi Elements Inc. U.S.A and contains 0.1 mole percent of Ho.

Because of the complexity of the Ho^{3+} spectrum, as discussed in Chapter 4, the spectra of Ho^{3+} in BaF_2 are not studied in detail. Some of the earlier studies on this system are listed at the end of the chapter. Bansilal [1] has recently reported the fluorescence spectrum of $Ho^{3+}:BaF_2$, recorded in the region from 5200 to 7600A. CW Ar^+ laser was used as the excitation source. He, however, did not attempt to analyse the spectrum. In the present work, the spectra are recorded using the N_2 laser pumped dye laser. Fluorescence and excitation spectra are recorded to classify the lines in the optical spectrum under different centres.

5.2 The Spectra Obtained

As discussed in Chapters 2 and 3, the fluorescence spectra are recorded at LNT using N_2 laser (a broad band excitation) and the dye laser (selective excitation). Three groups of fluorescence lines are observed in the optical region, from 5200 to 7700A. Another group around 4800A, is found to be very weak and is not studied in the present

experiments. A comparison of this spectra with that of $Ho^{3+}:CaF_2$ (Chapter 4) leads to the following transition assignments.

Fluorescence Group	Transition Assignment
5280 - 5650A	$^5F_4 + {}^5S_2$ (E) $\rightarrow {}^5I_8$(Z)
6300 - 6650A	$^5F_5$(D) $\rightarrow {}^5I_8$(Z)
	$^5F_3$(F) $\rightarrow {}^5I_7$(Y)
7450 - 7700A	$^5F_4 + {}^5S_2$ (E) $\rightarrow {}^5I_7$(Y)
	$^5I_4$(C) $\rightarrow {}^5I_8$(Z)

To classify the lines belonging to different centres, excitation spectra are recorded by monitoring all the lines in the 5300A group, which is the strongest. Monitoring most of the lines resulted in a spectrum as shown in figure 5.1. But, with some of the lines at 5397.1, 5562.6, 5527.5A etc., all the lines in the excitation spectrum (figure 5.1) are reproduced in intensity and position except for three lines at 4624.0, 4634.8 and 4642.5A in the $^5I_8$(Z) $\rightarrow {}^3K_8$(H) + $^5F_2$(G) transition, and one line at 4504.3A in the $^5I_8$(Z) $\rightarrow {}^5G_6 + {}^5F_1$(I) transition. These lines show a change in relative intensity depending on the lines monitored. On excitation at most of the other lines, all the lines in the fluorescence spectrum shown in figures 5.2 and 5.3 are reproduced with their relative intensities and positions. The variation in

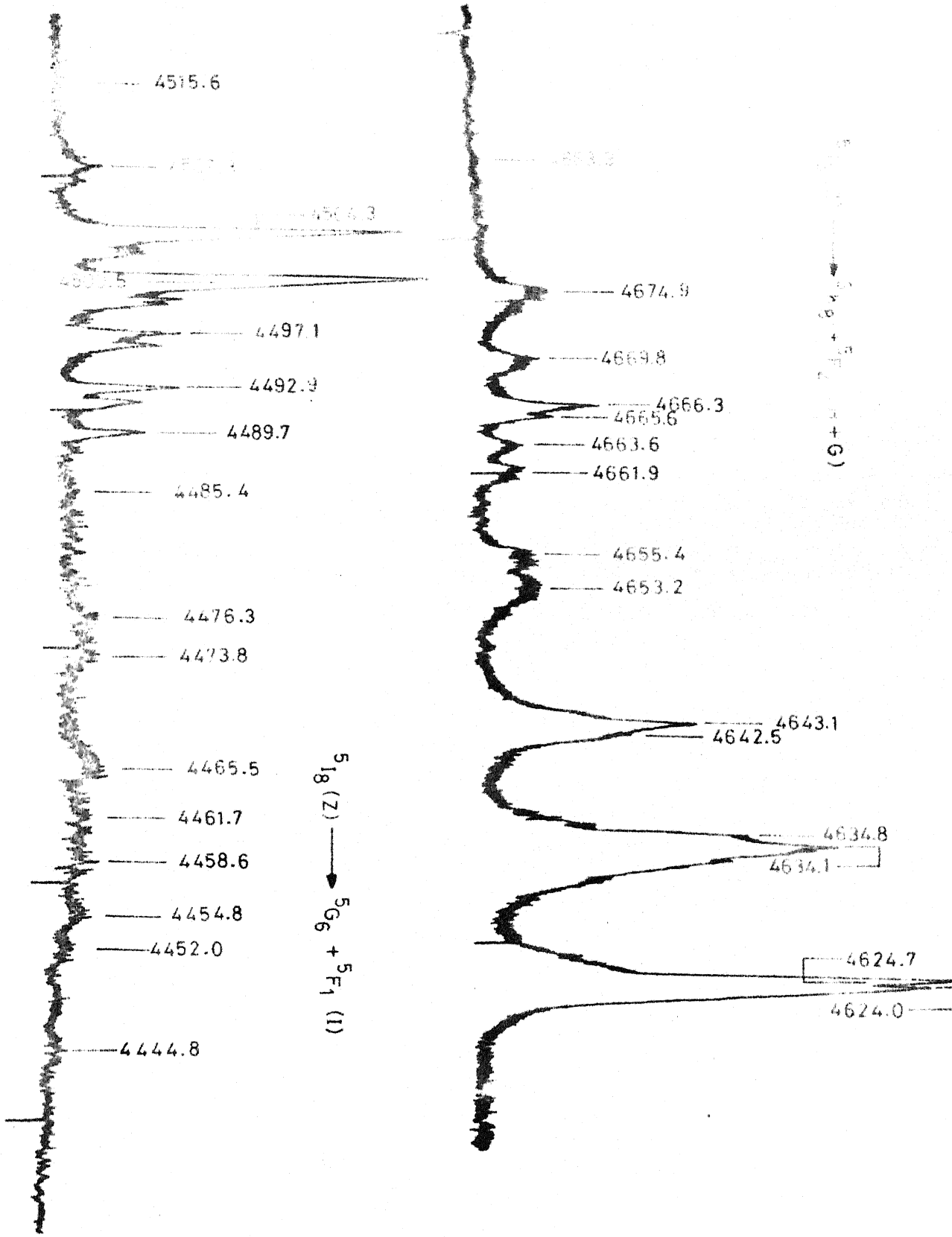
4515.6
4497.1
4492.9
4489.7
4485.4
4476.3
4473.8
4465.5
4461.7
4458.6
4454.8
4452.0
4444.8
5I8 (Z) ⟶ 5G6 + 5F1 (I)
4674.9
4669.8
4666.3
4665.6
4663.6
4661.9
4655.4
4653.2
4643.1
4642.5
4634.8
4634.1
4624.7
4624.0

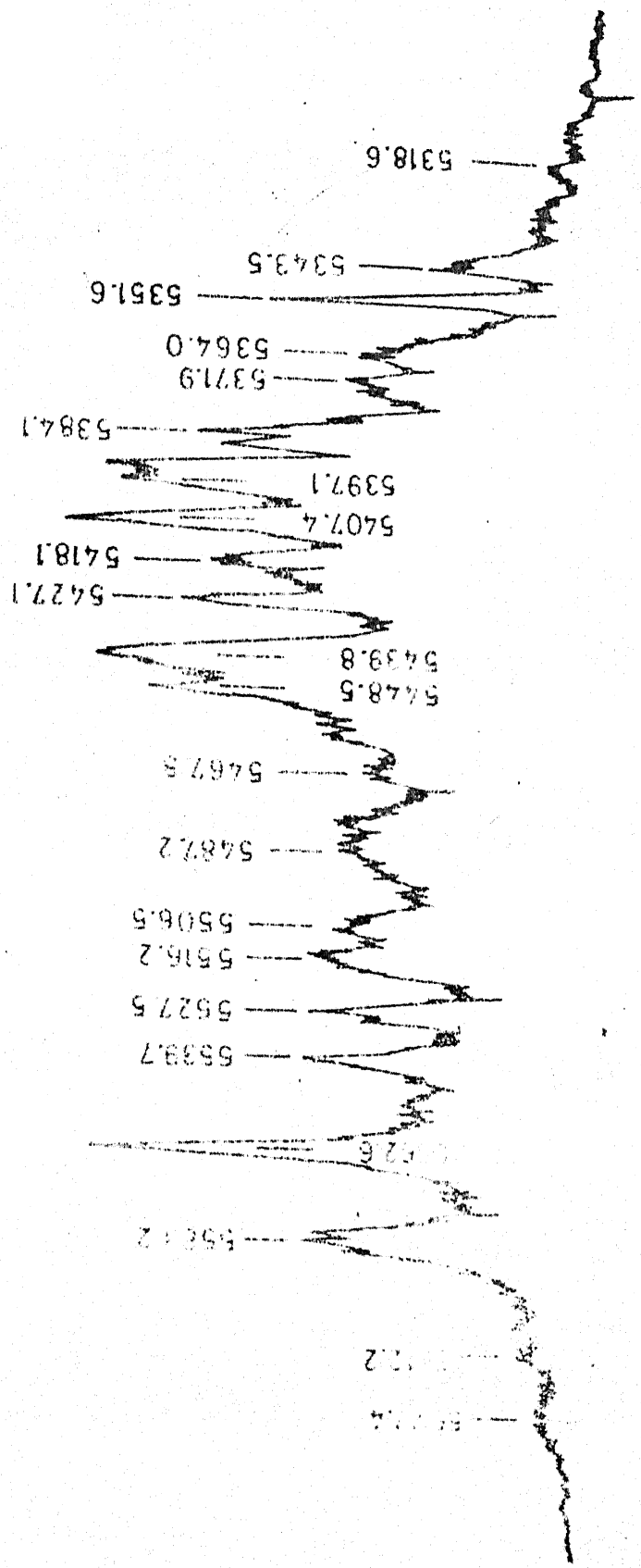

FIG. 5.2 FLUORESCENCE SPECTRUM OF Ho^{3+}: BaF_2 AT LNT; EX: 4624.7 A.

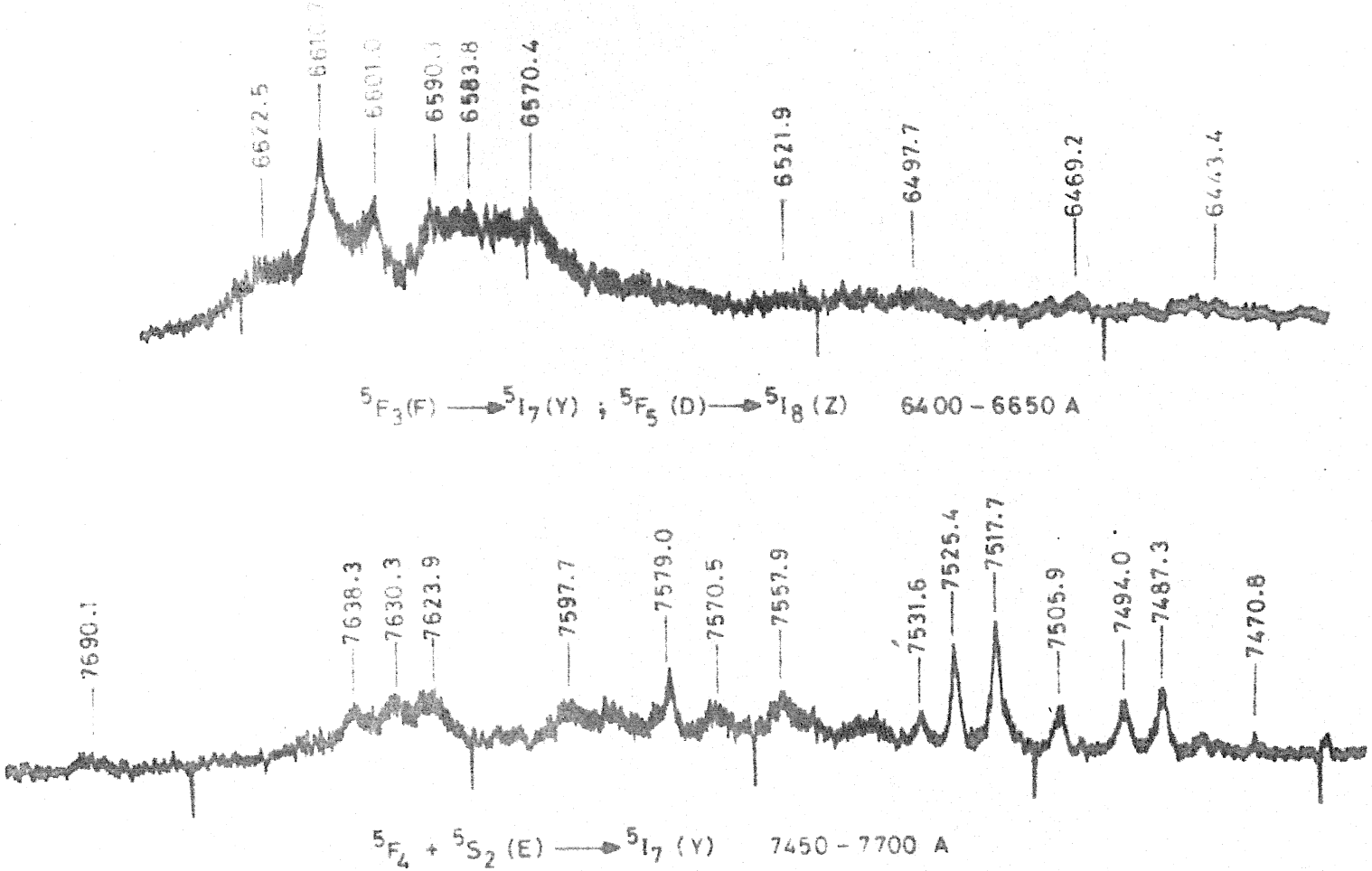

FIG. 5.3 FLUORESCENCE SPECTRUM OF Ho^{3+}: BaF_2 AT LNT ; EX: 4624.7 A.

the intensities of some of the lines in the spectra indicates the presence of more than one centre of Ho^{3+}. The centres other than the one which gives rise to the excitation and fluorescence spectra shown in figures 5.1 to 5.3, could not be studied in detail because of their weak fluorescence and excitation spectra.

As in the case of $Sm^{3+}:CaF_2$ and $Ho^{3+}:CaF_2$, this classification of all the lines shown in figures 5.1 to 5.3 under one centre, is confirmed from the studies of decay times of the fluorescence lines in the 5300A group.

The following discussion pertains to the strongly fluorescing centre only.

5.3 Discussion

5.3.1 The Ground Level, $^5I_8(Z)$

The ground level, Stark components below 150 cm^{-1} are derived from the $^5I_8(Z) \rightarrow {}^5G_6 + {}^5F_1$ (I) and $^5I_8(Z) \rightarrow {}^3K_8(H) + {}^5F_2(G)$ transitions in the excitation spectrum and $^5F_4 + {}^5S_2$ (E) $\rightarrow {}^5I_8(Z)$ transitions in the fluorescence spectrum. Higher Stark components of the ground level could not be derived since, only one group in the fluorescence spectrum terminating in $^5I_8$ is observed to be strong. The 6500A group, which also involves the

ground level $^5I_8$, is an overlap of $^5F_5(D) \rightarrow {}^5I_8(Z)$ and $^5F_3(F) \rightarrow {}^5I_7(Y)$ transitions, and further, the lines of this group are too broad and weak to analyse. The higher Stark components derived for the ground level from the $^5F_4 + {}^5S_2 \rightarrow {}^5I_8$ transition cannot be confirmed with the $^5F_5 \rightarrow {}^5I_8$ fluorescence, and therefore they are not given in the energy level scheme.+ The Stark components at 0, 37, 61, 86, 111 and 148 cm^{-1} are found to explain all the lines observed in the excitation spectrum. From the $^5F_4 + {}^5S_2 \rightarrow {}^5I_8$ fluorescence spectrum, which has a spread of about 1000 cm^{-1}, it is clear that the ground level has Stark components even upto about 900 cm^{-1} (assuming that Stark components upto 150 cm^{-1} above the lower most are only populated at LNT in the $^5F_4 + {}^5S_2$ manifold).

5.3.2 Trasitions Involving $^5G_6 + {}^5F_1$ (I) and $^3K_8$(H) + $^5F_2$(G)

Since these levels do not fluoresce, the Stark components are established from the excitation spectrum only. The excitation spectrum of $^5G_6 + {}^5F_1$ contains sharp and intense lines on the longer wavelength side and very weak and broad lines on the shorter wavelength side.

Absorption to $^3K_8 + {}^5F_2$ is observed to be the strongest in the 4400 to 6600A region. All the lines in this

+ In the case of Ho^{3+}:CaF_2 all the three groups $^5F_3$, $^5F_4 + {}^5S_2$ and $^5F_5$ to $^5I_8$ are strong, enabling the derivation of the upper Stark components of the ground level.

group have half widths of ~ 1.5A. The excitation spectrum of this group contains eighteen lines, which is a very small number, considering the large J values of the participating levels.

Figure 5.1 shows the excitation spectrum of these levels. Figure 5.4 shows the transition assignments made for this spectrum. Stark components at 21385, 21427, 21445, 21474, 21571, 21617 and 21657 cm^{-1} for $^3K_8 + {}^5F_2$ and 22186, 22231, 22256, 22288, 22304, 22334, 22388, 22458, 22476 and 22493 cm^{-1} for $^5G_6 + {}^5F_1$ are derived from the excitation spectrum.

5.3.3 Transitions Involving Levels $^5F_4 + {}^5S_2$ (E)

$^5F_4 + {}^5S_2 \rightarrow {}^5I_8$ is the strongest transition (figure 5.2) in the observed fluorescence spectrum. This group contains thirty eight lines. All these lines show a single value of decay time of 2450 μs within experimental errors. Excitation spectrum of this level could not be obtained as this absorption is weak. Hence, position of the Stark components of this level could not be derived.

The 7500A group shown in figure 5.3 contains only few sharp lines on the shorter wavelength side and large number of weak and broad lines on the longer wavelength side. Decay times of all the strong lines of this group (7487.3,

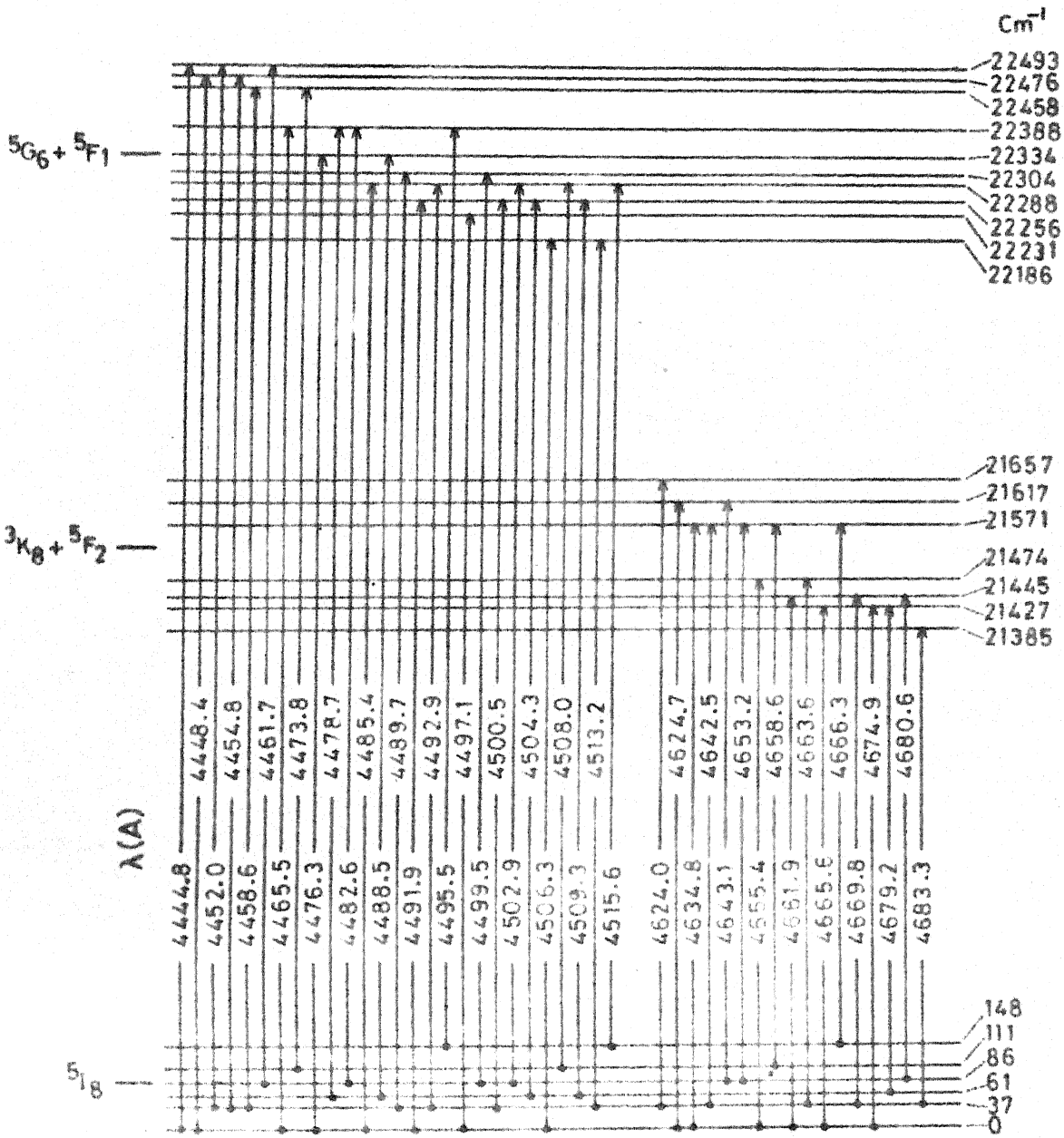

FIG. 5.4 PARTIAL ENERGY LEVEL DIAGRAM OF Ho^{3+}: BaF_2 SHOWING THE OBSERVED ABSORPTION LINES OF $^5I_8 \longrightarrow {}^5G_6 + {}^5F_1$ AND $^5I_8 \longrightarrow {}^3K_8 + {}^5F_2$ TRANSITIONS IN THE EXCITATION SPECTRUM AT LNT.

Table 5.1 : Excitation Spectrum of $Ho^{3+}:BaF_2$ at LNT; MON:5351.6A

Wavelength A	Energy cm^{-1}	Intensity (arb. units)	Wavelength A	Energy cm^{-1}	Intensity (arb. units)
$^5I_8 \rightarrow$	$^5G_6 + {}^5F_1$		$^5I_8 \rightarrow$	$^3K_8 + {}^5F_2$	
4444.8	22492	3	4624.0	21620	96
4448.4	22474	3	4624.7	21617	114
4452.0	22456	5	4634.1	21573	75
4454.8	22441	7	4634.8	21570	58
4458.6	22422	8	4642.5	21534	31
4461.7	22407	8	4643.1	21531	44
4465.5	22388	10	4653.2	21485	13
4473.8	22346	9	4655.4	21474	11
4476.3	22334	9	4658.6	21460	3
4478.7	22322	6	4661.9	21445	10
4482.6	22302	6	4663.6	21437	9
4485.4	22288	5	4665.6	21428	15
4488.5	22273	6	4666.3	21424	23
4489.7	22267	19	4669.8	21408	12
4491.9	22256	18	4674.9	21385	14
4492.9	22251	26	4679.2	21365	3
4495.5	22238	22	4680.6	21359	2
4497.1	22230	26	4683.3	21347	2
4499.5	22219	25			
4500.5	22214	81			
4502.9	22202	18			
4504.3	22195	75			
4506.3	22185	4			
4508.0	22177	7			
4509.3	22170	10			
4513.2	22151	3			
4515.6	22139	3			

Table 5.2 : Fluorescence Spectrum of Ho^{3+}:BaF_2 at LNT; Ex:4624.7A

Wavelength A	Energy cm^{-1}	Intensity (arb. units)
$^5F_4 + {}^5S_2$ (E) → $^5I_8$(Z)		
5309.6	18829	5
5318.6	18797	8
5328.3	18763	9
5331.6	18751	10
5341.3	18717	23
5343.5	18709	25
5351.6	18681	49
5364.0	18638	35
5366.2	18630	39
5371.9	18610	42
5374.9	18600	37
5380.8	18579	43
5384.1	18568	63
5387.3	18557	62
5392.8	18538	95
5397.1	18523	90
5407.4	18488	100
5418.1	18452	63
5427.1	18421	71
5439.8	18378	94
5448.5	18349	73
5459.3	18311	46
5467.8	18284	35
5474.3	18262	33
5480.2	18242	39
5487.2	18219	37
5506.5	18155	35
5516.2	18123	36
5527.5	18086	48
5529.6	18080	37
5539.7	18047	54
5550.3	18012	33
5562.6	17972	95
5572.7	17940	26
5583.2	17906	50
5605.2	17836	12
5612.2	17813	11
5627.4	17765	8
$^5F_3$(F) → $^5I_7$(Y) $^5F_5$(D) → $^5I_8$(Z)		
6435.2	15535	2
6443.4	15516	3
6447.5	15506	3
6457.8	15481	3
6469.2	15454	3
6473.8	15443	2
6483.0	15421	3
6497.7	15386	5
6521.9	15329	5
6570.4	15216	20
6583.8	15185	20
6590.3	15170	20
6601.0	15145	20

Table 5.2 : (continued)

Wavelength A	Energy cm^{-1}	Intensity (arb. units)	Wavelength A	Energy cm^{-1}	Intensity (arb. units)
6610.7	15123	33	7647.9	13072	5
6622.5	15096	12	7690.1	13000	3
$^5F_4 + {}^5S_2$ (E) $\rightarrow {}^5I_7$(Y)					
7470.8	13382	2			
7477.5	13370	2			
7480.6	13364	3			
7487.3	13352	11			
7494.0	13340	9			
7505.9	13319	8			
7517.7	13298	23			
7525.4	13285	18			
7531.6	13274	7			
7540.4	13258	6			
7543.4	13253	6			
7557.9	13228	10			
7563.5	13218	7			
7570.5	13206	9			
7579.0	13191	13			
7589.2	13173	9			
7597.7	13158	10			
7602.0	13151	6			
7607.3	13142	6			
7611.1	13135	5			
7623.9	13113	12			
7630.3	13102	11			
7638.3	13088	10			

7494.0, 7505.9 etc.) show that they originate from $^5F_4 + {}^5S_2$. Decay times of the weak lines could not be measured accurately, and their originating levels ($^5F_4 + {}^5S_2$ or $^5I_4$) are not known.

5.3.4 Transitions Involving $^5F_3$ and $^5F_5$

Fluorescence from these levels in the region around 6500A is found to be weak (figure 5.3). Because of the complexity of the 6500A group due to the overlap of transitions from $^5F_3$ and $^5F_5$, this group presently is not analysed. Further, $^5I_8 \rightarrow {}^5F_5$ absorption is found to be too weak to study the $^5F_5$ level alone. However, since the spectrum is recorded by selectively exciting only one centre, all the lines of the 6500A group are classified as due to one centre only.

It is planned to grow crystals of BaF_2 with higher concentrations of Ho to study the weak groups in the spectrum, and also other centres which have weak fluorescence.

CONCLUSIONS

From the fluorescence and excitation spectra it is concluded that there is only one centre for Ho^{3+} in BaF_2 (at this concentration), which has strong fluorescence and absorption. From the observed spectra, Stark components of $^5I_8$ (below 150 cm^{-1}), $^5G_6 + {}^5F_1$ and $^3K_8 + {}^5F_2$ are derived for this centre. A decay time of 2450 μs is observed for the fluorescence from $^5F_4 + {}^5S_2$ levels.

REFERENCES

1. Bansilal, Ph.D. Dissertation, I.I.T. Kanpur, India (1977).

2. V.V. Ovsyankin and P.P. Feofilov, Opt. Spektrosk, 31, 944 (1971).

CHAPTER 6

FLUORESCENCE SPECTRUM OF $Tb^{3+}:CaF_2$

ABSTRACT

Steady state fluorescence spectra of CaF_2 with different concentrations of Tb are reinvestigated using CW Ar^+ laser and N_2 laser. Variation in the relative intensity of various lines in the observed spectrum indicates the presence of more than one centre for Tb^{3+}.

6.1 Introduction

Terbium, with its outer shell configuration as $4f^8$ in the trivalent state, is of much interest to the spectroscopists since it gives strong fluorescence, practically in all the hosts. The ground state of this confirguration is ^7F, and the next state is ^5D which is well seperated from the ground state. Earlier works [1 to 13] have established the ^7F and ^5D multiplet positions in various lattices. The calculated values of the free ion energies [5] of $^7F_{5,4,3,2,1,0}$, $^5D_4$ and $^5D_3$ are 2020, 3279, 4258, 4947, 5405, 5632, 20455 and 26500 cm^{-1} respectively above the ground level, $^7F_6$. $^5D_4$ and $^5D_3$ are the only two levels that were observed to give rise to fluorescence in the visible region.

Stepanov et.al [1] and Feofilov [3] were the first to study, in detail, the optical spectrum of Tb^{3+} in CaF_2. They observed two types of spectra, viz., spectrum I and spectrum II, depending on the nature of crystal growth conditions. Spectrum I, appearing in the region 4900 to 6600A and spectrum II, appearing in the region 3800 to 4800A are attributed to the fluorescence from $^5D_4$ and $^5D_3$ respectively to the ground multiplet. Later, Rabbiner [7] also reported the fluorescence from $^5D_4$ and derived an energy level scheme consistent with the observed spectra, with the assumption

of a cubic symmetry. All the earlier spectra are photographed using 'broad band' excitations.

This work reports a preliminary attempt to reinvestigate this system using various laser excitations.

6.2 The Spectra Observed

As in the case of $Sm^{3+}:CaF_2$ and $Ho^{3+}:CaF_2$, the spectra are recorded using different laser excitations. Selective excitation of $^5D_4$ using dye laser did not yield detectable fluorescence because of very weak absorption of this level. $^5D_3$ and still higher levels could not be selectively excited because of the nonavailability of the needed laser dye. No excitation spectra is therefore available to make a complete analysis. Hence the work is carried out with N_2 laser and Ar^+ laser excitations only.

The Tb^{3+} fluorescence is recorded at LNT using crystals with different concentrations of Tb^{3+} (0.03, 0.09, 0.3, 1, 5 percent by weight of TbF_3 in CaF_2) and N_2 laser as the excitation source. As mentioned in the earlier chapters, this corresponds to a 'broad band' excitation. The fluorescence spectrum consists of six groups of lines in the range 5200 to 6900A, all of which are from $^5D_4$ to the ground multiplet, $^7F_{5,4,3,2,1,0}$. The spectrum corresponding to $^5D_4 \rightarrow {}^7F_{5,4,3}$ transitions is found to be similar to the spectrum I reported

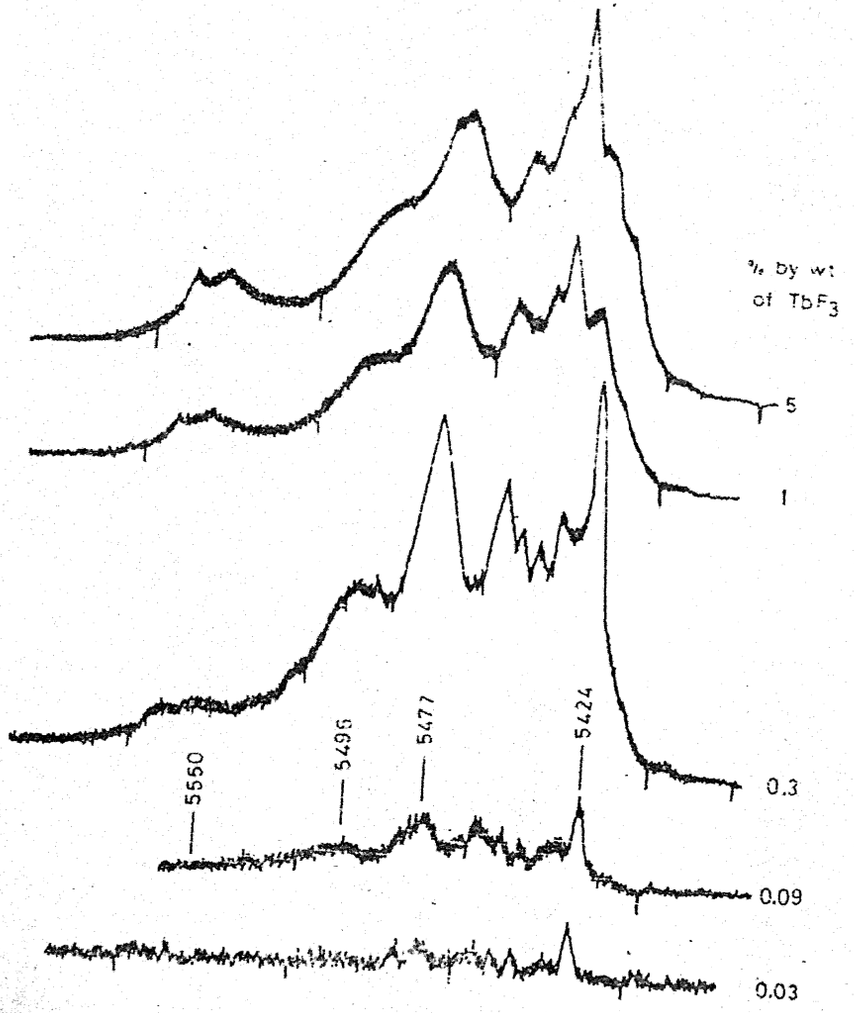

FIG. 6.1a FLUORESCENCE SPECTRUM OF Tb^{3+}: CaF_2 AT LNT; CONC. SERIES; $^5D_4 \longrightarrow {}^7F_5$ GROUP; EX : 3371 A.

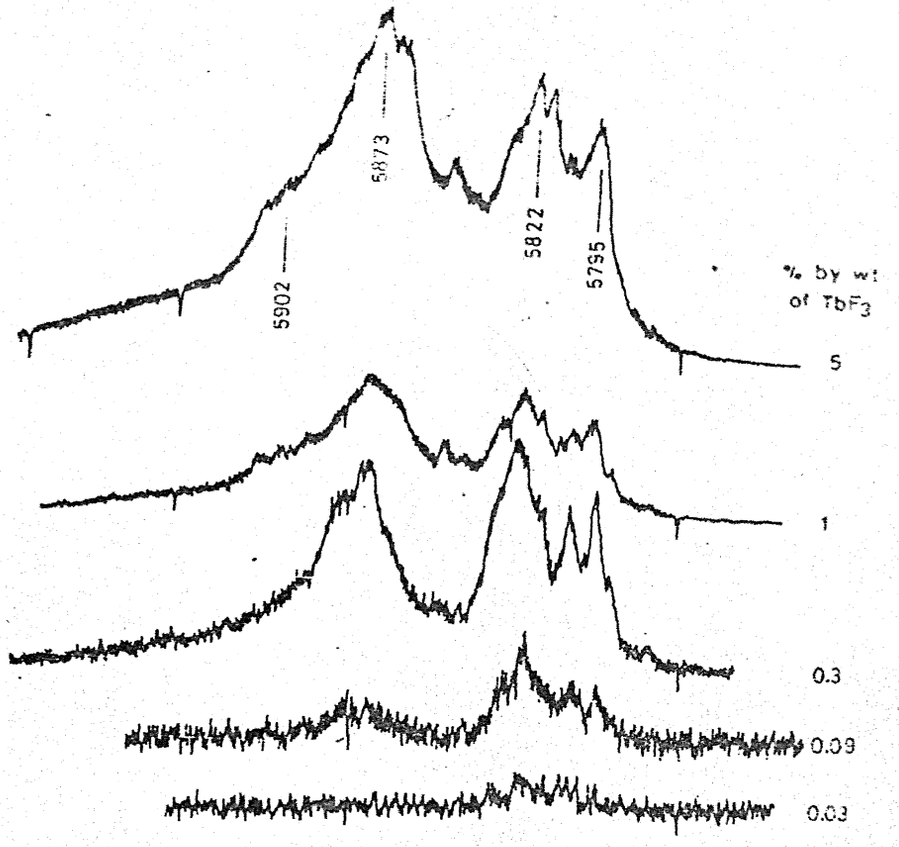

FIG.6.1b FLUORESCENCE SPECTRUM OF Tb^{3+}: CaF_2 AT LNT; CONC. SERIES; $^5D_4 \longrightarrow {}^7F_4$ GROUP; EX: 3371 A.

by Rabbiner. A search for the fluorescence from $^5D_3$, in the region from 4000 to 5000A did not yield any result.

Two of the groups, $^5D_4 \rightarrow {}^7F_5$ and $^5D_4 \rightarrow {}^7F_4$, obtained with 3371A ($N_2$ laser) excitation are shown in figure 6.1. The other four groups $^5D_4 \rightarrow {}^7F_{3,2,1,0}$ are very weak and are not shown in figures. It is seen that the spectra contain several weak and unresolved lines in addition to broad features.

With 4880A excitation, fluorescence is observed in the region 5300 to 6900A corresponding to the transitions $^5D_4 \rightarrow {}^7F_{5,4,3,2,1,0}$ (figures 6.2 and 6.3). 1 percent concentration crystal is used for these studies. The table 6.1 lists the observed fluorescence lines using 4880A excitation. It may be seen from the figures 6.1 and 6.2 that the relative intensities of some of the lines observed in the transitions $^5D_4 \rightarrow {}^7F_5$ and $^5D_4 \rightarrow {}^7F_4$ differ with excitation wavelength. This is attributed as due to the presence of more than one centre of Tb^{3+}. Also the spectra obtained in the present studies contain a much larger number of lines than reported earlier by Rabbiner. A site symmetry of Oh, as has been assumed by Rabbiner, cannot explain such large number of lines.

The relative intensity of gross features of the spectrum changes significantly with concentration. This can be

seen in figure 6.1. Some of the lines at 5423.8, 5802.6A, etc., show a large reduction in intensity with concentration. Whereas the intensity of the lines at 5430.6, 5451.9, 5872.6A, etc., increase with concentration. Lines at 5794.8, 5822.3A, etc., do not show much variation in the intensity with concentration. The spectra recorded showed some weak lines on the longer wavelength side of each group, which were not reported earlier. The intensity of these lines increases with increase of concentration. These intensity variations also indicate the presence of several centres of Tb^{3+}.

The following transition assignments, for different groups observed in the spectrum, are made after a comparison with the observed spectra of Tb^{3+} in various lattices.

Fluorescence Group	Transition Assignment
5350 - 5540A	$^5D_4 \rightarrow {}^7F_5$
5770 - 5960A	$^5D_4 \rightarrow {}^7F_4$
6140 - 6240A	$^5D_4 \rightarrow {}^7F_3$
6430 - 6520A	$^5D_4 \rightarrow {}^7F_2$
6650 - 6700A	$^5D_4 \rightarrow {}^7F_1$
6770 - 6830A	$^5D_4 \rightarrow {}^7F_0$

Fluorescence due to the $^5D_4 \rightarrow {}^7F_6$ transition is observed to be very weak, which probably is due to the very small transition probability between $^5D_4$ and $^7F_6$ levels.

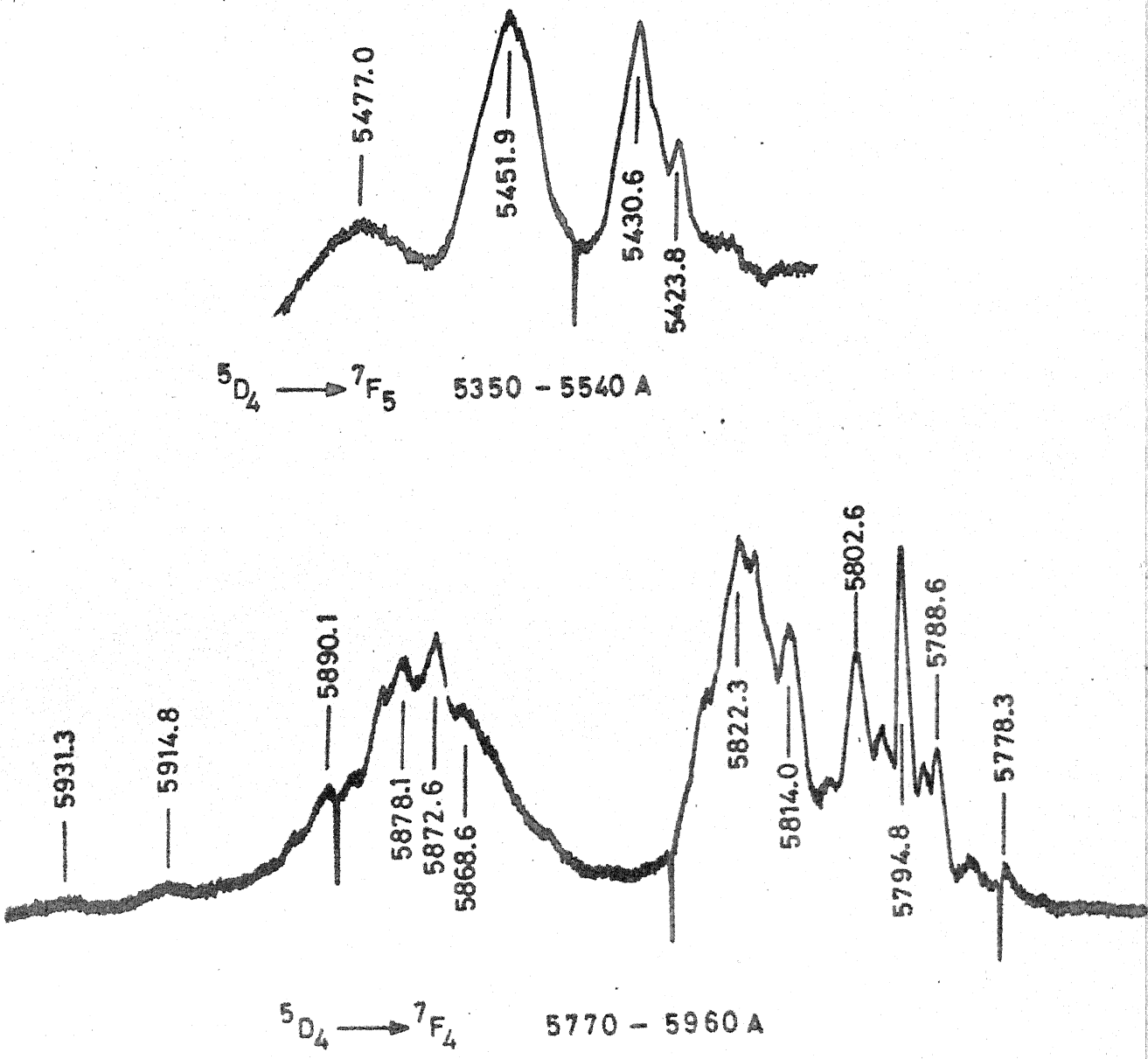

FIG. 6.2 FLUORESCENCE SPECTRUM OF Tb^{3+}: CaF_2 AT LNT; EX: 4880 A.

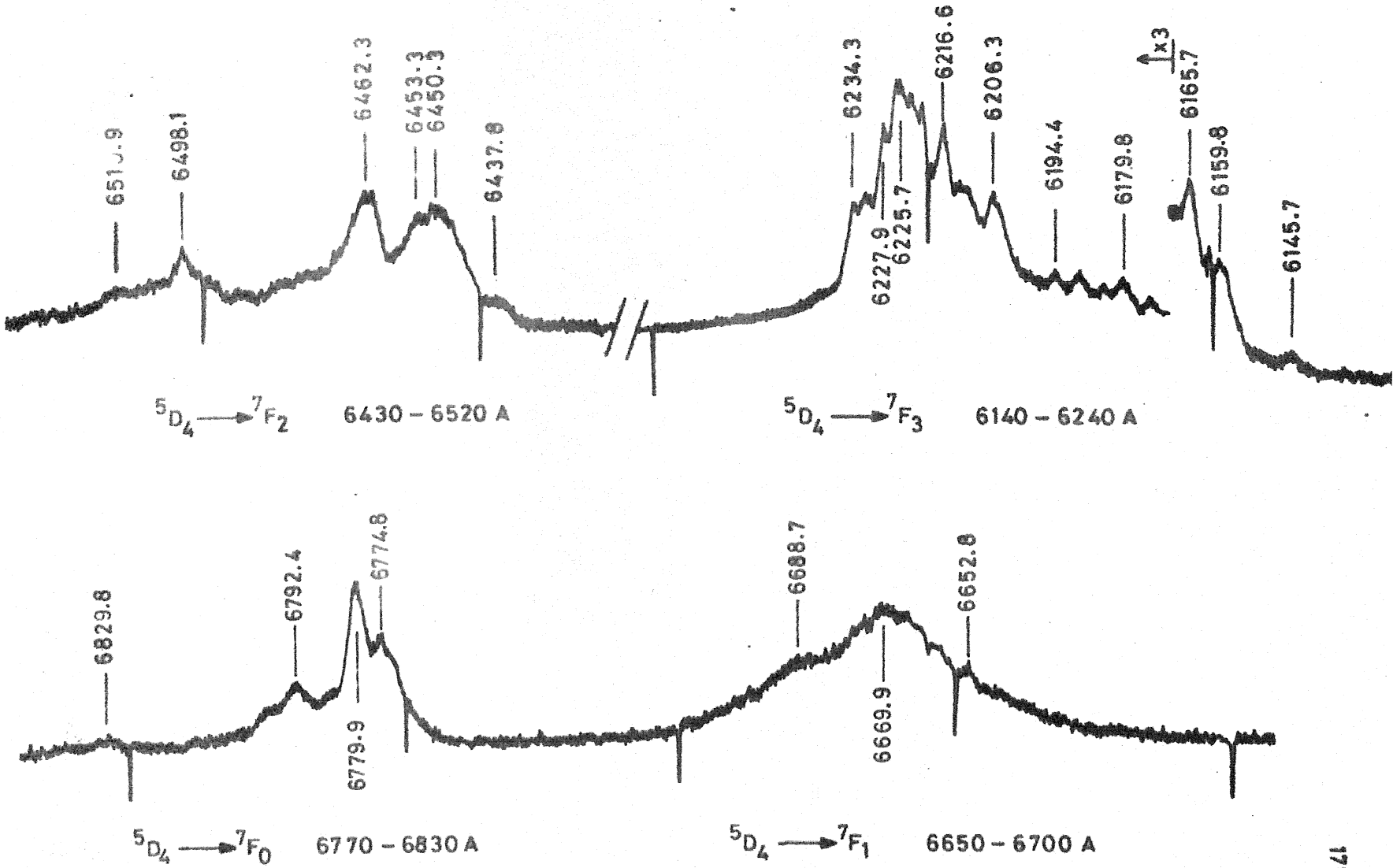

FIG. 6.3 FLUORESCENCE SPECTRUM OF Tb^{3+}: CaF_2 AT LNT; EX: 4880 A.

Table 6.1 : Fluorescence Spectrum of $Tb^{3+}:CaF_2$ at LNT; Ex:4880A of Ar^+ Laser

Wavelength A	Energy cm^{-1}
$^5D_4 \rightarrow {}^7F_5$	
5378.9	18585
5386.0	18561
5390.0	18548
5402.7	18504
5407.6	18487
5413.5	18467
5417.9	18452
5423.8	18432
5427.7	18419
5430.6	18409
5451.9	18337
5477.0	18253
5508.1	18150
5513.2	18133
5525.9	18092
5539.1	18049
$^5D_4 \rightarrow {}^7F_4$	
5772.2	17320
5778.3	17301
5783.4	17286
5788.6	17271
5791.7	17261
5794.8	17252
5798.0	17243
5802.6	17229
5807.8	17214
5814.0	17195
5819.2	17180
5822.3	17171
5828.5	17152
5838.7	17122
5845.7	17102
5853.7	17079
5868.6	17035
5872.6	17024
5878.1	17008
5881.1	16997
5886.1	16984
5890.1	16973
5895.6	16957
5914.8	16902
5931.3	16855
5953.0	16794
5956.0	16785
$^5D_4 \rightarrow {}^7F_3$	
6145.7	16267
6158.3	16234
6159.8	16230
6162.5	16223
6165.7	16214
6174.4	16192
6184.1	16166
6188.5	16155
6194.4	16139

Table 6.1 : (continued)

Wavelength A	Energy cm^{-1}
6206.3	16108
6212.8	16091
6216.6	16082
6220.4	16072
6222.5	16066
6225.7	16058
6227.9	16052
6231.1	16044
6234.3	16036
$^5D_4 \rightarrow {}^7F_2$	
6437.8	15529
6450.3	15499
6453.3	15492
6462.3	15470
6475.2	15439
6479.2	15430
6487.2	15411
6498.1	15385
6500.1	15380
6504.1	15371
6510.9	15355
$^5D_4 \rightarrow {}^7F_1$	
6652.8	15027
6669.9	14989
6688.7	14947
$^5D_4 \rightarrow {}^7F_0$	
6772.2	14762
6774.8	14757
6779.9	14745
6785.6	14733
6798.6	14705
6824.5	14649
6829.8	14638

$^5D_4 \rightarrow {}^7F_5$ transition is observed to be the strongest in the fluorescence spectrum. $^5D_4 \rightarrow {}^7F_{3,2,1,0}$ groups are found to be weak. In general, all groups are observed to be very broad, which is probably due to the presence of large number of lines due to several centres of Tb^{3+}.

Further detailed study to understand the spectra by selectively exciting each centre is planned. However, it is safe to conclude even at this preliminary stage that even the spectrum 1 itself is made of fluorescence from several kinds of Tb^{3+} centres.

REFERENCES

For the studies of Tb^{3+} in:

1. CaF_2 - I.V. Stepanov and P.P. Feofilov, Soviet Phys. Doklady 1, 350 (1956).

2. $Tb(C_2H_5SO_4)_3.9H_2O$, $Tb(BrO_3)_3.9H_2O$, $TbCl_3.6H_2O$, $Tb_2(SO_4)_3.8H_2O$, $Tb(NO_3)_3.6H_2O$, $Tb(C_2H_3O_2)_3.4H_2O$ and $Tb(HCO_2)_3$ - S. Singh, Dissertation, The Johns Hopkins University, 1957.

3. CaF_2 - P.P. Feofilov, Optika i Spektrosk (USSR) 10, 142 (1961).

4. $LaCl_3$ - K.S. Thomas, S. Singh and G.H. Dieke, J. Chem. Phys. 38, 2180 (1963).

5. Theoretical calculation - G.S. Ofelt, J. Chem. Phys. 38, 2171 (1963).

6. Ethyl Sulphate - J. A. Koningstein, Phys. Rev. 136, A726 (1964b).

7. CaF_2 - N. Rabbiner, J. Opt. Soc. Am. 55, 436 (1965).

8. Tungtates and Molybdates - W. Vichmann, J. Chem. Phys. 47, 875 (1967).

9. Hydroxides - P.D. Scott, H.E. Meissner, H.M. Crosswhite Phys. Letters 28a, 489 (1969).

10. Chelates - V.J. Rao and A.P.B. Sinha, Indian J. Chem. 9, 152 (1971).

11. TbAlG - B.D. Joshi and A.G. Page, J. Lumin. 6, 441 (1973).

12. CdF_2 - E. Grilliot and M. Brancie-Grilliot, J. Electrochem. Soc. 121, 95c (1974).

13. $CaWO_4$ - D. Fournier and A.C. Boccara, Phys. Status Solidi B64, 87 (1974).